Active Noise Control Over Spatial Regions

JIHUI ZHANG

Master of Engineering, Harbin Institute of Technology, China
Bachelor of Engineering, Harbin Institute of Technology, China

May 2019

A thesis submitted for the degree of Doctor of Philosophy
of The Australian National University

Research School of Engineering
College of Engineering and Computer Science
The Australian National University

Declaration

The contents of this thesis are the results of original research and have not been submitted for a higher degree to any other university or institution. Much of this work has either been published or submitted for publications as journal papers and conference proceedings. Following is a list of these papers.

Journal Publications

- J. Zhang, T. D. Abhayapala, P. N. Samarasinghe, W. Zhang, and S. Jiang, 'Multichannel active noise control for spatially sparse noise fields', *The Journal of the Acoustical Society of America*, vol. 140, no. 6, pp. EL510 − EL516, 2016.

- J. Zhang, T. D. Abhayapala, W. Zhang, P. N. Samarasinghe and S. Jiang, "Active Noise Control Over Space: A Wave Domain Approach," in *IEEE/ACM Transactions on Audio, Speech, and Language Processing*, vol. 26, no. 4, pp. 774-786, April 2018.

- J. Zhang, T. D. Abhayapala, W. Zhang, and P. N. Samarasinghe, "Active Noise Control over Space: A Subspace Method for Performance Analysis," *Applied Sciences*, vol. 9, no. 6, pp. 1250, March 2019.

Conference Proceedings

- J. Zhang, W. Zhang, and T. D. Abhayapala, Noise cancellation over spatial regions using adaptive wave-domain processing, in *Proc. IEEE Workshop on Applications of Signal Processing to Audio and Acoustics (WASPAA) 2015*, New Paltz, NY, USA, October 2015, pp. 1-5

- J. Zhang, T.D. Abhayapala, P. N. Samarasinghe, W. Zhang and S. Jiang, Sparse complex FxLMS for active noise cancellation over spatial regions, in *IEEE International Conference on Acoustics, Speech and Signal Processing (ICASSP)*, Shanghai, China, March 2016, pp. 524-528

- H. Chen, J. Zhang, P. N. Samarasinghe, and T. D. Abhayapala, Evaluation of spatial active noise cancellation performance using spherical harmonic analysis, in *Proc. IEEE International Workshop on Acoustic Signal Enhancement 2016*, Xi′an, China, September 2016, pp. 15.

The following papers are also results from my Ph.D. study, but not included in this thesis:

Journal Publications

- Y. Xu, J. Zhang, Real-time detection algorithm for small space targets based on max-median filter, *Journal of Information and Computational Science*, vol. 11, no. 4, pp. 1047-1055, 2014

- Y. Xu, J. Zhang, Y. Wei, Recent patents on real-time deep space target track system based on dual-DSP, *Recent Patents on Computer Science*, vol. 6, no. 3, pp. 227-232, Dec. 2013

Conference Proceedings

- Y. Xu, J. Zhang, X. Liu, The research on the design and application of a new configurable test instrument, *2014 IEEE AUTOTESTCON*, St. Louis, MO, USA, Sep. 2014, pp. 342-345

- Y. Xu, J. Zhang, X. Liu, The research on a new implementation scheme of the portable general purpose automatic test system, *2014 IEEE AUTOTESTCON*, St. Louis, MO, USA, Sep. 2014, pp. 173-176

The research work presented in this thesis has been performed jointly with Prof. Thushara D. Abhayapala, Dr. Wen Zhang, Dr. Prasanga N. Samarasinghe, and Prof. Shouda Jiang. Approximately 75% of this work is my own.

Jihui Zhang
Research School of Engineering
The Australian National University
Canberra ACT 2601
May 2019

Acknowledgments

Without the support of the many faces in my life, this work would not have been completed. I would like to acknowledge and thank each of the following.

- First and foremost, my supervisors, Prof. Thushara Abhayapala, Prof. Wen Zhang, and Dr. Prasanga Samarasinghe, for their valuable guidance and true friendship along my research.

  Special thanks goes to Thushara, for his unconditional support and care throughout all the difficulties.

  Thanks Wen, for her detailed guidance and support since the beginning of my ANC research, along all the variations of our lives.

  Thanks Prasanga, for providing many suggestions on the research and valuable feedback during the process of writing.

- Prof. Shouda Jiang and Dr. Yonghui Xu, my supervisors in the Harbin Institute of Technology, China, for supporting me to study in Australia.

- The Australian National University, for the PhD opportunity, Postgraduate Research Scholarship, HDR Fee Remission Merit Scholarship and many administrative supports.

- The China Scholarship Council, for the State Scholarship.

- My friends in the Audio & Acoustic Group, the Signal Processing Group, and the Communication Group, specially Farhana, Shama, Nicole, Hanchi, Jing, Fahim, Katrina and Yuting, for their true friendship.

- Mr. Yuki Mitsufuji, for giving me the internship opportunity at SONY Japan.

- My parents, for their constant encouragement and inspiration.
- Finally, my boyfriend Phil, for his love and company during my busiest days.

Abstract

This thesis investigates active noise control over a large spatial region using efficient control systems. Active noise control (ANC) utilises secondary sound sources to cancel primary noise based on the principle of destructive interference, and has the advantage of high flexibility and easy adaptability. ANC over a large spatial region (spatial ANC), which requires multiple sensors and multiple secondary sources in the system, creates a large-sized quiet zone for multiple listeners in three-dimensional spaces. The existing multichannel approaches are not very efficient in spatial ANC, as the noise cancellation is optimized only around the error sensors. This thesis provides new adaptive solutions for spatial ANC in general noise fields and optimal methods for spatial ANC in sparse noise fields.

In terms of adaptive solutions for spatial ANC in a general noise field, our approach is to utilize the wave-domain signal processing technique. Several outcomes resulting from this approach are (1) the design of the feedback wave-domain ANC system, and derivation of the filtered-x least mean square wave-domain approaches; (2) systematical formulation of the wave-domain ANC into different minimization problems and different updating variables, and derivation of four normalized wave-domain approaches. We show that, compared to the conventional multichannel approaches, the proposed wave-domain ANC approaches can achieve significant noise reduction over the entire spatial region with faster convergence speed.

In terms of the optimal methods for spatial ANC in a sparse noise field, our approach is to incorporate the ℓ_1-norm constraint from compressive sensing into the spatial ANC. Several outcomes resulting from this approach are (1) derivation of the ℓ_1-constrained multichannel approaches; (2) derivation of the ℓ_1-constrained wave-domain approach. We show that, compared to the conventional multichannel approaches, the proposed ℓ_1-norm constrained approaches can reduce the number of active secondary sources with faster convergence speed.

In addition, this thesis investigates the best possible spatial ANC performance

for a given system, by analyzing the signal space spanned by the secondary sources within a given acoustic environment. The proposed subspace method can obtain best possible ANC performance and is demonstrated to be a feasible solution, especially when the secondary sources are not sufficient to cover all orthogonal spatial modes according to the spherical harmonic theory.

List of Acronyms

ANC	Active noise control
SNR	Signal to noise ratio
ATF	Acoustic transfer function
PCA	Principal component analysis
3-D	Three-dimensional
2-D	Two-dimensional
LMS	Least-mean-square
FxLMS	Filtered-x least mean square algorithm
NLMS	Normalized least mean square algorithm
WFS	Wave field synthesis
WD	Wave domain
MP	Multi-point
NMP	Normalized multi-point algorithm
NWD-D	Normalized wave-domain algorithm updating driving signals
NWD-M	Normalized wave-domain algorithm updating mode coefficients
NEWD-D	Normalized energy-based wave-domain algorithm updating driving signals
NEWD-M	Normalized energy-based wave-domain algorithm updating the mode coefficients
APE	Acoustic potential energy
AED	Acoustic energy density
GED	Generalized acoustic energy density
Cℓ_1-MP	Complex ℓ_1 constrained multi-point algorithm
Sℓ_1-MP	Scalar ℓ_1 constrained multi-point algorithm
Leaky-MP	Leaky multi-point algorithm
NR	Noise reduction

WD-FxLMS	Wave-domain filtered-x least mean square algorithm
MP-FxLMS	Multi-point filtered-x least mean square algorithm
ℓ_1-WD-FxLMS	ℓ_1-norm constraint wave-domain FxLMS algorithm
ℓ_1-MP-FxLMS	ℓ_1-norm constraint multi-point FxLMS algorithm
WDLS	Wave-domain least square method

Notations and Symbols

$\lceil \cdot \rceil$	Ceiling operator
$[\cdot]^*$	Complex conjugate of a vector or matrix
$[\cdot]^T$	Transpose of a vector or matrix
$[\cdot]^H$	Complex conjugate transpose of a matrix
$\lvert \cdot \rvert$	Euclidean norm of a vector
$\lVert \cdot \rVert_1$	ℓ_1 Norm
$\lVert \cdot \rVert_2$	ℓ_2 Norm
$*$	Linear convolution
$\boldsymbol{A}^{-1}$	Matrix inverse
$\boldsymbol{A}^{\dagger}$	Matrix pseudoinverse
$\boldsymbol{x} \cdot \boldsymbol{y}$	Dot product between two vectors
$\mathrm{E}\{\cdot\}$	Expectation operator
$\Re\{\cdot\}$	Real part
$\Im\{\cdot\}$	Imaginary part
$\delta\{\cdot\}$	Dirac delta function
$\delta_{um}\{\cdot\}$	Kronecker delta function
$\exp\{\cdot\}$	Exponential function
$H_0^{(2)}(\cdot)$	Zero$^{\text{th}}$-order Hankel function of the second kind
$J_m(\cdot)$	Bessel function
$Y_{um}(\cdot)$	Spherical harmonics
$\nabla(\cdot)$	Gradient
$< \cdot >$	the dot product of two vectors
i	$\sqrt{-1}$

k	Wave number
c	Speed of sound propagation
ρ_0	Density of the media
M	Wave domain mode after truncation
n	Iteration number of the adaptation
u	Spherical harmonics order
m	Number of spherical harmonics basis of each order
x_{in}	Reference input of the FxLMS algoirthm
ω	Adaptive filter
r	Radius of arbitrary point with respect to origin
ϕ	Azimuthal angle
Δ_ϕ	Angles between two loudspeakers
p	Sound pressure on the arbitrary points
ψ	Polar angle (elevation angle)
x	Any arbitrary point inside the interest region
w	Angular frequency
y	Loudspeaker position
e	Residual noise field
α	Residual noise field coefficients in wave domain
P	Average energy of the residual signal over the entire region
v	Primary noise field
β	Primary noise field coefficients in wave domain
s	Secondary noise field
γ	Secondary noise field coefficients in wave domain
d	Loudspeaker weights
G	Acoustic transfer function
T	Acoustic transfer function coefficients in wave domain
ξ	Cost function
ω	Update variable
μ	Step size
μ_0	Normalized step size

ρ	Leakage factor
δ	Sparsity level (for ℓ_0 constraint)
λ	Sparsity parameter (for ℓ_1 constraint)
θ	Phases of complex driving signals
L	Loudspeaker number
Q	Microphone number
Z	Number of evaluation point inside the interest region
R_1	Radius of the interest region
R_2	Radius of the loudspeaker array
R_z	Radius of the microphone array
χ	Continuance loudspeaker distribution
τ	Continuance loudspeaker distribution in wave domain
σ	ATF for continuance loudspeaker array
$\boldsymbol{U}$	Acoustic potential energy weights
κ	Loudspeaker coefficients in the subspace
ϵ	Loudspeaker vector composed by eigenvalues and eigenfunctions
O	Basis of the subspace
N_r^{in}	Noise reduction inside the region of interest
N_r^b	Noise reduction on the boundary of the region

Contents

List of Figures

List of Tables

Chapter 1

Introduction

1.1 Motivation and Scope

Acoustic noise is a common disturbance throughout our daily life. For example, when reading this thesis, you may hear a wide range of noises which distract your attention, such as noise from a construction site across the road, or a door slammed by a colleague as they leave. As the amount of industrial equipment increases, such as engines, blowers, fans, transformers, noise problems become more and more evident [3]. Excessive amounts of acoustic noise above a certain level are the main cause of hearing loss, which drastically reduces the quality of life [4]. This thesis is focused on finding ways of reducing acoustic noises to improve our lives.

Noise control, or noise cancellation, is designed to control the noise we hear, to minimize the 'residual noise' after the cancellation process. There are two methods of controlling noise, passive noise control and active noise control (ANC), as shown in Figure 1.1.

One noise control method is passive noise control, in which noise-isolating materials and acoustic structures are applied to attenuate noise [5]. Example of noise-isolating materials includes insulation, sound-absorbing tiles, and mufflers. Passive noise control capability is achieved through a range of different variables including frequency of sound, material type, material thickness, and geometry of the material. When the wavelength of the sound is thicker than the material, it is difficult for the material to absorb the sound [6]. Passive noise control is more effective at mid

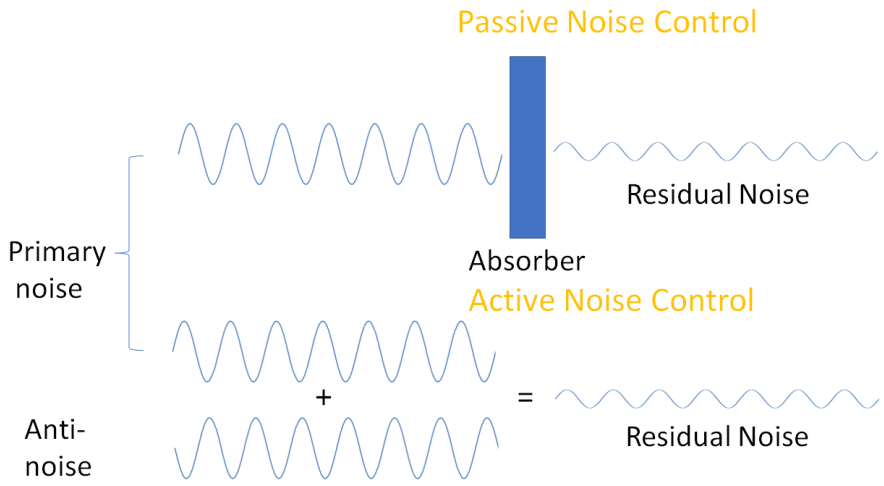

Figure 1.1: Passive noise control and active noise control [1].

and high frequency ranges, but it is less effective in the low frequency range[1] [8].

The second method used to control noise is active noise control (ANC). In ANC systems, the noise to be cancelled is called 'primary noise'. The system uses 'secondary sound sources' to generate 'anti-noise signals' to reduce the primary noise. This is achieved through the principle of destructive interference [9, 10, 11]. ANC has the advantages of high flexibility and easy adaptability and over the last 30 years has become a well-researched topic. ANC has many applications, such as noise cancelling headphones [12, 13], noise control in industrial machines [14] and in-car noise cancellation [15,16,17,18,19]. Unlike the passive noise control strategy, ANC works better in the low frequencies [20]. Low frequency noise is dominant in many real-world scenarios, e.g., air-conditioning noise, vehicle engine noise [21, 19] and wind noise [18]. In this thesis, we apply the ANC technique to cancel low frequency noise over a spatial region.

As typical noise sources and acoustic environments are always time-varying and unknown, adaptive systems are commonly applied to iteratively calculate secondary source driving signals[2]. Adaptive systems are in either feed-forward or feedback control configurations, depending on with or without reference sensors.

[1]Low frequency range is typically between 20 Hz to 500 Hz [7].
[2]Here, driving signal represents the signal of the driver of the secondary source.

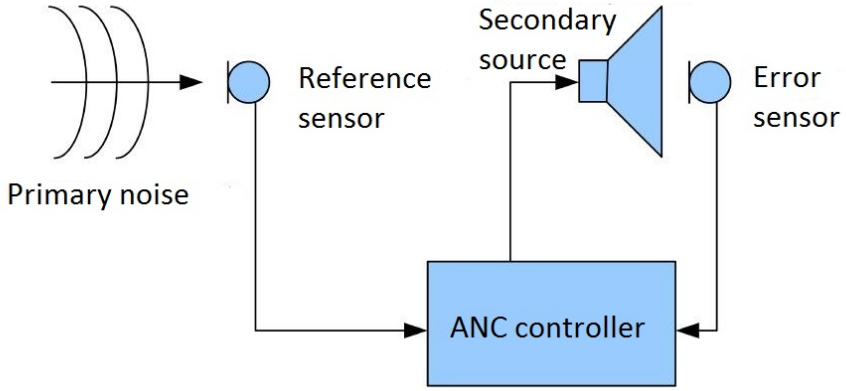

Figure 1.2: Basic ANC system structure.

Feed-forward configuration uses a reference sensor and an error sensor, as shown in Figure 1.2 [22], while the feedback configuration only uses an error sensor. Hybrid systems, a combination of feed-forward and feedback control structures, are also used in ANC applications. In the ANC controller, some well-known algorithms for implementation include the least-mean-square (LMS) method or its variants, such as filtered-x LMS (FxLMS), adjoint LMS and recursive LMS [23]. The details of feed-forward/feedback ANC structures and algorithms are given in Chapter 2, Section 1.

There is a growing research interest in creating a large quiet zone for multiple listeners in three-dimensional (3-D) spaces, such as noise cancellation in aircrafts [24] and automobiles [17, 25, 18, 26]. In these applications, the control zones of interest are large, and there are requirements for noise cancellation over the entire region, instead of at spatial points. When people sit around a particular region, such as around a desk in Figure 1.3, or when there are several people all requiring a noise-free acoustic environment, noise cancellation is required to cover the relevant spatial region. Meanwhile, ANC throughout a spatial region enables listeners to move freely within the region. Therefore, in this thesis, we investigate ANC over a spatially extended region, which is termed as *'Spatial ANC'*.

In spatial ANC applications, multichannel ANC systems equipped with multiple sensors and multiple secondary sources are adopted [27]. In these systems, multiple

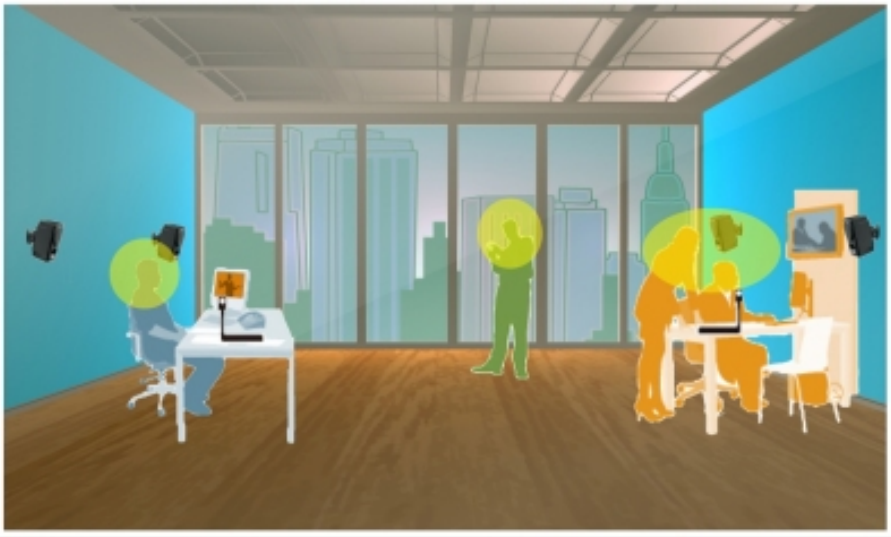

Figure 1.3: An example of shared office space with personal sound zones for each individual [2].

sensors are placed to measure the residual signals and multiple secondary sources are utilized to generate the anti-noise signals. In the feed-forward control system, additional reference sensors are placed to measure the primary noise. Both time-domain [28, 29] and frequency-domain [30, 31] algorithms have been implemented in multichannel ANC systems. For example, the frequency domain multichannel ANC [32] and its variations (such as Leaky ANC [33]) are now widely developed for noise cancellation at error sensor positions and their close surroundings [31]. The details of multichannel ANC algorithms and applications are reviewed in Chapter 2, Section 2.

The multichannel method is not very efficient in spatial noise control over a region, as the noise cancellation is optimized only on the error sensors. One method for solving this problem is to increase the number of sensors so as to cover more space, which dramatically increases the cost of the ANC system. More efficient spatial sound field control and sound reproduction techniques can be applied to address spatial ANC problems including wave field synthesis (WFS) and spherical/cylindrical harmonic based wave domain processing.

Wave field synthesis, introduced by Berkhout [34, 35], is one of the spatial sound field control and sound reproduction techniques, which can be applied to

spatial ANC. WFS uses a holographic technique to reproduce a desired sound field over a large area with a relatively large number of loudspeakers [36]. The WFS approach is based on the Kirchhoff-Helmholtz integral [37, 38, 39]. In theory, WFS uses continuous distribution of appropriately driven secondary sources arranged on the boundary of the desired listening area to reproduce a virtual sound field [37]. This technique has already been applied in ANC applications [40, 41]. However, WFS-based spatial sound control has the disadvantage of requiring many secondary sources to approximate the continuous distribution on the boundary of the desired listening area, which is not always practical to implement for noise cancellation over the region of interest.

Spherical/cylindrical Harmonic based wave domain processing [42] is another spatial sound field control and sound reproduction technique, which can be applied to spatial ANC. This method transfers the measurements into a spherical/cylindrical harmonic domain [43, 44, 45], and controls the entire spatial region by manipulating the spherical/cylindrical harmonic coefficients. This technique does not require secondary sources to be placed on the boundary of the region, and can therefore be more feasible. The details of wave domain sound field representation are reviewed in Chapter 2, Section 3. Up untill the beginning of this research, Spherical/cylindrical Harmonic based wave domain processing had not been applied to spatial ANC.

From the foregoing discussion, the key question which drives this thesis is as follows:

How can we achieve ANC over a large spatial region using efficient control systems?

1.2 Problem Description

We elaborate this problem into two further questions:

(i) How to achieve ANC over a large continuous region in a general noise field[3] *?*

[3]Here, general noise field includes free field and reverberant field, diffuse noise field and directional sparse noise field.

(ii) How to exploit the sparse characteristics in a specific noise field, and based on which to optimize the spatial ANC system?

For Question (i), we develop an ANC system to cancel the noise over a designated region of space. To achieve ANC in a large continuous region, the control objective should be the sound field over the entire region rather than multiple observation points within the region. The generic solution can be applied to a general noise field, regardless of the acoustic environment and the features of the primary sources. In the ANC system over a region, secondary source placement and adaptive algorithms are two critical factors to be investigated. Noise cancellation performance for a given secondary source arrangement is also important to ANC system design in real implementations.

For Question (ii), we optimize the spatial ANC system in directional sparse noise fields. In noise fields which have directional sparse features, noise sources are sparsely distributed in space, and are located in one or a few directions with respect to the origin of the region. As in general noise field, spatial ANC systems require large numbers of secondary sources and high computational complexity, the problem in the directional sparse noise field becomes:

How to reduce the number of secondary sources in the array, and how to reduce the computational complexity of the algorithms?

1.3 Thesis Outline

Motivated by the above problems, in this thesis, we develop adaptive solutions for spatial ANC within a continuous region. As shown in Figure 1.4, we investigate the spatial ANC in general noise field, as well as in sparse noise field.

For noise cancellation in a general noise field, we (1) formulate the problem in the wave domain based on cylindrical harmonics or spherical harmonics) to achieve ANC over large continuous regions, and propose the wave-domain ANC algorithms; (2) investigate wave-domain ANC in different cost functions and adaptations; and (3) derive a subspace to represent the secondary sources and the acoustic environment, and evaluate the ANC performance in this subspace.

For noise cancellation in a sparse noise field, we exploit sparse features, and introduce constraints from compressive sensing into the conventional multichan-

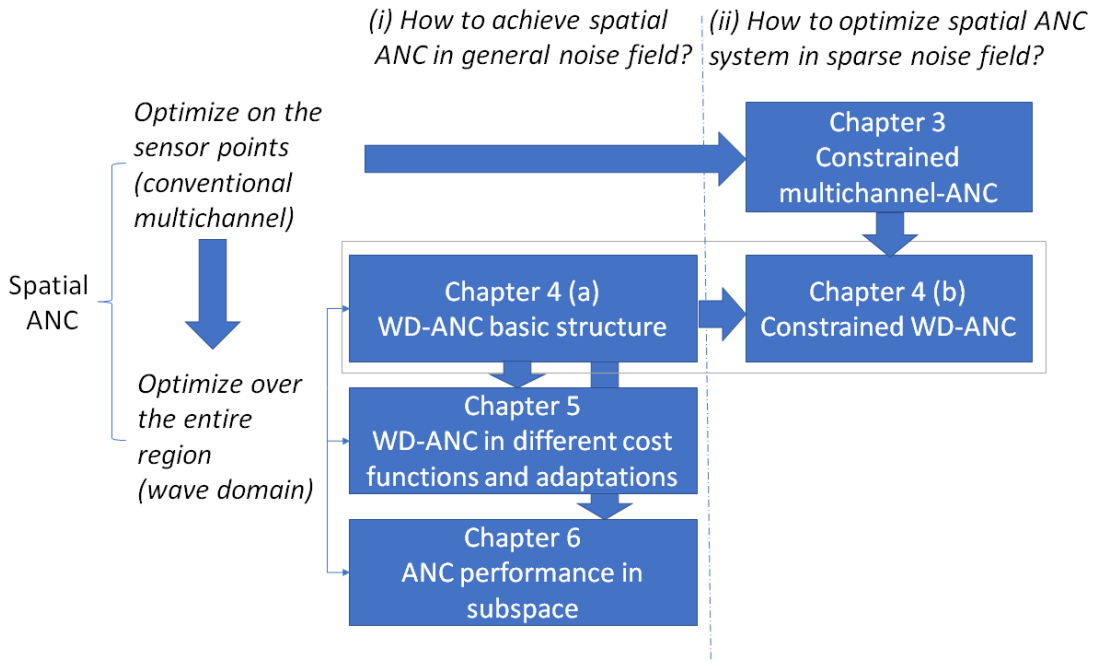

Figure 1.4: Breakdown of the spatial ANC problem into each chapter. WD-ANC denotes the wave-domain ANC.

nel ANC structure and the proposed wave-domain ANC structure to reduce the number of secondary sources in the array and the computational complexity in the algorithms.

The performance of the proposed systems and techniques are verified through numerical simulations.

The structure of the thesis is as follows:

Chapter 2: Literature Review and Background Theory

In Chapter 2, we review the literature on ANC methods and the wave domain noise field control technique. We first review the single-channel ANC method. In terms of the control structure, we review the feed-forward and feed-back configurations. In terms of the adaptive control, we review LMS, FxLMS, and normalized LMS (NLMS) algorithms. Thereafter, we review the multichannel ANC algorithm and different applications. We review the classical multichannel algorithm, and then discuss the variations in global ANC applications and regional ANC applications. The classical multi-point algorithm which is commonly used for solution of ANC in a large area, is one of the typical algorithms against which we compare

new algorithms. We also study typical sound fields and the wave domain sound field representation. The theory and methods reviewed in this chapter form the fundamentals of my thesis.

Chapter 3: Multiple-point ANC for Directional Sparse Fields

In Chapter 3, we address question (ii) and investigate the noise control over a region using a multichannel ANC framework in a directional sparse noise field. We first review the conventional multi-point algorithm and Leaky multi-point algorithm using the feedback control structure. Thereafter, we introduce the ℓ_1-norm penalty to the multi-point algorithm, resulting in the complex ℓ_1-norm constrained multi-point ($C\ell_1$-MP) algorithm and the scalar ℓ_1-norm constrained multi-point ($S\ell_1$-MP) algorithm. In this chapter, driving signals of the secondary sources are designed by minimizing the addition of a squared residual noise field and ℓ_1 norm of the driving signal magnitude. We conduct simulations for spatial ANC applications while the noise sources are coming from a few directions. The simulation results indicate that when the noise field has directional sparsity, the proposed $C\ell_1$-MP algorithm and proposed $S\ell_1$-MP algorithm can reduce the number of active secondary sources, with reasonable noise reduction performance.

Chapter 4: Wave Domain ANC: Basic Structure

The conventional multi-point algorithm and variations are not efficient in ANC over a large continuous region. In Chapter 4, we apply a wave-domain signal processing technique to spatial ANC applications. To addresses question (i), after representing all the variables in the control system into wave-domain coefficients, we propose a wave-domain FxLMS algorithm. Using this algorithm, we control the noise field over the entire region directly. This results in significant noise reduction with fast convergence speed. This advantage is evaluated in both free field and reverberant environments. To address question (ii), we also propose the ℓ_1-constrained wave-domain FxLMS algorithm, by introducing the ℓ_1-norm penalty into the wave-domain ANC. This can be applied to spatial ANC in directional sparse noise fields.

Chapter 5: Wave Domain ANC: Different Cost Functions and Adaptations

In this chapter, we further address question (i) and investigate the wave-domain spatial ANC. We represent the acoustic potential energy of the residual sound field

in terms of the wave domain residual signal coefficients. We implement normalized LMS adaptive algorithms in the wave domain by solving two minimization algorithms: (i) minimizing the squared wave-domain residual signal coefficients, and (ii) minimizing the acoustic potential energy. For each minimization problem, we derive the update equations with respect to two variables: (i) updating the driving signals, and (ii) updating the wave-domain coefficients. This results in four different wave domain algorithms (i) normalized wave domain algorithm updating driving signals (NWD-D), (ii) normalized wave domain algorithm updating mode coefficients (NWD-M), (iii) normalized energy-based wave domain algorithm updating driving signals (NEWD-D), and (iv) normalized energy-based wave domain algorithm updating mode coefficients (NEWD-M). We compare the four proposed algorithms as well as the conventional multi-point algorithms in the simulation section. We evaluate these five algorithms using three criteria: acoustic potential energy reduction, convergence speed, and energy of the secondary-source driving signals. These numerical simulations are conducted in the free field, as well as in the reverberant environment.

Chapter 6: ANC Subspace Performance Analysis

In Chapter 6, we investigate the noise control performance in any 3-D reverberant environment. We discuss a wave-domain least square method, which matches the primary noise field coefficients to the secondary noise field coefficients in the wave domain. Based on the wave-domain coefficients of the acoustic transfer function between loudspeakers and the control region, we derive the subspace representing the secondary sources and the acoustic environment. We then propose a subspace method by matching the projection of the primary noise field coefficients to the secondary noise field coefficients in the subspace. We conduct the simulations to compare the proposed subspace method with the wave-domain least square method. We compare the ANC performance under different noise source positions and different loudspeaker configurations.

Chapter 7: Conclusion and Future Research Directions

Chapter 7 provides concluding remarks and possible directions for future work.

Chapter 2

Literature Review and Background Theory

***Overview:** This chapter provides a brief overview of the background knowledge concerning spatial ANC over a region. We first review conventional single-channel active noise control structures, and then focus on the use of multichannel active noise control techniques for 3-D noise field control. Furthermore, we discuss the sound field and acoustic environment considered in this thesis. To further develop the spatial ANC strategies in the later chapters, we review the basic formulation of harmonics-based sound field representation. The theory and methods reviewed in this chapter form the foundation for the rest of the thesis.*

2.1 Single-channel ANC Techniques

In ANC systems, noise sources are unknown and acoustic environments are time-varying. Therefore, adaptive filters are employed to produce anti-noise signals. The control structure of ANC can be broadly classified into two classes: feed-forward control and feedback control. We review the basis of both theories and structures in the next two subsections. The basic formulations we mentioned here can be extended to multichannel cases as well.

2.1.1 Feed-forward control system

The feed-forward ANC scheme requires a reference signal as an input to the adaptive filter. This scheme is widely used for industrial applications such as reducing duct noises [46].

The objective of feed-forward ANC is to design the driving signal of the secondary source, using sound measurements captured by a reference sensor and an error sensor. The fundamental block diagram of a feed-forward ANC system is shown in Figure 2.1. Here, the ANC system consists of an error sensor, a reference

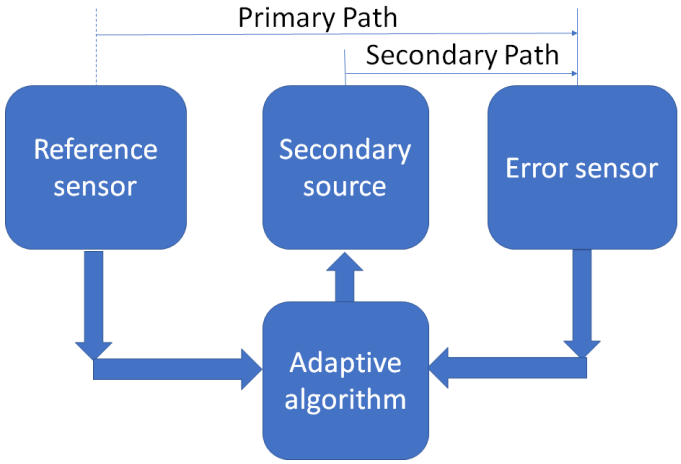

Figure 2.1: Fundamental components in a feed-forward ANC system.

sensor, a secondary source, and an adaptive algorithm. Here, we assume that there is no acoustic feedback from the secondary source to the reference sensor [1].

Some well-known adaptive algorithms used to implement feed-forward ANC include the least-mean-square (LMS) method or its variants, such as FxLMS [47], NLMS [48], adjoint LMS [49] and recursive LMS [33]. LMS algorithms are a class of adaptive algorithms, which minimize the least mean squares of the error signal. In the following subsections, we review the LMS algorithm, FxLMS algorithm and NLMS algorithm. Here, we introduce the secondary-path transfer function $\boldsymbol{G}(n)$ into each algorithm.

[1] There are several solutions to eliminate the acoustic feedback. One solution is to use a separate 'feedback path neutralization filter' [9].

LMS algorithm

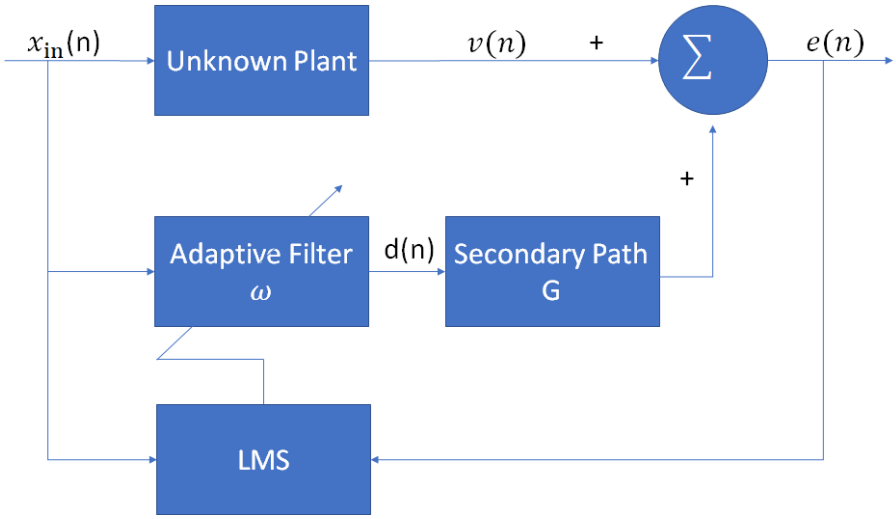

Figure 2.2: Block diagram of feedforward ANC using LMS algorithm, where $x_{\text{in}}(n)$ is the input reference signal, $v(n)$ is the primary signal on the error microphone position, $e(n)$ is the error signal, and $d(n)$ is the driving signal.

The block diagram of a single-channel feed-forward ANC system using LMS algorithm is shown in Figure 2.2. In this system, the controller is the adaptive filter using the LMS algorithm. The adaptive filter ω continuously tracks variations in the primary noise field.

In the LMS algorithm, the error signal $e(\cdot)$ for each iteration can be written by

$$e(n) = v(n) + G(n) * d(n), \tag{2.1}$$

where n is the iteration number, $G(\cdot)$ is the impulse response of secondary path from the secondary source to the error sensor, $v(\cdot)$ is the primary noise field at the error sensor, and

$$d(n) = \boldsymbol{x}_{\text{in}}(n) * \boldsymbol{\omega}(n), \tag{2.2}$$

is the driving signal of the secondary source.

Here, $*$ denotes linear convolution, $\boldsymbol{\omega}(n) = [\omega_0(n), \omega_1(n), ..., \omega_{L_\omega - 1}(n)]^T$ are the filter coefficients with the filter order of L_ω, $\boldsymbol{x}_{\text{in}}(n) = [x(n), x(n-1), ..., x(n-L_\omega +$

$1)]^T$ are the input reference signal.

Minimizing the mean square of the error signal, the cost function becomes

$$\xi(n) = e^2(n). \tag{2.3}$$

Since the LMS algorithm is based on the steepest descent method, the update equation is as follows,

$$\boldsymbol{\omega}(n+1) = \boldsymbol{\omega}(n) - \frac{\mu}{2}\nabla\xi(n), \tag{2.4}$$

where μ is the adaptation step size, and ∇ is the gradient operator.
From (2.1) and (2.3), the gradient of the cost function with respect to the filter coefficients $\boldsymbol{\omega}$ is written as

$$\begin{aligned}\nabla\xi(n) &= \nabla(e^2(n)) \\ &= 2e(n)\nabla e(n) \\ &= 2e(n)\boldsymbol{x}'_{\text{in}}(n),\end{aligned} \tag{2.5}$$

where

$$\boldsymbol{x}'_{\text{in}}(n) = G(n) * \boldsymbol{x}_{\text{in}}(n). \tag{2.6}$$

Substituting (2.5) into (2.4), the final update equation of the LMS algorithm is written as

$$\boldsymbol{\omega}(n+1) = \boldsymbol{\omega}(n) - \mu\boldsymbol{x}'_{\text{in}}(n)e(n). \tag{2.7}$$

In (2.7), the filter coefficients $\boldsymbol{\omega}$ in the next iteration are based on the error signal and the filtered reference signal on the current iteration, by finding the gradient of the mean square error.

The step size μ in (2.7) controls the convergence speed of the adaptive process, which should be chosen properly based on the individual scenario. The upper bound of the step size μ is given as follows [50],

$$\mu < \frac{2}{\lambda_{\text{in}}^{\max}}, \tag{2.8}$$

where $\lambda_{\text{in}}^{\max}$ is the largest eigenvalue of the autocorrelation matrix of the input

reference signal $E\{\boldsymbol{x}_{\text{in}}(n)\boldsymbol{x}_{\text{in}}^{H}(n)\}$.

FxLMS algorithm

The performance of an ANC system depends largely on the secondary-path transfer function G [3]. In the LMS algorithm, however, due to the secondary-path transfer function, the error signal and the reference signal are not aligned in time. This effect will generally cause instability [51].

One effective solution to compensate for the effect of the secondary-path is to add an identical filter on the reference signal path, which is called the FxLMS algorithm. The block diagram is illustrated in Figure 2.3. Compared with Figure 2.2, the reference signal is filtered by the estimation of the secondary path $\widehat{G}$, before being used in the LMS filter. This is the main difference between the LMS algorithm and the FxLMS algorithm.

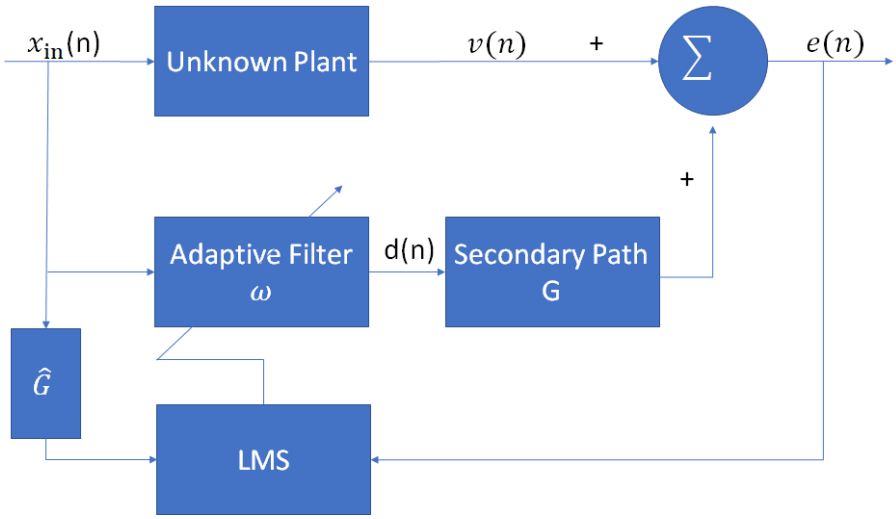

Figure 2.3: Block diagram of FxLMS feed-forward ANC.

Therefore, the update equation of FxLMS algorithm can be written as:

$$\boldsymbol{\omega}(n+1) = \boldsymbol{\omega}(n) - \mu \boldsymbol{x}'_{\text{in}}(n)e(n), \tag{2.9}$$

where $\boldsymbol{x}_{\text{in}}^{'}(n)$ is the filtered reference signal, and

$$\boldsymbol{x}_{\text{in}}^{'}(n) = \boldsymbol{x}_{\text{in}}(n) * \widehat{G}(n). \tag{2.10}$$

FxLMS is very tolerant of error between the secondary path G and the estimation filter $\widehat{G}$, which can be estimated using the off-line model during initial training in most ANC applications [3]. Adaptive online secondary path modelling has also been applied [52, 53]. Variations of the FxLMS algorithm exist, such as the Leaky FxLMS [54,55] and the filtered-x normalized LMS algorithm [32], which are proposed to improve the performance of the FxLMS.

NLMS algorithm

The normalized LMS algorithm also minimizes the mean square error, with the same cost function as LMS algorithm. The normalization term is according to the energy of the reference input signal $\boldsymbol{x}_{\text{in}}(n)$. The step size in LMS algorithm has been modified to a data-dependent step size $\frac{\mu}{a+\|\boldsymbol{x}_{\text{in}}(n)\|_2^2}$.

Therefore, the update equation of the NLMS algorithm is given by:

$$\boldsymbol{\omega}(n+1) = \boldsymbol{\omega}(n) - \frac{\mu}{a + \|\boldsymbol{x}_{\text{in}}(n)\|_2^2}\boldsymbol{x}_{\text{in}}^{'}(n)e(n), \tag{2.11}$$

where $\|\cdot\|_2$ denotes the ℓ_2 norm, and $a > 0$ is a constant to overcome the possible numerical difficulties when $\|\boldsymbol{x}_{\text{in}}(n)\|_2^2$ is very close to zero.

The algorithm is stable for $0 < \mu < 2$. Like the LMS algorithm, the next iteration of the NLMS algorithm is based on the error signal and the filtered reference signal on the current iteration. Compared to the LMS algorithm, the NLMS algorithm has superior robustness [56].

2.1.2 Feedback control system

In the feed-forward control system described in Section 2.1.1, we assume that there is no acoustic feedback from the secondary source to the reference sensor. Unfortunately, in some applications, the upstream sound field from the secondary source (loudspeaker) to the reference microphone can corrupt the reference signal. One

solution is to model the acoustic feedback transfer function and incorporate it into the system with a separate feedback cancellation filter [23]. Another solution is to utilize the feedback structure, which is reviewed as follows.

In the feedback ANC system, only an error sensor (error microphone) and a secondary source (loudspeaker) are utilised [57], as shown in Figure 2.4. The active noise controller attempts to cancel the noise without the benefit of reference input. There have been growing interests in implementing the feedback system as it avoids the need for separate reference sensors to measure the primary noise [58]. This reduces the number of system components and associated hardware. In particular, it is more cost-effective and more suitable for use in large 3-D acoustic environments with multiple noise sources [59]. However, in most cases, feedback control system is only effective for dealing with narrowband noise.

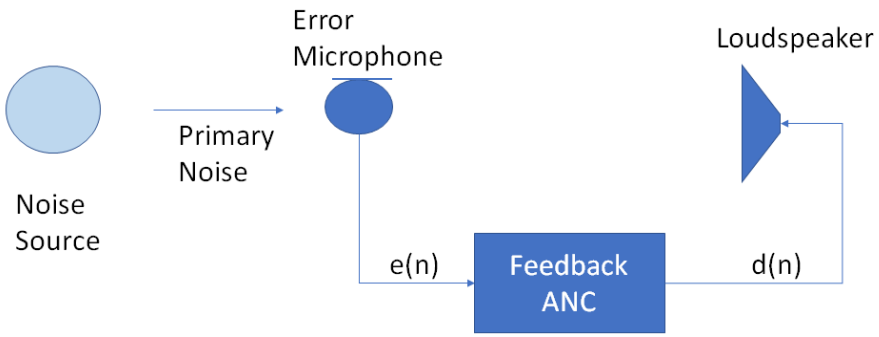

Figure 2.4: Single-channel feedback ANC system.

2.2 Multichannel ANC Techniques

As discussed in Section 2.1, the single-channel configuration, with one error sensor and one secondary source, is well suited for both narrowband and broadband cancellation in narrow ducts or small areas. When the noise field is monitored at a specific spatial point by an error sensor, noise cancellation can be achieved around the error sensor with the spatial limit being approximately $\lambda_{\max}/10$ [31], where $\lambda_{\max}$ is the wavelength of the highest undesired frequency. However, the single-channel system is clearly insufficient for more complex enclosures or large dimension environments. To achieve noise cancellation for an increased area, we can extend the

single-channel ANC systems to multichannel ANC systems by employing multiple error sensors and multiple secondary sources [33].

In the following subsections, we first review the basic multichannel ANC theory and variations, and then discuss the investigations in global and regional ANC applications.

2.2.1 Multichannel algorithm and variation

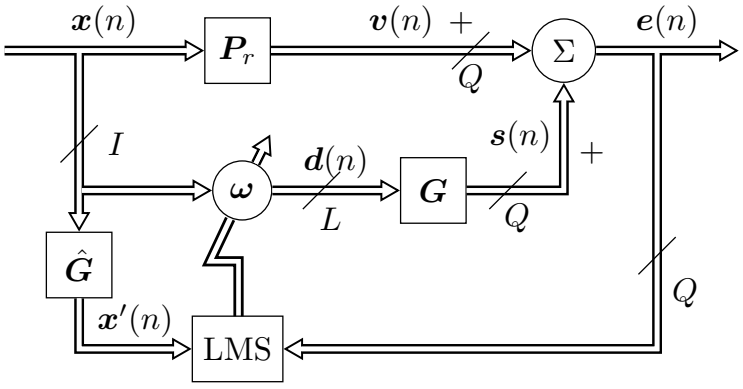

Figure 2.5: Block diagram of multichannel feedforward ANC system, where $\boldsymbol{P}_r$ is the primary path from reference sensors to error sensors, $\boldsymbol{G}$ and $\widehat{\boldsymbol{G}}$ represent the secondary path and the estimation of secondary path, respectively.

A block diagram of the commonly used FxLMS multichannel algorithm is shown in Figure 2.5. In the figure, $\boldsymbol{P}_r$ is the primary path, which is the acoustic path from reference sensors to error sensors. $\boldsymbol{G}$ and $\widehat{\boldsymbol{G}}$ represent the secondary path from adaptive filters to error microphones and its estimation, i.e., the secondary path model, respectively.

The reference input signals are $x_i(n), i = 1, \ldots, I$, and the instantaneous error microphone measurements are $e_q(n), q = 1, \ldots, Q$. Here, I is the number of reference input signals, Q is the number of error microphones.

The error signals at the error microphones can be written as

$$e_q(n) = v_q(n) + s_q(n), \tag{2.12}$$

where $s_q(n)$ is the secondary noise field on the q^{th} microphone, and $v_q(n)$ is the

primary noise field on the q^{th} microphone.

$$s_q(n) = \sum_{l=1}^{L} d_l(n) * G_{lq}(n), \tag{2.13}$$

where $G_{lq}(n)$ denotes the impulse response from the l^{th} secondary source to the q^{th} error microphone, $d_l(n)$ are the loudspeaker driving signals.

The l^{th} secondary speaker driving signal is generated as

$$d_l(n) = \sum_{i=1}^{I} \boldsymbol{w}_{il}^T(n)\boldsymbol{x}_i(n), \text{for } l = 1, 2, \ldots, L, \tag{2.14}$$

where $\boldsymbol{\omega}_{il}(n) = [\omega_{il,0}(n), \omega_{il,1}(n), \ldots, \omega_{il,L_w-1}(n)]^T$ are the adaptive filter coefficients of the l_{th} loudspeaker in the nth iteration, $\boldsymbol{x}_{il}(n) = [x_i(n), x_i(n-1), \ldots, x_i(n - L_w + 1)]^T$, and L_w is the length of the FIR adaptive filters.

The multichannel feedforward ANC minimizes the sum of mean squared error signal, as follows:

$$\xi(n) = \sum_{q=1}^{Q} |e_q(n)|^2. \tag{2.15}$$

Therefore, the update equation of the multichannel feed-forward algorithm for $\boldsymbol{\omega}_{il}(n)$ is given by

$$\boldsymbol{\omega}_{il}(n+1) = \boldsymbol{\omega}_{il}(n) - \mu \sum_{q=1}^{Q} \boldsymbol{x}'_{ilq}(n)e_q(n), \tag{2.16}$$

where μ is the step size, $\boldsymbol{x}'_{ilq}(n) = [x'_{ilq}(n), \ldots, x'_{ilq}(n - L_w + 1)]^T$ is a vector of filtered reference signals, and

$$x'_{ilq}(n) = x_i(n) * \widehat{G}_{lq}(n). \tag{2.17}$$

The positions and numbers of microphones and loudspeakers play important roles in the multichannel ANC performance. The locations of the error microphones are very important for estimating the residual noise field, as it has a significant effect on the ANC performance.

There are several multichannel variations, which can improve the ANC performance. Thomas et al. proposed an eigenvalue equalization filtered-x LMS algorithm, which can increase the convergence speed of the FxLMS multichannel algorithm [60]. M. Bouchard proposed multichannel affine and fast affine projection algorithms, which can provide better convergence performance when non ideal noisy acoustic plant models are used in the adaptive systems [61].

Compared to single-channel ANC, multichannel ANC can increase the control region, which is applicable to spatial ANC. Meanwhile, compared to the single-channel ANC, the computational complexity of the multichannel ANC system is significantly increased. This is one of the main challenges for implementing multichannel ANC systems in real applications.

Next, we review some spatial ANC applications using multichannel algorithms. In particular, we examines ANC in an enclosure, such as in a car cabin or inside an aeroplane. Depending on whether the objective is the entire enclosure or only a partial region, a multichannel algorithm has been applied in global ANC and regional ANC.

2.2.2 Global ANC using multichannel algorithms

Global ANC aims to minimize the sound pressure level over a continuous space throughout the enclosure. The effective cancellation frequency range is determined by the acoustic modes of relevant noise components and the number and placement of microphones and loudspeakers [62].

The performance of global ANC is dependent on a number of factors. The number and location of the error sensors [63] is one factor. For example, to cover more acoustic modes, error microphones can be located in opposite corners to ensure wider coverage. The number of secondary sources is also a factor. To control all the acoustic modes, the number of secondary sources must be approximately equal to the number of acoustic modes [64]. Adaptive algorithm is another factor. Traditional adaptive algorithms minimize the squared error signals, and some newly proposed methods minimize the acoustic potential energy (APE) or energy density of the noise field.

Minimization of the squared error signals

Theoretically, global ANC using the multichannel method can be achieved by minimizing the total APE within an enclosure. However, in the initial investigations, in practice, this must be approximated by minimizing the sum of the squared pressures measured at a sufficient number of error microphone locations [65].

Minimization of the APE or energy density

To enlarge the control region, some researchers have proposed ANC systems based on APE or energy density of the region.

Instead of minimizing the squared error signals, Romeu et al. modified the cost function to the APE [63]. This method ensures to reach the optimal attenuation that can be obtained by a set of secondary sources. Using APE as a cost function is also more robust than the squared error signal methods and its robustness does not depend on the location of the error sensors. Montazeri et al. described the APE in terms of room modes, which depends greatly on the room geometry [66].

By utilizing acoustic energy density sensors [67, 68], Parkins sensed and minimized the acoustic energy density (AED), which is the sum of the potential energy density and the kinetic energy density. The energy density measurement is more capable of observing the modes of a sound field. Using this method, Parkins used approximately one-fourth of the number of sensors compared to the squared error signal method.

Xu et al. proposed a similar ANC method by minimizing the generalized acoustic energy density (GED) [69, 70]. The GED method is defined by introducing weighting factors into the formulation of the total AED. The results demonstrated that GED-based ANC can further improve the results of AED-based ANC, when the frequency was below the Schroeder frequency of a room [2]. Compared to squared error signal methods, by varying the weighting value of GED, it is possible to increase the size of the control region as much as three times. As a trade off, the maximum noise reduction may decrease to around 1.25 dB.

From the literatures above, we can conclude that, minimizing the APE or energy

[2]Schroeder frequency refers to the frequency at which rooms go from being resonators to being reflectors/diffusors as the 'crossover frequency'.

density is more robust than minimizing the squared error signal, and the energy density sensor is more suitable to observe the modes of the sound field.

2.2.3 Regional ANC using multichannel algorithms

In industrial applications, the large volumes of rooms makes the implementation of global ANC difficult and costly [71]. Regional ANC, or locally global ANC, is often used in real applications. The objective of the regional ANC strategy is to achieve noise reduction in the region of interest. Using limited microphones and loudspeakers, regional ANC using the multichannel method can achieve noise cancellation in small regions around the error microphones [71]. Compared with global ANC, regional ANC can reduce the scale of the ANC system and the computational complexity.

There are several researchers investigated locally global ANC. Li and Hodgson [71] examined optimal microphones/loudspeaker placements to ensure that squared error signals were minimized and the potential energy in the region of interest was also significantly reduced. Cheer has published works related to regional ANC in the automobile [25], and in a yacht [64]. For instance, in automobile noise cancellation, the region of interest is the small areas around the passengers' heads.

In this thesis, we focus on regional ANC. This area of research has been selected as regional ANC which has advantages requiring lower system costs and computational complexity. To achieve spatial noise cancellation over the entire region of interest, we apply wave-domain sound field processing technique rather than the method in Section 2.2.1.

2.3 Wave-domain Sound Field Representation

Wave-domain signal processing[3] is a technique commonly used for spatial sound field recording/reproduction over spatial regions using discrete transducer arrays. The principle of harmonic representation of sound fields is to use fundamental solutions of the Helmholtz wave-equation as basis functions to express sound fields

[3]Note that in this thesis, we use the term 'wave-domain signal processing' to refer to harmonics (cylindrical/spherical) based sound field processing.

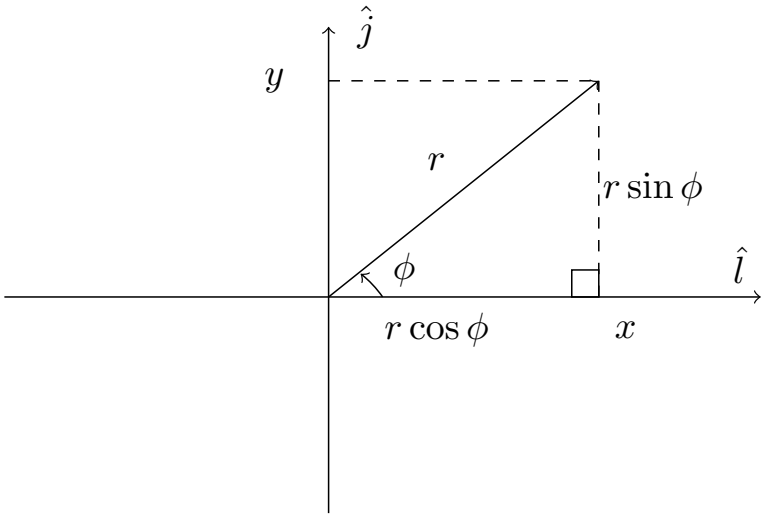

Figure 2.6: An arbitrary point in Cartesian coordinates and polar coordinates in 2-D space.

over a spatial region [72]. Thus, the sound field can be thought of as a superimposed set of orthogonal and continuous basis fields (cylindrical/spherical harmonics) with corresponding knobs to control relative weights (coefficients) of each basis wave field. Since wave-domain signal processing controls propagating sound fields as a whole rather than as a distributed set of target points, it naturally provides a more insightful and efficient method for sound control over space.

Recently, wave-domain technique has been applied to achieve sound control over large spatial regions, such as echo cancellation [73, 74, 75], room equalization for massive multichannel sound field reproduction systems [76, 77, 78], acoustic quiet zone generation [79, 80, 81, 82, 83, 84], and to design higher order loudspeakers [85, 86, 87].

We review the basic theory of sound field and wave-domain sound field representation technique in this section, and apply the wave-domain method for spatial ANC investigation in Chapters 4, 5 and 6.

2.3.1 Sound field and acoustic environment in a space

Coordinate systems

We start with defining the coordinate systems used in this thesis to represent a sound field. We utilize both 2-D and 3-D coordinate systems.

In 2-D space, the polar coordinate system is shown in Figure 2.6. The transformation formulas between Cartesian coordinates and polar coordinates are

$$\begin{aligned} x &= r\cos\phi \\ y &= r\sin\phi, \end{aligned} \tag{2.18}$$

where r is the radius of the arbitrary point with respect to the origin, and ϕ is the azimuthal angle. In the sound field, the sound pressure is relevant to time and space. Therefore, the pressure of an observation point $\boldsymbol{x}$ in space can be represented by $P = p(r, \phi, t)$.

In 3-D space, as shown in Figure 2.7, a position $\boldsymbol{x}$ can be represented as follows,

$$\boldsymbol{x} = \begin{pmatrix} x \\ y \\ z \end{pmatrix} = \begin{pmatrix} r\cos\phi \\ r\sin\phi \\ z \end{pmatrix} = \begin{pmatrix} r\sin\psi\cos\phi \\ r\sin\psi\sin\phi \\ r\cos\psi \end{pmatrix}, \tag{2.19}$$

where $(x, y, z)^T$ denotes the representation in Cartesian coordinates, $(r\cos\phi, r\sin\phi, z)^T$ denotes the representation in cylindrical coordinates, and $(r\sin\psi\cos\phi, r\sin\psi\sin\phi, r\cos\psi)^T$ is in spherical coordinates. Here, ψ is elevation angle, with the range of $[0, 180°]$. Using spherical coordinates, the pressure of a point in 3-D space can be represented by $P = p(r, \phi, \psi, t)$.

In the next subsection, we further discuss the representation of sound pressures p.

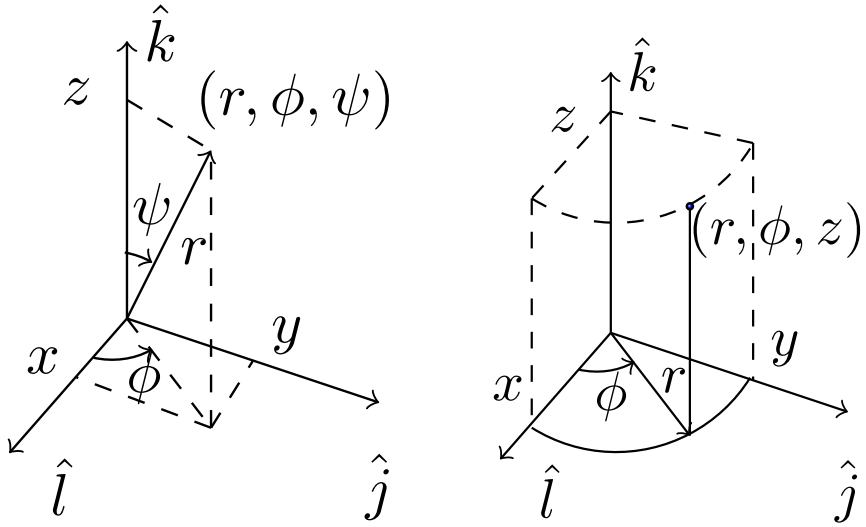

(a) (b)

Figure 2.7: Coordinate system in 3D space: (a) Cartesian coordinates and spherical coordinates; (b) Cylindrical coordinates.

Sound pressure

Considering the propagation of the sound wave, the wave equation at an arbitrary $\boldsymbol{x}$ and time t can be represented by

$$\nabla^2 p(\boldsymbol{x}, t) = \frac{1}{c^2} \frac{\partial^2 p(\boldsymbol{x}, t)}{\partial t^2}, \tag{2.20}$$

where c denotes the speed of sound propagation, and ∇^2 is the Laplacian operator, which is variant in different coordinate systems. For instance, in Cartesian coordinates, the Laplacian operator can be written by

$$\nabla^2 = \frac{\partial^2}{\partial x^2} + \frac{\partial^2}{\partial y^2} + \frac{\partial^2}{\partial z^2}. \tag{2.21}$$

Using the Fourier transform, time domain sound pressure $p(\boldsymbol{x}, t)$ can be transformed to the frequency domain $p(\boldsymbol{x}, w)$,

$$p(\boldsymbol{x}, w) = \int_{-\infty}^{\infty} p(\boldsymbol{x}, t) \exp(-iwt) dt, \tag{2.22}$$

where w is the angular frequency, $i = \sqrt{-1}$, and $\exp(\cdot)$ denotes the exponential function.

In this thesis, we focus more on the space-dependent part of the sound field $p(\boldsymbol{x}, w)$. Therefore, in the following chapters, the time dependence t in a sound pressure is omitted for notational simplicity.

In the next subsection, we discuss the noise field and acoustic environments considered in this thesis.

Noise field and acoustic environment

In terms of the relation between the source position and the region position, the sound field is divided into two cases: *interior sound field* and *exterior sound field*. The term *interior sound field* is used to describe the wave field within a spatial region caused by sources completely outside the outer boundary, as shown in Figure 2.8. The term *exterior sound field* is used to describe the situation where the sound sources are positioned within a limited area, and the region of interest is defined

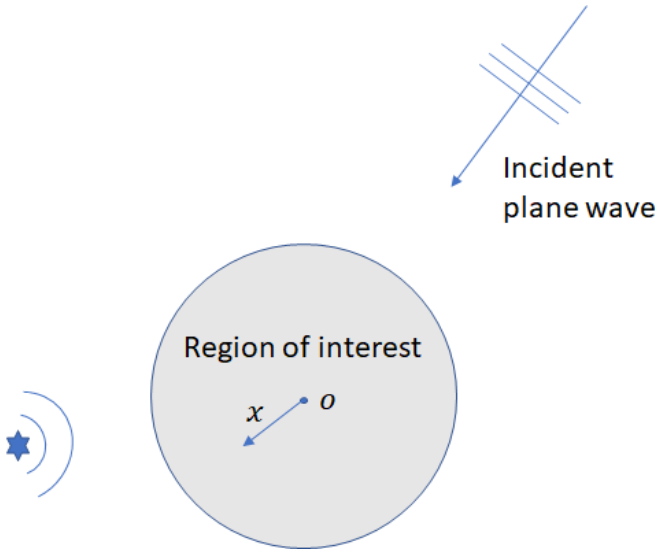

Figure 2.8: Interior sound field. The stars are positions of the noise sources.

as the space outside the source area. In this thesis, only the interior sound field is considered.

In terms of acoustic environment, in this thesis, we mainly utilize the free-field model and room reverberant model for spatial ANC investigation.

(i) *Free-field environment:*
Free-field is a noise field where sound waves propagate in an open space. The free-field can be an open space without boundaries, or an anechoic chamber which can absorb sound energy in all directions. The free-field model is a simple model, which is applied for investigations and evaluations of new acoustic methods.

(ii) *Room-reverberant environment:*
In a typical environment, the received sound is never an exact copy of the original sound. The received sound is comprised of sound scattered/reflected/diffracted off various surfaces in the environment [36]. The collective effect of sound interaction with the room walls and contents (e.g., loudspeakers) is known as reverberation [88] [89]. A room reverberant environment is an enclosure with reflections. The model of a 'Room reverberant environment' is applied to many enclosed environments, such as office rooms, automobiles, aeroplanes and trains. ANC becomes difficult under complex environments such as reverberant environments.

2.3.2 Wave-domain expansion of a sound field

Wave domain sound field representation uses the weighted sum of a set of orthogonal basis functions to describe the pressure field of propagating sound. The basis are fundamental solutions to the Helmholtz wave-equation. In this subsection, we begin from the wave-domain expansion of a general sound field, and then discuss the wave-domain expansion in the near field and far field, respectively.

General sound field wave-domain expansion

The Helmholtz equation can be derived by substituting (2.22) into (2.20),

$$\nabla^2 p(\boldsymbol{x}, w) = -k^2 p(\boldsymbol{x}, w), \tag{2.23}$$

where k denotes the wavenumber, and

$$k = \frac{w}{c} = \frac{2\pi}{\lambda_0}, \tag{2.24}$$

where λ_0 is the wavelength.

This Helmholtz equation (2.23) determines all the sound fields in this thesis. Assuming the speed of the sound is constant in the sound field, we often use wavenumber k instead of angular frequency w to represent 'frequency' in this thesis. In that case, we represent the sound pressure at an arbitrary point $\boldsymbol{x}$ as $p(\boldsymbol{x}, k)$.

By solving equation (2.23) in different coordinate systems, we can represent the sound field in the wave domain. This formulation applies directly to a narrow band sound field. It can be extended to the broadband sound fields as well.

In a 3D sound field, to solve the Helmoltz equation in a spherical coordinate system, we apply the technique of variable separation. We assume that the solution can be rewritten by a product of functions of each coordinate, as:

$$p(\boldsymbol{x}, w) = X(r, w)\Theta(\psi, w)\Phi(\phi, w). \tag{2.25}$$

The Laplacian operator in spherical coordinates can be written by

$$\nabla^2(\cdot) = \frac{1}{r^2}\frac{\partial}{\partial r}[r^2\frac{\partial}{\partial r}(\cdot)] + \frac{1}{r^2\sin\psi}\frac{\partial}{\partial\psi}[\sin\psi\frac{\partial}{\partial\psi}(\cdot)] + \frac{1}{r^2\sin^2\psi}\frac{\partial^2}{\partial\phi^2}(\cdot). \tag{2.26}$$

Substituting (2.26) into the Helmholtz equation (2.23), three ordinary difference equations can be written as [90]

$$\frac{d^2\Phi}{d\phi^2} + m^2\Phi = 0, \tag{2.27}$$

$$\frac{1}{\sin\psi}\frac{d}{d\psi}(\sin\psi\frac{d\Theta}{d\psi}) + [u(u+1) - \frac{m^2}{\sin^2\psi}]\Theta = 0, \tag{2.28}$$

$$\frac{1}{r^2}\frac{d}{dr}(r^2\frac{dX}{dr}) + k^2X - \frac{u(u+1)}{r^2}X = 0, \tag{2.29}$$

where u and m are integers.

The solution to (2.27) is

$$\Phi(\phi) = \Phi_1\exp(im\phi) + \Phi_2\exp(-im\phi), \tag{2.30}$$

where Φ_1 and Φ_2 are arbitrary constants.

To further solve the (2.28), the finite solution is

$$\Theta(\psi) = \Theta_1 P_{um}(\cos\psi), \tag{2.31}$$

where $P_{um}(\cdot)$ is the first kind of associated Legendre function, Θ_1 is an arbitrary constant.

The definitions of $P_{um}(\cdot)$ are

$$P_{um}(t) = \frac{(1-t^2)^{m/2}}{2^u u!}\frac{d^{m+u}}{dt^{m+u}}(t^2-1)^u. \tag{2.32}$$

When $m < 0$ and $m \leq u$,

$$P_{u(-m)}(t) = (-1)^m\frac{(u-m)!}{(u+m)!}P_{um}(t); \tag{2.33}$$

when $m > u$,

$$P_{um}(\cdot) = 0. \tag{2.34}$$

Further solving (2.29), we obtain

$$X(r) = X_1 j_u(kr) + X_2 y_u(kr), \tag{2.35}$$

where X_1 and X_2 are arbitrary constants, $j_u(\cdot)$ and $y_u(\cdot)$ are the first and the second kind of Bessel functions, respectively. Another solution of (2.29) can be written by

$$X(r) = X_3 h_u(kr) + X_4 h_u^{(2)}(kr), \tag{2.36}$$

where X_3 and X_4 are arbitrary constants, $h_u(\cdot)$ and $h_u^{(2)}(\cdot)$ are the first and the second kind of spherical Hankel functions, respectively.

To simplify the calculation, we combine the angle frequency of (2.30) and (2.31) into a new function, which is called 'spherical harmonics' [90, 91]

$$Y_{um}(\phi, \psi) = \sqrt{\frac{(2u+1)}{4\pi}\frac{(u-m)!}{(u+m)!}} P_{um}(\cos\psi)\exp(im\phi), \tag{2.37}$$

where u is the spherical harmonics order, $m = -u, \ldots, u$ is the number of spherical harmonics basis of each order.

One important property of spherical harmonics is that, for different m and u, all the spherical harmonics basis are orthogonal to each other [90], as follows:

$$\int_0^{2\pi}\int_0^{\pi} Y_{um}(\phi,\psi) Y^*_{u'm'}(\phi,\psi)\sin\psi d\psi d\phi = \delta_{mm'}\delta_{uu'}, \tag{2.38}$$

where $(\cdot)^*$ is the complex conjugate, $\delta_{uu'}$ is the Kronecker delta function, and

$$\delta_{uu'} = \begin{cases} 1, u = u' \\ 0, u \neq u'. \end{cases}$$

From the derivation above, the general solution of the Helmholtz function is

$$p(\boldsymbol{x},k)=\sum_{u=0}^{\infty}\sum_{m=-u}^{u}\big(\beta_{um}(k)j_u(kr)+\widehat{\beta}_{um}(k)y_u(kr)\big)Y_{um}(\phi,\psi), \tag{2.39}$$

where $\beta_{um}(k)$ and $\widehat{\beta}_{um}(k)$ are the wave domain coefficients, which are dependent on frequency.

In (2.39), the first kind of Bessel function is finite in the region. However, since the origin is inside the sound field, the second kind of Bessel function $y_u(kr)$ is infinite on the origin. We use (2.39) to express interior sound field, and set $\widehat{\beta}_{um}(k)=0$.

Therefore, in an interior sound field, any arbitrary point can be represented by

$$p(\boldsymbol{x},k)=\sum_{u=0}^{\infty}\sum_{m=-u}^{u}\beta_{um}(k)j_u(kr)Y_{um}(\phi,\psi). \tag{2.40}$$

where $\beta_{um}(k)$ is the representation in the spherical harmonics domain.

A similar derivation, the cylindrical harmonics expansion for an interior sound field can be written by

$$p(\boldsymbol{x},k)=\sum_{m=-\infty}^{\infty}\beta_m(k)J_m(k||\boldsymbol{x}||)\exp(im\phi_x), \tag{2.41}$$

where $J_m(\cdot)$ is the Bessel function of of order m.

Near-field and far-field wave-domain expansion

When sources are located outside of the region, we consider the near field and the far field in this thesis depending on how far they are located.

(i) Near field: spherical wave model and cylindrical wave model

The near field of a source is the region close to a source where the sound pressure and acoustic particle velocity are not in phase. When a point source is suitably close to the region of interest, we apply the spherical wave model and cylindrical wave model in this thesis.

In 3-D space, using the spherical wave model, the Green's function of a point

source at $\boldsymbol{x}_s$ can be written by

$$g(\boldsymbol{x} \mid \boldsymbol{x}_s, k) = \frac{\exp(ik\|\boldsymbol{x} - \boldsymbol{x}_s\|)}{4\pi\|\boldsymbol{x} - \boldsymbol{x}_s\|}, \tag{2.42}$$

where $\boldsymbol{x} = (r, \phi, \psi)$ and $\boldsymbol{x}_s = (r_s, \phi_s, \psi_s)$ are in spherical coordinates.
In the wave domain, (2.42) can be expanded as [42]

$$g(\boldsymbol{x} \mid \boldsymbol{x}_s, k) = ik \sum_{u=0}^{\infty} \sum_{m=-u}^{u} h_u(kr_s) Y_{um}^*(\phi_s, \psi_s) j_u(kr) Y_{um}(\phi, \psi), r_s > r. \tag{2.43}$$

Therefore, the wave-domain coefficients of Green's function using spherical harmonics expansion can be written by

$$\beta_{um}^{(g)}(k) = ikh_u(kr_s) Y_{um}^*(\phi_s, \psi_s). \tag{2.44}$$

In 2-D space, using the cylindrical wave model, the Green's function can be written by

$$g(\boldsymbol{x}|\boldsymbol{x}_s, k) = \frac{i}{4} H_0(k\|\boldsymbol{x} - \boldsymbol{x}_s\|). \tag{2.45}$$

Using the addition property of Hankel function [92], $H_0(k\|\boldsymbol{x} - \boldsymbol{x}_s\|)$ in (2.45) can be written by

$$H_0(k\|\boldsymbol{x} - \boldsymbol{x}_s\|) = \sum_{m=-\infty}^{\infty} H_m(kr_s) \exp(-im\phi_s) J_m(kr) \exp(im\phi). \tag{2.46}$$

Therefore, the wave-domain coefficients of Green's function using cylindrical harmonics expansion can be written by

$$\beta_m^{(g)}(k) = \frac{i}{4} H_m(kr_s) \exp(-im\phi_s). \tag{2.47}$$

(ii) Far field: plane wave model
The far field of a source begins where the near field ends and extends to infinity. When the radial distance r_s is much greater than the wavelength of the sound radiated, the source can be assumed to be at an infinite distance ($r_s \to \infty$) from the region of interest and hence the received waveform from a single point source is

planar. In this case, we use far-field approximation. The common rule of thumb for the approximate distance at which the far-field approximation begins to be valid is $r_s = 2R_1^2/\lambda$ [42], where λ is the operating wavelength and R_1 is the radius of the region.

The sound field at arbitrary point $p(\boldsymbol{x}|\boldsymbol{x}_s, k)$ produced by plane wave source can be represented by [72]

$$p(\boldsymbol{x}|\boldsymbol{x}_s, k) = \sum_{u=0}^{\infty} \sum_{m=-u}^{u} 4\pi i^u j_u(kr) Y^*(\phi_s, \psi_s) Y(\phi, \psi). \tag{2.48}$$

The wave-domain expansion of the plane wave also satisfies (2.40). Therefore, in 3-D space, wave domain coefficients of a plane wave can be written by

$$\beta_{um}(k) = 4\pi i^u Y^*(\phi_s, \psi_s). \tag{2.49}$$

As reviewed above, the wave-domain expansion represents the sound field in wave-domain coefficients, as shown in (2.40) and (2.41). In the ANC system, we can also represent the loudspeaker signals and microphone signals in wave-domain coefficients. Details of wave-domain representation of ANC systems are discussed in Section 4.2. In Chapter 4 and Chapter 5, we control the region of interest using these wave-domain coefficients and achieve spatial ANC over the entire region of interest. In Chapter 6, we investigate noise cancellation performance based on the wave-domain coefficients representing the secondary source to the region of interest.

2.4 Summary

This chapter reviewed basic ANC techniques and harmonic-based wave-domain sound field representation. The chapter is comprised of three sections: single-channel ANC, multichannel ANC, and wave-domain sound field representation technique. From single-channel ANC to multichannel ANC, the control system becomes more complex and the control area is enlarged. To reduce the complexity of the system in specific noise field environments, we modify the existing multichannel ANC algorithm in Chapter 3. To further cancel the spatial sound field over a continuous region of interest, we apply the wave-domain processing technique in

Chapters 4, 5 and 6 to investigate new strategies for spatial ANC over a region.

Chapter 3

Multiple-point ANC for Directional Sparse Noise Fields

***Overview:** Multichannel active noise control is currently an attractive solution for the attenuation of low-frequency noise, in 3-D space. This chapter develops multichannel ANC algorithms for the case when the noise source components are sparsely distributed in space. We design the loudspeaker driving signals as in conventional ANC to minimize the residual signals but with an additional term containing an ℓ_l norm regularization applied to the driving signal magnitude. Only secondary sources close to the noise sources are required to be active for cancellation of sparse noise fields. We propose adaptive algorithms with low computational complexity and faster convergence speeds.*

3.1 Introduction

As discussed in Section 2.2, multichannel algorithms have been utilized to achieve noise cancellation in general noise fields. When the noise sources are sparsely distributed in space, (i.e., directional sparse noise field constructed by a few noise sources), an effective strategy is to use only the secondary sources that are close to the noise sources for noise cancellation. This means that many secondary source candidates in the multichannel ANC system can be inactive, so that the overall

system power and system complexity can be reduced. Such systems have applications in controlling industry noise fields in an open area and directional sources in less reverberant rooms.

In sound field reproduction and system identification applications, the sparse feature is exploited by introducing an additional term to the minimization problem [93, 94, 95]. In particular, motivated by the least-absolute shrinkage and selection operator (Lasso) algorithm, some algorithms have been proposed which introduce an ℓ_1-norm penalty [94] on the adaptive coefficients of the cost function.

In ANC applications, the ℓ_1-norm penalty is applied on the loudspeaker driving signals, which can be added onto the cost function of residual error signals. It is important to note that, for frequency domain multichannel ANC, the adaptive filters are designed in terms of complex vectors, so the ℓ_1-norm constraint should be applied accordingly.

In this chapter, we develop two constrained multichannel ANC formulations to deal with spatially sparse distribution of noise sources. We derive these algorithms via combining two variants of the ℓ_1 norm of complex vectors into the conventional multichannel cost function. This is the first time for the ℓ_1-norm constraint is introduced to multichannel ANC. The complex ℓ_1 constrained multi-point algorithm (Cℓ_1-MP) adds ℓ_1-norm constraint to the complex driving signals, and the scalar ℓ_1-constrained multi-point algorithm (Sℓ_1-MP) adds constraint on the sum of ℓ_1 norm to the real and imaginary parts of the loudspeaker driving signals. Simulations are conducted to evaluate the two proposed algorithms in comparison with the conventional multi-point and Leaky multi-point algorithms.

The rest of the chapter is organized as follows. In Section 3.2 we formulate the spatial noise cancellation problem and set up the ANC system. We review the conventional multichannel ANC system in Section 3.3, and propose the constrained multichannel ANC system in Section 3.4. In Section 3.5, we present the effect and the selection of the sparsity parameter in the new algorithms. We demonstrate the simulation results in Section 3.6 and draw some conclusions in Section 3.7.

3.2 Spatial ANC Problem Formulation

In this section, we formulate the spatial ANC problem assuming a 2-D (or height-invariant 3-D) sound field, to cancel the noise over a spatial region.

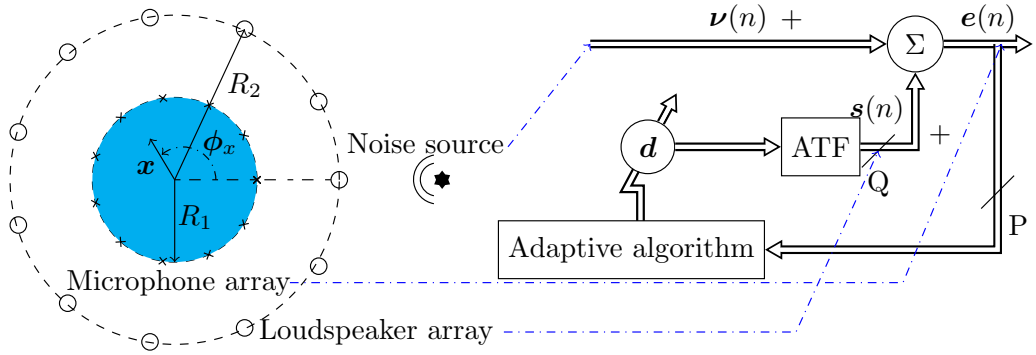

Figure 3.1: ANC setup with a circular region of interest and the block diagram of the multi-point feedback ANC system.

Let the control zone of interest be a circular region with a radius R_1. Assume that the noise sources are located outside the region of interest, as shown in Figure 3.1. We consider an ANC system in two-dimensional space using (i) a single microphone array (Q microphones) on the boundary of the control region to measure the residual signals and (ii) a single loudspeaker array (L loudspeakers) outside the region to generate the secondary sound field [96]. The theory we developed in this chapter can be extended to 3-D space.

The objective of spatial ANC is to cancel the noise field over the entire region of interest using the loudspeaker array.

Any arbitrary observation point within the control region is denoted as $\boldsymbol{x} \equiv \{r, \phi_{\boldsymbol{x}}\}$. In the ANC system, the residual signal at this point is given by

$$e(\boldsymbol{x}, k) = \nu(\boldsymbol{x}, k) + s(\boldsymbol{x}, k), \tag{3.1}$$

where $k = 2\pi f/c$ is the wave number, f is the frequency, c is the speed of sound propagation, $\nu(\boldsymbol{x}, k)$ is the primary noise signal and $\boldsymbol{s}(\boldsymbol{x}, k)$ is the secondary sound field generated by the loudspeakers.

The secondary sound field generated by the loudspeaker array can be represented by

$$s(\boldsymbol{x}, k) = \sum_{l=1}^{L} d_l(k) G(\boldsymbol{x}|\boldsymbol{y}_l, k), \tag{3.2}$$

where $d_l(k)$ is the driving signal for the l^{th} loudspeaker, and $G(\boldsymbol{x}|\boldsymbol{y}_l, k)$ denotes the acoustic transfer function (ATF) between the l^{th} loudspeaker and the observation point $\boldsymbol{x}$. For example, for sound propagation in free field, $G(\boldsymbol{x}|\boldsymbol{y}_l, k) = \frac{i}{4}\mathcal{H}_0^{(2)}(k\|\boldsymbol{y}_l - \boldsymbol{x}\|)$, where $\mathcal{H}_0^{(2)}(\cdot)$ is the zero$^{\text{th}}$-order Hankel function of the second kind.

Let the microphones be positioned at $\boldsymbol{x}_q, q = 1, \cdots, Q$ with respect to the origin O. Then the residual signal vector at the microphone array is given by

$$\boldsymbol{e}(k) = \boldsymbol{\nu}(k) + \boldsymbol{G}(k)\boldsymbol{d}(k), \tag{3.3}$$

where $\boldsymbol{G}(k)$ is a $Q \times L$ matrix with the (q, l) element given by $G(\boldsymbol{x}_q|\boldsymbol{y}_l, k)$, and

$$\begin{aligned}
\boldsymbol{e}(k) &\triangleq [e(\boldsymbol{x}_1, k), \ldots, e(\boldsymbol{x}_Q, k)]^T, \\
\boldsymbol{\nu}(k) &\triangleq [\nu(\boldsymbol{x}_1, k), \ldots, \nu(\boldsymbol{x}_Q, k)]^T, \\
\boldsymbol{d}(k) &\triangleq [d_1(k), \ldots, d_L(k)]^T.
\end{aligned}$$

Here, we assumed $\boldsymbol{G}(k)$ to be prior knowledge obtained from pre-calibration or room modelling.

The objective is to design the driving signals $\boldsymbol{d}(k)$, using the minimum number of active secondary sources to generate secondary sound field and force the residual error signals $\boldsymbol{e}(k)$ towards zero.

In this chapter, we assume that the noise fields have directional sparsity.[1] We first briefly review the conventional multichannel algorithms, and then propose our new constrained algorithms. The multichannel algorithms in this chapter apply multiple microphone points in the region, and minimize the residual signals around these points. In order to differentiate the multichannel algorithms in wave domain in the later chapters, here onwards, we utilize the terminology 'multi-point

[1]Here the directional sparsity means that the noise signals are arriving from few distinct directions.

algorithm' instead of 'multichannel algorithm'.

3.3 Conventional Multi-point Algorithms

In this section, we briefly outline the existing frequency domain multi-point adaptive ANC algorithm and its variation using a feedback structure. A block-wise operation is adopted and the microphone measurements are transformed into time-frequency domain.

3.3.1 Multi-point algorithm

The conventional multi-point (MP) approach minimises the sum of squares of the residual signals with the cost function

$$\xi(n,k) = \sum_{q=1}^{Q} |e_q(n,k)|^2, \tag{3.4}$$

where n is the iteration index of the adaptive algorithm and $e_q(n,k)$ is the frequency domain pressure $e_q(k)$ in the n_{th} time frame.

In vector form, (3.4) can be written as

$$\xi(n,k) = \boldsymbol{e}^H(n,k)\boldsymbol{e}(n,k). \tag{3.5}$$

It can also be represented by the ℓ_2 norm of the residual signals, as follows

$$\xi(n,k) = \|\boldsymbol{e}(n,k)\|_2^2. \tag{3.6}$$

By using the steepest descent algorithm, the driving signals are updated by

$$\boldsymbol{d}(n+1,k) = \boldsymbol{d}(n,k) - \frac{\mu}{2}\nabla\xi(n,k), \tag{3.7}$$

where μ is the adaptation step size, and $\nabla(\cdot)$ denotes the gradient.

The gradient of the cost function can be written as

$$\nabla\xi(n,k) = \nabla(\|\boldsymbol{e}(n,k)\|_2^2). \tag{3.8}$$

Substituting (3.3) into (3.8), the gradient can be represented by

$$\nabla\xi(n,k) = 2\boldsymbol{G}^H(k)\boldsymbol{e}(n,k). \tag{3.9}$$

Thus the loudspeaker update equation is [97]

$$\boldsymbol{d}(n+1,k) = \boldsymbol{d}(n,k) - \mu\boldsymbol{G}^H(k)\boldsymbol{e}(n,k). \tag{3.10}$$

In (3.10), the loudspeaker driving signals $\boldsymbol{d}(k)$ are updated directly. The block diagram of the frequency domain multi-point feedback LMS algorithm is shown in Figure 3.1.

3.3.2 Leaky multi-point algorithm

The traditional LMS algorithm may suffer from divergence due to insufficient spectral excitation, like a sinusoid signal without noise, which consequently may cause overflow for the weight vector during the updating process. This divergence problem can be resolved by proposing a 'leaky term' during the update process of the weight vector. A Leaky algorithm introduces output power constraints (leakage factor) to the adaptive filter [98, 99, 54, 100]. This results in inferior performance; however, the leakage factor is controlled, which is necessary to balance for the lost performance. In addition, this adds complexity, but achieves more robustness of the adaptive filter. Moreover, the leakage term can stabilize the LMS algorithm.

When the leaky factor is applied to the multi-point algorithm, the problem becomes minimizing the sum of squared residual signals and the weighted sum of loudspeaker driving signals [101]. Therefore, the modified cost function of the Leaky multi-point (Leaky-MP) algorithm is written as

$$\xi_{\text{Leaky}}(n,k) = \|\boldsymbol{e}(n,k)\|_2^2 + \rho\|\boldsymbol{d}(n,k)\|_2^2, \tag{3.11}$$

where $\rho > 0$ is the leakage factor, $\|\boldsymbol{d}(n,k)\|_2$ denotes the ℓ_2 norm of the loudspeaker driving signals.

Substituting (3.3) into (3.11), the gradient of the cost function of the Leaky-MP

algorithm can be written by

$$\nabla\xi_{\text{Leaky}}(n,k) = 2\boldsymbol{G}^H(k)\boldsymbol{e}(n,k) + 2\rho\boldsymbol{d}(n,k). \tag{3.12}$$

Hence, the adaptive weights of the Leaky-MP algorithm are updated as

$$\boldsymbol{d}(n+1,k) = (1-\mu\rho)\boldsymbol{d}(n,k) - \mu\boldsymbol{G}^H\boldsymbol{e}(n,k). \tag{3.13}$$

Compared to the update equation (3.10) in the multi-point algorithm, (3.13) reduces the strength of driving signals in the previous iteration, which makes the adaptive algorithm more stable.

3.4 Sparsity Constrained Multi-point Algorithms

In the multi-point algorithm and the Leaky multi-point algorithm discussed above, the focus is in the general noise field without any directional constraint. These approaches often result in large numbers of active loudspeakers. However, in real applications, some noise fields have directional sparsity. In this section, we exploit the sparse nature of the noise sources to reduce the active loudspeaker numbers and improve the ANC systems. For spatially sparse noise fields, inspired by Leaky-MP, we introduce an additional constraint on the loudspeaker driving signals in the cost function of the conventional multi-point approach.

3.4.1 ℓ_0-norm constrained multi-point algorithm

One method to enforce a reduction in the number of loudspeakers in multi-point ANC systems is by utilizing compressed sensing techniques [102]. This can be done by selecting the amplitude of each of the loudspeakers' driving signals to achieve more zero elements in $\boldsymbol{d}$. To be more specific, it is the solution of the following constrained minimization problem

$$\min_{\boldsymbol{d}(k)} \quad \|\boldsymbol{e}(k)\|_2^2 + \delta(k)\|\boldsymbol{d}(k)\|_0, \tag{3.14}$$

where $\delta(k)$ is the sparsity level of each frequency bin, and $\|\boldsymbol{d}(k)\|_0$ represents the total number of non-zero elements in the loudspeaker driving signal vector.

However, the problem in (3.14) is Non-Polynomial (NP) hard as it entails an exhaustive search. Therefore, the ℓ_0 norm is either approximated by a continuous function [103] or replaced by the ℓ_1 norm [93].

Because the ℓ_1-norm regularization is a convex problem, it can provide a sparse solution with less computational time. In the following two subsections, we propose two regularization methods involving ℓ_1 norm.

3.4.2 Complex ℓ_1-norm constrained multi-point algorithm

In the first method, we replace the ℓ_0 norm in (3.14) with the ℓ_1 norm on the complex vector

$$\min_{\boldsymbol{d}(k)} \quad \|\boldsymbol{e}(k)\|_2^2 + \lambda(k)\|\boldsymbol{d}(k)\|_1, \tag{3.15}$$

where $\|\boldsymbol{d}(k)\|_1$ is the sum of the magnitudes of the complex entries of the vector $\boldsymbol{d}(k)$, $\lambda(k)$ is a controllable parameter to determine the degree of sparse constraint for the adaptive coefficients.

In the frequency domain adaptive algorithm, combining the squared residual error signals with the ℓ_1 norm of the weight vector, the cost function becomes

$$\xi_{\mathrm{C}\ell_1\text{-MP}}(n,k) = \|\boldsymbol{e}^H(n,k)\|_2^2 + \lambda(k)\|\boldsymbol{d}(n,k)\|_1, \tag{3.16}$$

where n is the adaptive index.

The gradient of the cost function can be written as

$$\nabla\xi_{\mathrm{C}\ell_1\text{-MP}}(n) = \underbrace{\nabla\|\boldsymbol{e}^H(n)\|_2^2}_{\nabla\xi_1(n)} + \underbrace{\nabla\lambda\|\boldsymbol{d}(n)\|_1}_{\nabla\xi_2(n)}, \tag{3.17}$$

where we dropped the frequency dependency k for notational simplicity.

Theorem 3.4.1 *The gradient of the cost function $\xi_{C\ell_1\text{-}MP}(n)$ is given by*

$$\nabla\xi_{C\ell_1\text{-}MP}(n) = 2\boldsymbol{G}^H\boldsymbol{e}(n) + \lambda\exp(i\boldsymbol{\theta}(n)), \tag{3.18}$$

where $\boldsymbol{\theta}(n)$ is the vector of phases of complex driving signals $d_q(n)$, $q = 1, ..., Q$,

and $\exp(\cdot)$ *denotes the exponential function.*

Proof

The term $\nabla\xi_1(n)$ of (3.17) is the same as that of the conventional MP algorithm, i.e., $\nabla\xi_1(n) = 2\boldsymbol{G}^H\boldsymbol{e}(n)$.

From (3.17), we write $\nabla\xi_2$ as follows [50],

$$\nabla\xi_2 = 2\lambda\frac{\partial(\|\boldsymbol{d}\|_1)}{\partial\boldsymbol{d}^*} = 2\lambda\frac{\partial(\sum_{q=1}^{Q}|d_q|)}{\partial\boldsymbol{d}^*}, \tag{3.19}$$

where we dropped the iteration dependency n for notational simplicity. Then

$$\frac{\partial(\sum_{q=1}^{Q}|d_q|)}{\partial\boldsymbol{d}^*} = \begin{bmatrix}\frac{\partial|d_1|}{\partial d_1^*}\\ \vdots \\ \frac{\partial|d_Q|}{\partial d_Q^*}\end{bmatrix} = \frac{1}{2}\begin{bmatrix}\frac{\partial|d_1|}{\partial\Re(d_1)} + i\frac{\partial|d_1|}{\partial\Im(d_1)}\\ \vdots \\ \frac{\partial|d_Q|}{\partial\Re(d_Q)} + i\frac{\partial|d_Q|}{\partial\Im(d_Q)}\end{bmatrix}. \tag{3.20}$$

Given the absolute value of a complex number $|d_q| = \sqrt{\Re(d_q)^2 + \Im(d_q)^2}$, we have

$$\begin{aligned}\frac{\partial|d_q|}{\partial\Re(d_q)} &= \frac{\Re(d_q)}{\sqrt{\Re(d_q)^2 + \Im(d_q)^2}} = \cos\theta_q,\\ \frac{\partial|d_q|}{\partial\Im(d_q)} &= \frac{\Im(d_q)}{\sqrt{\Re(d_q)^2 + \Im(d_q)^2}} = \sin\theta_q.\end{aligned} \tag{3.21}$$

By substituting (3.21) into (3.20), $\nabla\xi_2$ can be simplified to $\lambda\exp(i\boldsymbol{\theta})$. This completes the proof.

Following the steepest descent updating and substituting (3.18) into (3.7), the final update equation of the complex ℓ_1-constrained multi-point algorithm (Cℓ_1-MP) can be written as

$$\boldsymbol{d}(n+1) = \boldsymbol{d}(n) - \mu\boldsymbol{G}^H\boldsymbol{e}(n) - \frac{1}{2}\mu\lambda\exp(i\boldsymbol{\theta}(n)). \tag{3.22}$$

Compared to the conventional multi-point approach, the additional constraint $\frac{1}{2}\mu\lambda\exp(i\boldsymbol{\theta}(n))$ tends to shrink more entries in the loudspeaker driving signals vector to zero. As evidenced in Section 3.6, this method speeds up the convergence in spatially sparse noise fields.

In the first method, there is complex number calculation involved in the ℓ_1 constraint, which is computationally costly. In the next subsection, we propose the second method to reduce the computational cost.

3.4.3 Scalar ℓ_1-norm constrained multi-point algorithm

In the second method, we replace the ℓ_0 norm in (3.14) with the sum of the ℓ_1 norm on the real and imaginary parts of the loudspeaker driving signals. The new cost function becomes

$$\xi_{\mathrm{S}\ell_1\text{-MP}}(n) = \|\boldsymbol{e}^H(n)\|_2^2 + \lambda(\|\Re(\boldsymbol{d}(n))\|_1 + \|\Im(\boldsymbol{d}(n))\|_1). \tag{3.23}$$

Instead of forcing the complex weight entries towards zero directly, we force the real and imaginary parts of the complex entries towards zero at the same rate.

Theorem 3.4.2 *The gradient of the cost function $\xi_{S\ell_1\text{-}MP}(n)$ is given by*

$$\nabla\xi_{S\ell_1\text{-}MP}(n) = \underbrace{\nabla\|\boldsymbol{e}^H(n)\|_2^2}_{\nabla\xi_1(n)} + \underbrace{\nabla\lambda(\|\Re(\boldsymbol{d}(n))\|_1 + \|\Im(\boldsymbol{d}(n))\|_1)}_{\nabla\xi_2'(n)} \tag{3.24}$$

$$= 2\boldsymbol{G}^H\boldsymbol{e}(n) + \lambda\big(\operatorname{sgn}(\Re(\boldsymbol{d}(n))) + i\operatorname{sgn}(\Im(\boldsymbol{d}(n)))\big) \tag{3.25}$$

where $\operatorname{sgn}(\cdot)$ *is a component-wise function which is defined as* $\operatorname{sgn}(d) = \begin{cases} d/|d| & d \neq 0 \\ 0 & d = 0 \end{cases}$.

Proof

The second term in (3.24) can be represented by

$$\nabla\xi_2' = 2\lambda\left(\frac{\partial(\|\Re(\boldsymbol{d})\|_1)}{\partial\boldsymbol{d}^*} + \frac{\partial(\|\Im(\boldsymbol{d})\|_1)}{\partial\boldsymbol{d}^*}\right). \tag{3.26}$$

The complex partial differentiation based on $\boldsymbol{d}^*$ can be separated by [104]

$$\begin{aligned}\frac{\partial\|\Re(\boldsymbol{d})\|_1}{\partial\boldsymbol{d}^*} &= \frac{1}{2}\left(\frac{\partial\|\Re(\boldsymbol{d})\|_1}{\partial\Re(\boldsymbol{d})} + i\frac{\partial\|\Re(\boldsymbol{d})\|_1}{\partial\Im(\boldsymbol{d})}\right), \\ \frac{\partial\|\Im(\boldsymbol{d})\|_1}{\partial\boldsymbol{d}^*} &= \frac{1}{2}\left(\frac{\partial\|\Im(\boldsymbol{d})\|_1}{\partial\Re(\boldsymbol{d})} + i\frac{\partial\|\Im(\boldsymbol{d})\|_1}{\partial\Im(\boldsymbol{d})}\right).\end{aligned} \tag{3.27}$$

Each item in the (3.27) is given by

$$\frac{\partial \|\Re(\boldsymbol{d})\|_1}{\partial \Re(\boldsymbol{d})} = \operatorname{sgn}(\Re(\boldsymbol{d})),$$

$$\frac{\partial \|\Re(\boldsymbol{d})\|_1}{\partial \Im(\boldsymbol{d})} = \frac{\partial \|\Im(\boldsymbol{d})\|_1}{\partial \Re(\boldsymbol{d})} = 0,$$

$$\frac{\partial \|\Im(\boldsymbol{d})\|_1}{\partial \Im(\boldsymbol{d})} = \operatorname{sgn}(\Im(\boldsymbol{d})). \tag{3.28}$$

By substituting (3.27) and (3.28) into (3.26), we obtain the second term of (3.25). Also note from Theorem 1 $\nabla\xi_1(n) = 2\boldsymbol{G}^H\boldsymbol{e}(n)$ which is the first term of (3.25).

Thus, substituting (3.25) into (3.7), the scalar ℓ_1-norm constrained multi-point algorithm (Sℓ_1-MP) can be written as

$$\boldsymbol{d}(n+1) = \boldsymbol{d}(n) - \mu\boldsymbol{G}^H\boldsymbol{e}(n) - \frac{1}{2}\mu\lambda\big(\operatorname{sgn}(\Re(\boldsymbol{d}(n))) + i\operatorname{sgn}(\Im(\boldsymbol{d}(n)))\big). \tag{3.29}$$

Compared to (3.22), in (3.29), the exponential function of a complex vector is replaced by the sign function of two real vectors, which can save computational complexity in each iteration. It is a significant advantage in real time implementations.

3.5 Parameter Selection

The most important parameter in both Cℓ_1-MP and Sℓ_1-MP is the sparsity-tuning parameter $\lambda(k)$. It is a frequency dependent positive number which controls the relative importance of the sparsity constraint when generating loudspeaker driving signals. A large value of $\lambda(k)$ emphasizes the role of the ℓ_1-norm penalty in the cost functions (3.16) and (3.23), that is, forcing more entries in the loudspeaker weights $\boldsymbol{d}(k)$ towards zero or close to zero.

For the selection of sparsity level $\lambda(k)$, in the Lasso algorithm [93], $\lambda(k)$ is searched over the set $[0, \|G^H(k)\boldsymbol{\nu}(k)\|_\infty)$. A nominal value for selecting the sparsity-tuning parameter is

$$\lambda(k) = \frac{1}{20}\|G(k)^H\boldsymbol{\nu}(k)\|_\infty, \tag{3.30}$$

around which $\lambda(k)$ is selected within a set $[(\|G(k)^H\boldsymbol{\nu}(k)\|_\infty)/30, (\|G(k)^H\boldsymbol{\nu}(k)\|_\infty)/10]$.

In ANC applications, the primary noise field is often unknown and varying. To calculate the searching range of $\lambda(k)$, we utilize the initial recordings on the error microphones to estimate the primary noise level. During the adaptive process, if significant changes occur in the microphone recordings, we reset the value of $\lambda(k)$ to follow the varying noise field.

We conduct a simulation to further investigate the effect of $\lambda(k)$. Let the desired quiet zone be a circular region of radius of 1 m. The ANC system consists of 11 microphones placed equi-angularly on the boundary of the region and 11 loudspeakers placed on a circle of $R = 2$ m. A signal-to-noise ratio (SNR) of 40 dB white Gaussian noise is added at each microphone recording. The primary sound field is generated by a point noise source placed at 0° at a radius of 2.5 m. Here, $\lambda(k)$ is in the range of [0, 0.2].

Figure 3.2 demonstrates the noise reduction performance and active loudspeaker number under different $\lambda(k)$. From Figure 3.2(a), it is evident that as the value of $\lambda(k)$ increases, the noise reduction level in the region decreases. For both Cℓ_1-MP and Sℓ_1-MP algorithms, large $\lambda(k)$ results fewer loudspeakers and reduce total energy of the loudspeakers, as shown in Figure 3.2(b). Overall, in selection of $\lambda(k)$, there is a trade-off between the noise reduction level and the number of active loudspeakers. Meanwhile, the step size μ has an effect on the sparsity-tuning parameter selection. If we choose a large step size as well as a large sparse parameter, the system will become unstable, as demonstrated by the red curve in Figure 3.2(b).

3.6 Simulation Results

In this section, we compare the proposed algorithms (Cℓ_1-MP and Sℓ_1-MP) with the Multi-point (MP) algorithm [32] and the Leaky multi-point (Leaky-MP) algorithm [101] in a free-field environment. Let the desired quiet zone be a circular region of 1 m radius. The ANC system consists of 11 microphones placed equi-angularly on the boundary of the region and 11 loudspeakers placed on a circle of $R = 2$ m. A signal-to-noise ratio (SNR) of 40 dB white Gaussian noise is added at each

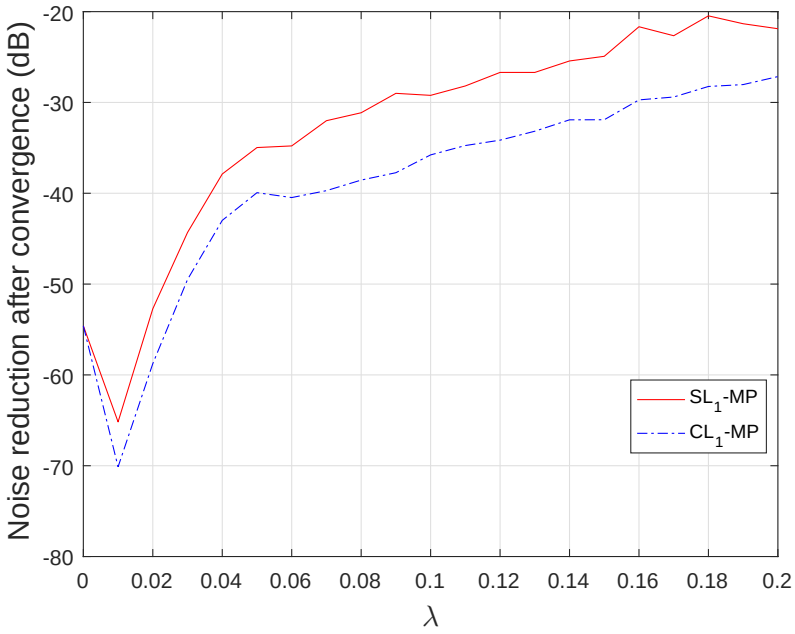

(a)

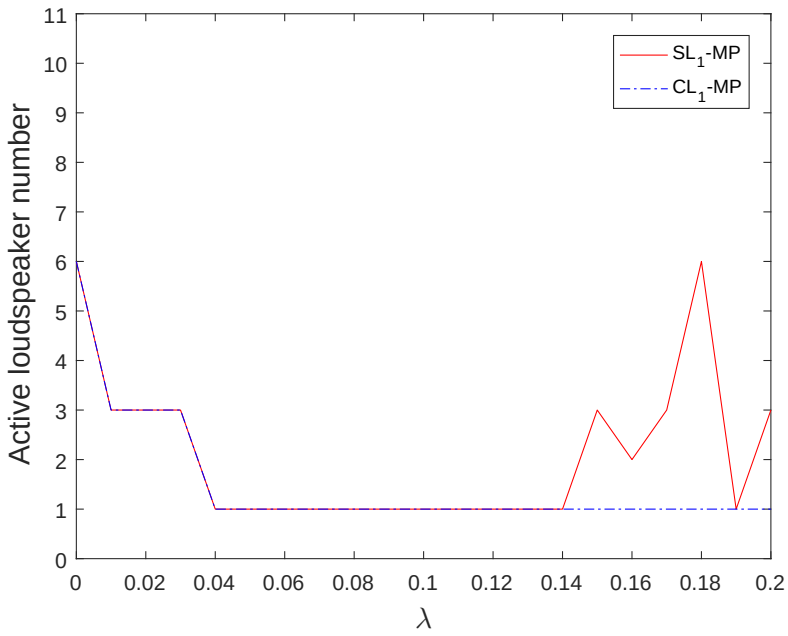

(b)

Figure 3.2: Noise reduction and active loudspeaker number after convergence using the ℓ_1-norm constrained ANC algorithm for different value of λ. (a) Noise reduction over the region, (b) Active loudspeaker numbers.

microphone recording [2]. The transfer function is simulated based on the modeling of sound propagation under the free-field assumption.

To evaluate the noise reduction performance inside the region (NR_{in}), sound pressures ($\boldsymbol{e}_{in}$) at $M = 1296$ uniformly placed points inside the regions are examined. We define $NR_{\text{in}}(n)$ as,

$$NR_{\text{in}}(n) = 10\log_{10}\frac{\|\boldsymbol{e}_{\text{in}}(n)\|_2^2/M}{\|\boldsymbol{e}_{\text{in}}(0)\|_2^2/M}, \tag{3.31}$$

where $\boldsymbol{e}_{\text{in}}(n)$ denotes the residual signals on the points inside the region at the nth iteration, and $\boldsymbol{e}_{\text{in}}(0)$ represents the primary noise field in the region. We choose the sparsity parameter $\lambda(k) = 0.02$ and $\lambda(k) = 0.04$.

3.6.1 Single primary source scenario

In this subsection, the primary sound field is generated by one point noise source placed at 0° at a radius of 2.5 m.

First, we investigate the narrowband performance of different algorithms. The frequency of the noise field is 200 Hz. The initial value of $\boldsymbol{d}$ is $\boldsymbol{d}(0) = [0, 0, ..., 0]^T$, and hence $\boldsymbol{\theta}(0) = [0, 0, ..., 0]^T$. Figure 3.3 shows the convergence performance and the noise reduction (NR) level for each iteration. Compared with MP, adding the ℓ_1 constraint will dramatically increase the convergence speed, especially for noise reduction inside the region, but adding the power constraint (Leaky-MP) can only slightly increase the speed. For noise reduction performance, adding the constraint to the loudspeaker driving signals (Cℓ_1-MP, Sℓ_1-MP and Leaky-MP) will decrease NR in the steady state. Larger value of λ results in less noise reduction, as shown in the comparison of $\lambda = 0.02$ and $\lambda = 0.04$. From the comparison of Figure 3.3(a) and Figure 3.3(b), it is evident that for the Leaky-MP algorithm, after convergence, the noise reduction performance inside the region is much worse than the noise reduction on the boundary. While for the same λ, both Cℓ_1-MP and Sℓ_1-MP can achieve similar noise reduction levels in the steady state on the microphone points and inside the region. Since our motivation is to cancel the

[2]Here, the SNR level is with respect to the primary noise field level on error microphones.

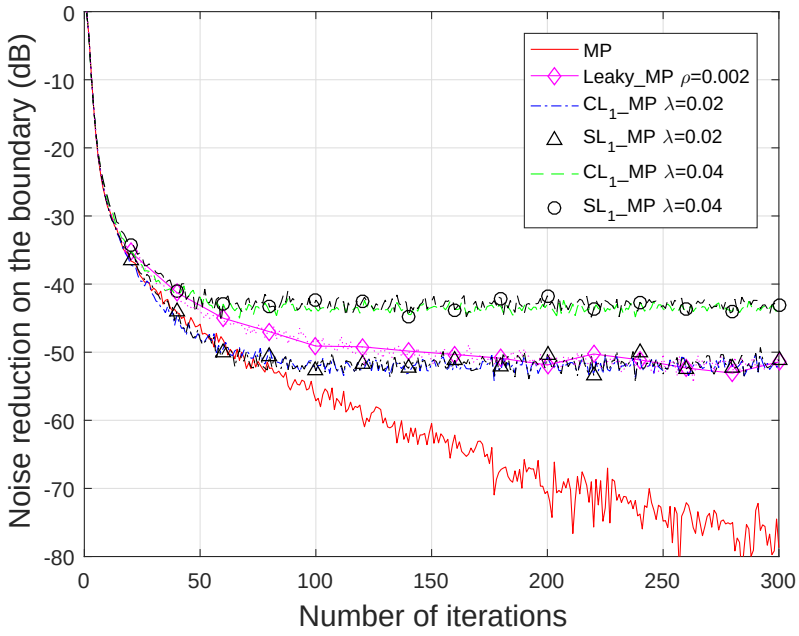

(a)

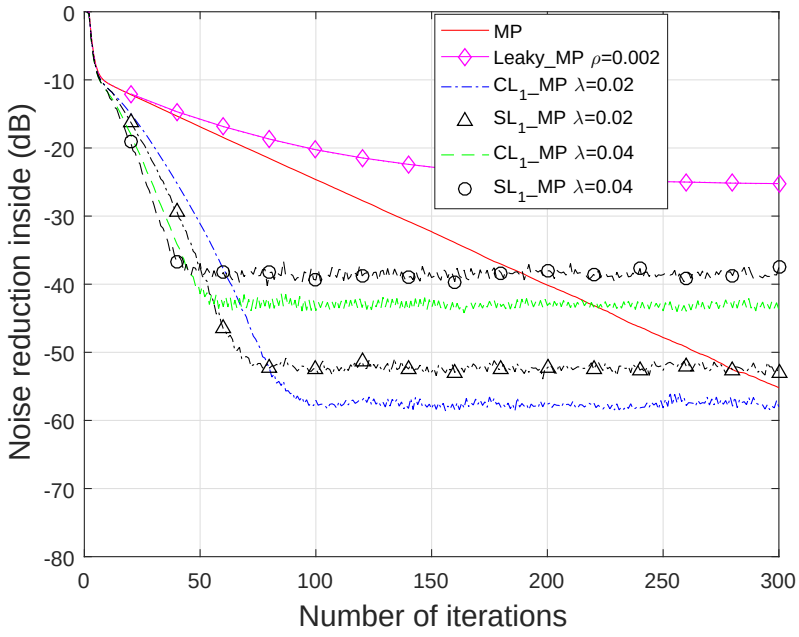

(b)

Figure 3.3: Comparison of the convergence speed and noise reduction level using different ANC algorithms, when the primary sound field is constructed by a primary source: (a) noise reduction on the boundary, (b) noise reduction inside the region.

Table 3.1: Noise reduction on the boundary, noise reduction inside the region, and active loudspeaker numbers after convergence in different frequency bins using different ANC algorithms, when the primary sound field is constructed by a primary source.

Frequency(Hz)	NR boundary (dB)			NR inside (dB)			Active speaker number		
	MP	Cℓ_1-MP	Sℓ_1-MP	MP	Cℓ_1-MP	Sℓ_1-MP	MP	Cℓ_1-MP	Sℓ_1-MP
50	-53.04	-49.50	-48.83	-69.47	-62.28	-58.67	11	4	5
100	-48.30	-38.62	-38.76	-65.94	-49.39	-48.25	9	3	3
150	-46.88	-43.58	-40.49	-38.43	-49.61	-49.69	9	3	3
200	-50.89	-43.25	-40.41	-20.84	-41.04	-35.84	11	1	2
250	-81.20	-41.81	-38.57	-66.44	-41.22	-35.73	7	1	1
300	-49.85	-41.98	-40.05	-22.22	-38.98	-38.98	9	1	1

noise over the entire region, the proposed Cℓ_1-MP and Sℓ_1-MP algorithm exhibit considerable improvement over the conventional MP and Leaky-MP algorithm.

Figure 3.4 demonstrates the performance in terms of the energy of loudspeaker driving signals and active loudspeaker numbers. Here we define the jth loudspeaker is active when $\|\boldsymbol{d}_j\| > 0.02 * \|\boldsymbol{d}_{\max}\|$. From Figure 3.4(a), compared to MP, the constrained MP algorithms can reduce the total energy of the loudspeaker driving signals, which can avoid the overloading of the secondary sources. A large value of λ results in a lower energy of the loudspeaker driving signals. For the Leaky-MP algorithm, all the loudspeaker candidates are active in the steady state, as shown in Figure 3.4(b). Whereas both Cℓ_1-MP and Sℓ_1-MP can reduce the active loudspeaker numbers, over the conventional algorithms. After convergence, the loudspeakers which are distant from the noise source are non-active. Larger values of λ will force more loudspeakers to be non-active. When $\lambda = 0.04$, both Cℓ_1-MP and Sℓ_1-MP can reduce the active loudspeaker numbers from 11 to 1, which corresponds to the case in which only the loudspeaker candidate located at 0° is active in the steady state.

Table 3.1 shows the performance in the case of multi- frequency noise field for different algorithms after 50 iterations. The frequency range of the noise field is [50, 300] Hz. For the MP algorithm, the noise reduction is not converged, thus the NR inside the region is not stable over the frequency range. For the proposed

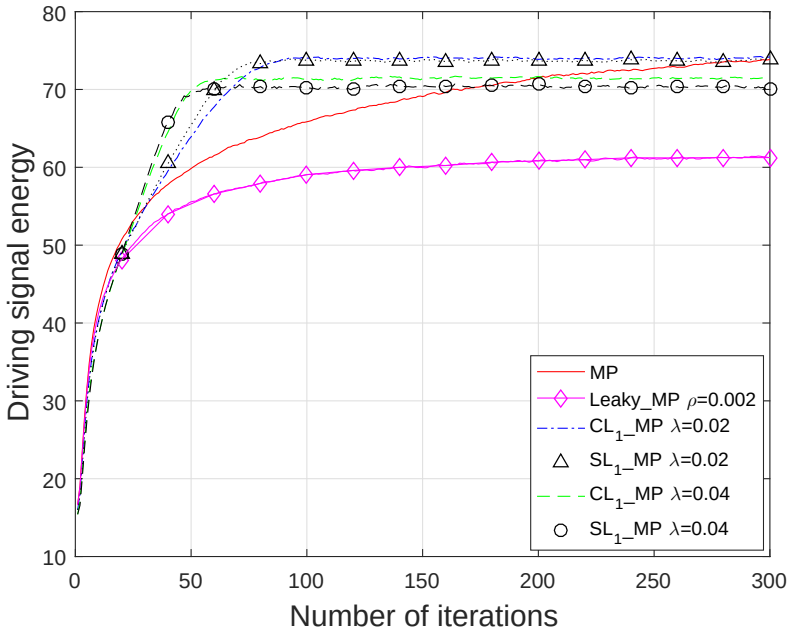

(a)

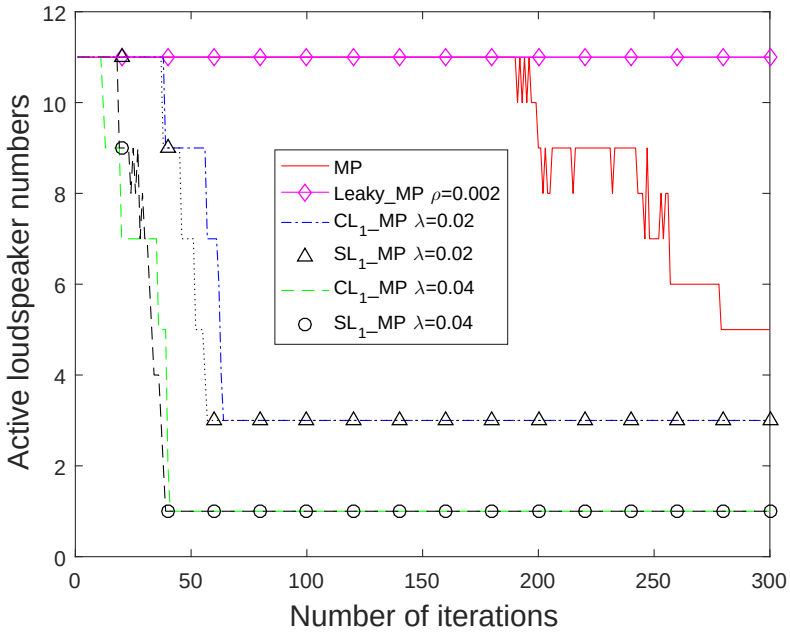

(b)

Figure 3.4: Comparison of the loudspeakers using different ANC algorithms, when the primary sound field is constructed by a primary source: (a) loudspeaker driving signal energy for each iteration, (b) active loudspeaker numbers for each iteration.

algorithms, by selecting proper parameter values for each frequency, 40 to 50 dB NR can be achieved on the boundary and inside the region. Compared to the MP algorithm, both Cℓ_1-MP and Sℓ_1-MP can reduce the active loudspeaker numbers. From the comparison of the proposed algorithms, it is evident that Cℓ_1-MP has slightly better noise reduction performance than Sℓ_1-MP in multiple frequency bins, but Sℓ_1-MP can achieve significant noise reduction with less computational complexity.

3.6.2 Multiple primary source scenario

If the primary sound field is constructed by multiple primary sources, for example two primary sources in different locations, the proposed ℓ_1-norm constrained ANC algorithms can still reduce the active loudspeaker numbers. To verify this, we place one of the point sources to 0° at the radius of 2.5 m, and move the other source from 0° to 360° at the radius of 2.2 m. The frequency of the noise field is 200 Hz. The performance of the ANC system after 300 iterations is shown in Table 3.2. The results are found to be similar to that containing a single primary source. The noise reduction inside the region shows the worst performance when two noise sources are located in the opposite direction (180°).

Table 3.2: Noise reduction inside the region and active loudspeaker numbers after convergence in different source locations, when the primary sound field is constructed by two primary sources.

Direction	NR boundary (dB)			NR inside (dB)			Active speaker number		
	MP	Cℓ_1-MP	Sℓ_1-MP	MP	Cℓ_1-MP	Sℓ_1-MP	MP	Cℓ_1-MP	Sℓ_1-MP
0°	-80	-47	-46	-52	-50	-50	5	1	1
60°	-80	-43	-40	-52	-45	-42	10	5	5
120°	-80	-43	-40	-52	-38	-30	11	5	5
180°	-80	-36	-35	-52	-34	-25	11	5	7
240°	-80	-40	-35	-52	-38	-30	11	5	6

3.7 Summary and Contributions

In this chapter, we investigated constrained multi-point methods for active noise control over a spatial region, in the directional sparse noise field. We derived Cℓ_1-MP algorithm via combining the ℓ_1-norm constraint on the complex loudspeaker driving signals to the cost function of the conventional multi-point algorithm. We derived Sℓ_1-MP algorithm via replacing the constraint in Cℓ_1-MP by sum of the ℓ_1 norm to the real and imaginary part of the loudspeaker driving signals, which can reduce the computational complexity.

We conducted the simulation in a single source noise field as well as a multiple sources noise field, and compared the proposed Cℓ_1-MP algorithm, proposed Sℓ_1-MP algorithm, conventional MP algorithm, and conventional Leaky-MP algorithm. From the simulation results in the directional sparse noise field, we concluded that the proposed algorithms (Cℓ_1-MP and Sℓ_1-MP) could i) increase the convergence speed, ii) reduce the active loudspeaker numbers in the steady state, and iii) decrease the noise reduction level in the steady state.

The major contribution made in this chapter is:

- We introduced ℓ_1 penalty to the multi-point algorithm to reduce the number of secondary sources and the computational complexity in a directional sparse noise field, resulting in two new algorithms: (i) the complex ℓ_1-norm constrained multi-point algorithm (Cℓ_1-MP), and (ii) the scalar ℓ_1-norm constrained multi-point algorithm (Sℓ_1-MP).

3.8 Related Publications

This chapter's work has been published in the following journal paper.

[105] J. Zhang, T. D. Abhayapala, P. N. Samarasinghe, W. Zhang, and S. Jiang, "Multichannel active noise control for spatially sparse noise fields", *J. Acoust. Soc. Am.*, vol. 140, no. 6, pp. EL510 – EL516, 2016.

Chapter 4

Wave Domain ANC: Basic Structure

Overview: *This chapter proposes wave-domain adaptive structure for noise cancellation within a large spatial region. We use fundamental solutions of the Helmholtz wave-equation as a basis function to express the noise field over a spatial region and show the wave-domain processing directly on the decomposition coefficients to control the entire region. A feedback control system is implemented using a microphone array and a loudspeaker array. The microphone array is placed at the boundary of the control region to measure the residual signals. The loudspeaker array is placed outside the region to generate the anti-noise signals. We develop an adaptive wave-domain filtered-x least mean square algorithm in a general noise field. We also incorporate a sparsity constraint to the wave-domain noise cancellation, and propose an ℓ_1-constrained wave-domain filtered-x least mean squared algorithm, which is mainly applicable to directional sparse noise fields. Simulation results demonstrate the performance and advantages of the proposed methods in terms of convergence speed and noise reduction levels over space.*

4.1 Introduction

As discussed in Chapter 3, the multi-point version of the LMS algorithm in the frequency domain (Section 3.3.1) and its variations (Section 3.3.2, etc.), are fairly straightforward and have been widely used in practice [31, 32, 106, 30]. One drawback of the conventional multichannel ANC system is that to achieve a continuous quiet zone, a large number of error microphones need to be uniformly placed inside the region to measure the residual signals so that the noise energy within the entire region can be cancelled completely.

Recently, ANC over space has been approached via wave field synthesis (WFS) based adaptive algorithms [107, 40, 41]. For example, in S. Spors and H. Buchner's work [40, 41], one loudspeaker array and two microphone arrays, including one reference microphone array placed outside the loudspeaker array and one error microphone array placed at the boundary of the quiet zone, are adopted and the feedforward ANC system is implemented. Significant noise cancellation over the entire region of interest has been achieved, for both interior and exterior noise control problems.

In this chapter, we propose a feedback ANC system in the wave domain using one loudspeaker array and one microphone array: a loudspeaker array to produce anti-noise signals and an error microphone array placed at the boundary of the desired quiet zone to measure the residual signals (see Figure 4.1). We represent the sound field using cylindrical harmonics expansion. We make a continuous loudspeaker array assumption, and propose an adaptive wave-domain FxLMS algorithm. After calculating the loudspeaker distribution coefficients, we utilize a discrete loudspeaker array to approximate the continuous loudspeaker distribution. In addition, we introduce the wave-domain algorithm with the ℓ_1-norm constraint, and design the discrete loudspeaker array directly to cancel noise in the directionally sparse noise field. The proposed wave-domain algorithms demonstrate good performance for spatial noise cancellation.

The rest of this chapter is organized as follows. In Section 2, we formulate the spatial ANC problem in the wave domain. We derive an adaptive wave-domain processing algorithm in Section 3, and further develop an ℓ_1-constrained wave-domain algorithm in Section 4. In Section 5, simulations are conducted to evaluate

the proposed algorithms in comparison with the conventional multi-point ANC algorithm. Summary and contributions are provided in Section 6.

4.2 Wave Domain ANC Formulation

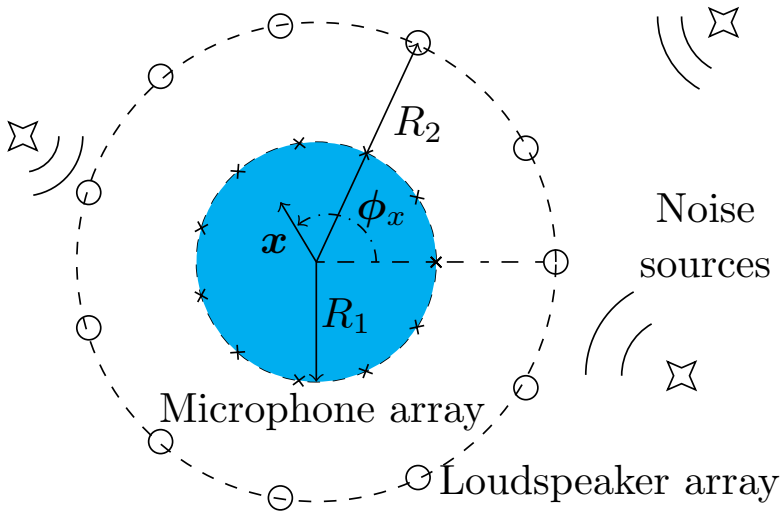

Figure 4.1: A spatial ANC region (blue) consists of a circular microphone array of radius R_1 and a circular loudspeaker array of radius R_2.

Instead of using measurements at the microphone points directly, the wave-domain approach employs the wave equation solutions as basis functions to express the sound field over the entire spatial region of interest, and designs the secondary signals accordingly.

For convenience, we rewrite (3.1) in Chapter 3. In the ANC system, as shown in Figure 4.1, the residual signal at any arbitrary observation point $\boldsymbol{x} \equiv \{r, \phi_{\boldsymbol{x}}\}$ is given by

$$e(\boldsymbol{x}, k) = \nu(\boldsymbol{x}, k) + s(\boldsymbol{x}, k). \tag{4.1}$$

Below we first transform each component in multi-point ANC system into the wave domain using cylindrical harmonic based wave equation solution, and then formulate the active noise control problem in terms of the wave-domain coefficients.

4.2.1 Primary noise field

As described in (2.41), the cylindrical harmonic based wave equation solution decomposes any homogeneous incident wave field $v(\boldsymbol{x}, k)$ observed at $\boldsymbol{x}$ into

$$v(\boldsymbol{x}, k) = \sum_{m=-\infty}^{\infty} \beta_m(k) J_m(kr) \exp(im\phi_{\boldsymbol{x}}), \tag{4.2}$$

where $J_m(\cdot)$ is the Bessel function of order m and $\exp(\cdot)$ denotes the exponential function [90]. The decomposition coefficients $\beta_m(k)$ represent the primary noise field in the wave domain.

Within the circular region $r \leq R_1$, we can use a finite number of modes to approximate[1] the noise field [108], thus (4.2) reduces to

$$v(\boldsymbol{x}, k) \approx \sum_{m=-M}^{M} \beta_m(k) J_m(kr) \exp(im\phi_{\boldsymbol{x}}), \tag{4.3}$$

where $M = \lceil ekR_1/2 \rceil$ [108, 109].

4.2.2 Secondary sound field

A circular array of L equiangularly placed loudspeakers are used to generate the control signals. Below, we represent the secondary sound field in two strategies: (i) Make a continuous loudspeaker array assumption first, and then design a discrete loudspeaker array to approximate the continuous source distribution; (ii) Design the discrete loudspeaker array directly.

Continuous loudspeaker array assumption

Using the strategy (i), we first assume a circular continuous loudspeaker array. A continuous loudspeaker array is an aperture that is a function of space variables and frequency [110].

Since the aperture function of the circular continuous loudspeaker $\chi(\boldsymbol{y}, k)$ is

[1] The infinite summation in (4.2) can be truncated at $M = \lceil ekr/2 \rceil$ [108, 109] due to inherent properties of Bessel functions

periodic with respect to the angle ϕ, using Fourier series expansion, $\chi(\boldsymbol{y}, k)$ can be represented as

$$\chi(\boldsymbol{y}, k) = \sum_{m=-\infty}^{\infty} \tau_m(k) \exp(im\phi_{\boldsymbol{y}}), \tag{4.4}$$

where $\tau_m(k)$ is the distribution coefficients.

Thus, the sound field generated can be written as

$$s(\boldsymbol{x}, k) = \int_0^{2\pi} \chi(\boldsymbol{y}, k) G(\boldsymbol{x}|\boldsymbol{y}, k) d\phi_{\boldsymbol{y}}. \tag{4.5}$$

When the observation points are inside the quiet zone, the ATF can also be parameterised in the wave domain [76] as

$$G(\boldsymbol{x}|\boldsymbol{y}, k) \approx \sum_{m=-M}^{M} T_m(\boldsymbol{y}, k) J_m(k\|\boldsymbol{x}\|) \exp(im\phi_{\boldsymbol{x}}), \tag{4.6}$$

where $T_m(\boldsymbol{y}, k)$ are ATF coefficients and assumed to be prior knowledge obtained from pre-calibration or room modelling.

Substituting (4.4) and (4.6) into (4.5) leads to the wave-domain representation of the sound field generated by the control sources, that is

$$s(\boldsymbol{x}, k) \approx \sum_{m=-M}^{M} \tau_m(k) \sigma_m(k) J_m(k\|\boldsymbol{x}\|) \exp(im\phi_{\boldsymbol{x}}), \tag{4.7}$$

where

$$\sigma_m(k) = \int_0^{2\pi} T_m(\boldsymbol{y}, k) \exp(im\phi_{\boldsymbol{y}}) d\phi_{\boldsymbol{y}}. \tag{4.8}$$

For example, for sound propagation in the free field, $G(\boldsymbol{x}|\boldsymbol{y}, k) = \frac{i}{4} H_0^{(1)}(k\|\boldsymbol{y} - \boldsymbol{x}\|)$ and $\sigma_m(k) = \frac{i}{4} H_m^{(1)}(kR_1)$, where $H_m^{(1)}(\cdot)$ denotes the first kind Hankel function of order m.

Given the estimated source distribution coefficients $\tau_m(k)$, a discrete loudspeaker array is designed to approximate the continuous loudspeaker distribution. For example, assuming $L \geq 2M + 1$ loudspeakers equiangularly placed in the cir-

cular array, the l^{th} loudspeaker driving signal is

$$d_\ell = \chi(\boldsymbol{y}_l, k)\Delta_\phi, \tag{4.9}$$

where $\Delta_\phi = 2\pi/L$.

Using the continuous loudspeaker array assumption to formulate the system, we can obtain the loudspeaker aperture function without using matrix inversion [110]. While, using strategy (i), two steps are required to calculate the loudspeaker driving signals: (a) make the continuous loudspeaker array assumption, and b) utilize the discrete loudspeaker array to approximate.

Discrete loudspeaker array

Using the second strategy, we design the discrete loudspeaker array $\boldsymbol{d}(k)$ directly without the continuous loudspeaker assumption.

For convenience, we rewrite the (3.2) in Chapter 3. The secondary sound field generated by discrete loudspeaker array can be represented by

$$s(\boldsymbol{x}, k) = \sum_{l=1}^{L} d_l(k) G(\boldsymbol{x}|\boldsymbol{y}_l, k), \tag{4.10}$$

where $G(\boldsymbol{x}|\boldsymbol{y}_l, k)$ is the acoustic transfer function, as defined in Chapter 3.

Using the cylindrical harmonic expansion, the generated secondary sound field inside the control region can also be represented by

$$s(\boldsymbol{x}, k) \approx \sum_{m=-M}^{M} \gamma_m(k) J_m(kr) \exp(im\phi_{\boldsymbol{x}}), \tag{4.11}$$

where coefficients $\gamma_m(k)$ represent the secondary sound field in the wave domain, and $M = \lceil ekR_1/2 \rceil$.

Similar to (4.6), the ATF in (4.10) can be parameterized in the wave domain [76] as

$$G(\boldsymbol{x}|\boldsymbol{y}_l, k) \approx \sum_{m=-M}^{M} T_{m,l}(k) J_m(kr) \exp(im\phi_{\boldsymbol{x}}). \tag{4.12}$$

By substituting (4.11) and (4.12) into (4.10), we can get

$$\gamma_m(k) = \sum_{l=1}^{L} d_l(k) T_{m,l}(k), \text{ for } m = -M, \cdots, M. \tag{4.13}$$

Therefore, in matrix form, the relationship between the secondary source decomposition coefficients and the loudspeaker weights is given by

$$\boldsymbol{\gamma}(k) = \boldsymbol{T}\boldsymbol{d}(k), \tag{4.14}$$

where $\boldsymbol{T}$ is a $(2M+1) \times L$ matrix, $\boldsymbol{d}$ is the vector of loudspeaker driving signals, and

$$T = \begin{bmatrix} T_{-M,1} & \cdots & T_{-M,L} \\ \vdots & \ddots & \vdots \\ T_{M,1} & \cdots & T_{M,L} \end{bmatrix}, d = \begin{bmatrix} d_1 \\ \vdots \\ d_L \end{bmatrix}. \tag{4.15}$$

Using the discrete loudspeaker array directly to formulate the system, wave-domain coefficients of the loudspeakers become $\gamma_m(k)$. Therefore, using strategy (ii), we calculate the vector form of the loudspeaker driving signals directly. While, matrix inversion is involved in the further derivation.

4.2.3 Residual signals

Substituting (4.3) and (4.11) into (4.1), the residual signals can be represented by

$$e(\boldsymbol{x}, k) \approx \sum_{m=-M}^{M} (\underbrace{\beta_m(k) + \gamma_m(k)}_{\alpha_m(k)}) J_m(kr) \exp(im\phi_{\boldsymbol{x}}), \tag{4.16}$$

where $\alpha_m(k)$ is the residual signal decomposition coefficients. In the ANC system, $e(\boldsymbol{x}, k)$ is the frequency domain sound pressure measured by the error microphones. From (4.16), we can obtain the wave-domain $\alpha_m(k)$, which is a good indicator of the residual sound field over the entire region.

In the proposed system (Figure 4.1), a circular microphone array is placed on the boundary of the quiet zone to measure the residual signals. Q microphones are equiangularly placed in the error microphone array to measure the residual noise

field $e(\boldsymbol{x}, k)$, i.e., the superposition of the noise field and sound field generated by the secondary noise sources. The error signals in the wave domain are written as

$$\alpha_m(k) = \frac{1}{QJ_m(kr)} \sum_{q=1}^{Q} e(\boldsymbol{x}_q, k) \exp(-i2\pi m(q-1)/Q),$$
$$m = -M, \ldots, M. \tag{4.17}$$

It is clear that the number of microphones required is $Q \geq 2M + 1$ so that all the wave-domain error signals can be obtained without causing a spatial aliasing problem. When Bessel function $J_m(kr)$ is close to zero, the coefficient error is amplified. The stability of the calculation will be reduced accordingly.

4.2.4 Wave-domain ANC

For the continuous loudspeaker array assumption, wave-domain noise cancellation is to design the secondary source coefficients $\tau_m(k)$ based on the ATF information $\sigma_m(k)$ so that the noise field $v(\boldsymbol{x}, k)$ characterised by its coefficients $\beta_m(k)$ is completely cancelled within the desired quiet zone. An optimal solution would be $\tau_m(k) = -\beta_m(k)/\sigma_m(k)$ if a stable noise field is assumed. However, in practice the noise field is always unknown and could be time-varying, so an adaptive algorithm is proposed in the next section.

For the discrete loudspeaker array without the continuous loudspeaker array assumption, the objective of wave-domain adaptive ANC is to design the loudspeaker driving signals $\boldsymbol{d}(k)$ based on the wave-domain residual signal $\alpha_m(k)$ and the acoustic transfer function coefficients $\boldsymbol{T}(k)$, so that the noise field $\boldsymbol{v}(\boldsymbol{x}, k)$ is cancelled by the generated secondary sound field $\boldsymbol{S}(\boldsymbol{x}, k)$ over the control region of interest.

The proposed ANC algorithms are introduced in the following sections.

4.3 Wave-domain FxLMS Algorithm

Now let us discuss the development of the wave-domain filtered-x least mean square (WD-FxLMS) algorithm for cancelling the above noise field. Here, for secondary

sound field, we make a continuous loudspeaker array assumption first, and then design the discrete loudspeaker array to approximate the continuous source distribution.

The residual signal in each iteration is expressed as

$$\widehat{\alpha}_m(n) = \beta_m(n) + \sigma_m \times \tau_m(n), \tag{4.18}$$

where n denotes the iteration step, and the wavenumber k is omitted for notational simplicity. The sourse coefficients $\tau_m(n)$ can be written by

$$\tau_m(n) = \omega_m(n)\tau_m^{(0)}, \tag{4.19}$$

where $\tau_m^{(0)}$ represents an arbitrary initial estimate of the source distribution coefficients, and $\omega_m(n)$ are the updated weights.

The adaptive algorithm minimises the instantaneous squared error, so that the cost function becomes

$$\xi_m(n) = |\widehat{\alpha}_m(n)|^2 = \widehat{\alpha}_m(n)\widehat{\alpha}_m^*(n). \tag{4.20}$$

Adopting the steepest descent algorithm, we have

$$\omega_m(n+1) = \omega_m(n) - \frac{\mu}{2}\nabla\xi_m(n). \tag{4.21}$$

Note that complex numbers are involved here, and thus we use the complex LMS algorithm to update the weights [111].

From (4.18) and (4.19), we can obtain

$$\frac{\partial\widehat{\alpha}_m^*(n)}{\partial\omega_m^*(n)} = [\sigma_m\tau_m^{(0)}]^*. \tag{4.22}$$

The gradient of the cost function can be written by

$$\nabla\xi_m(n) = 2\frac{\partial\xi_m(n)}{\partial\omega_m^*(n)}. \tag{4.23}$$

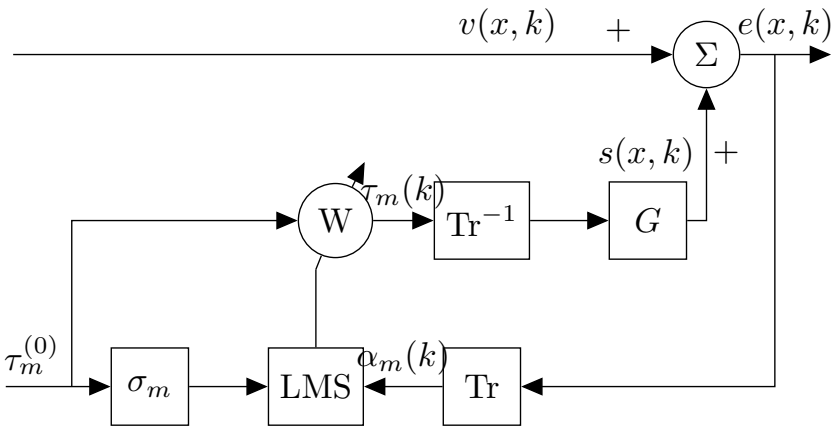

Figure 4.2: Block diagram of the wave-domain FxLMS algorithm for ANC. Blocks of Tr and Tr^{-1} represent the wave-domain transform and the inverse wave-domain transform, respectively.

Therefore, substituting (4.20) and (4.22) into (4.23), we can get

$$\nabla\xi_m(n) = 2\widehat{\alpha}_m(n)[\sigma_m\tau_m^{(0)}]^*. \tag{4.24}$$

Substituting (4.24) into (4.21), we have the wave-domain FxLMS algorithm,

$$\omega_m(n+1) = \omega_m(n) - \mu\widehat{\alpha}_m(n)[\sigma_m\tau_m^{(0)}]^*, \tag{4.25}$$

where the maximum step size $\mu_{\max} = 1/\|\sigma_m\tau_m^{(0)}\|^2$ [23]. The block diagram of the algorithm is shown in Figure 4.2.

4.4 Sparse Constrained Wave-domain FxLMS Algorithm

In this section, we develop an ℓ_1-norm constrained complex FxLMS algorithm for wave-domain noise cancellation. Differ from Section 4.3, for secondary sound field, here we solve the sparsity constrained ANC problem by focusing directly on the discrete loudspeaker array.

From (4.3), the cylindrical harmonic coefficients of the primary noise field are

represented by $\beta_m(k)$. Similarly, from (4.17), the cylindrical harmonic coefficients of the residual signal are represented by $\alpha_m(k)$.

Therefore, the wave-domain error function is given by

$$\boldsymbol{\alpha}(n) = \boldsymbol{\beta}(n) + \boldsymbol{\gamma}(n), \tag{4.26}$$

where $\boldsymbol{\alpha}(n) = \{\alpha_{-M}(n), \ldots, \alpha_M(n)\}^T$, $\boldsymbol{\beta}(n) = \{\beta_{-M}(n), \ldots, \beta_M(n)\}^T$ and $\boldsymbol{\gamma}(n) = \{\gamma_{-M}(n), \ldots, \gamma_M(n)\}^T$. The wavenumber k is omitted for notational simplicity.

All three terms are $(2N+1)-$long vectors in the complex domain. An FxLMS type formulation of (4.26) is

$$\boldsymbol{\alpha}(n) = \boldsymbol{\beta}(n) + \mathrm{diag}(\boldsymbol{\sigma})\boldsymbol{w}(n), \tag{4.27}$$

where $\boldsymbol{\sigma}$ is ATF coefficients in the wave domain, and $\boldsymbol{\sigma} = [\sigma_{-M}, \cdots, \sigma_M]$.

Note that $\boldsymbol{w}$ is not directly populated with loudspeaker weights $\boldsymbol{d}$ as before. The relationship between $\boldsymbol{w}$ and $\boldsymbol{d}$ is

$$\boldsymbol{w} = \boldsymbol{E}\boldsymbol{d}, \tag{4.28}$$

where $\boldsymbol{E}$ is the transformation matrix, and

$$\boldsymbol{E} = \begin{bmatrix} e^{iM\phi_1} & \ldots & e^{iM\phi_L} \\ \vdots & \ddots & \vdots \\ e^{-iM\phi_1} & \ldots & e^{-iM\phi_L} \end{bmatrix}. \tag{4.29}$$

Similar to the multi-point case in Chapter 3, the cost function of the ℓ_1 constrained wave-domain algorithm can be written by

$$\boldsymbol{\xi}_{\ell_1-\mathrm{WD}}(n) = \frac{1}{2}\boldsymbol{\alpha}(n)^2 + \lambda\|\boldsymbol{d}(n)\|_1, \tag{4.30}$$

where λ is a controllable parameter that determines the degree of zero attraction for the adaptive filter coefficients [112].

Using the steepest descent algorithm to calculate the updated equation in the

wave domain, the gradient term in (4.21) can be written as

$$\nabla \boldsymbol{\xi}_{\ell_1-\mathrm{WD}}(n) = \underbrace{\nabla \frac{1}{2}\boldsymbol{\alpha}(n)^2}_{\nabla \boldsymbol{\xi}_1} + \underbrace{\nabla \lambda \|\boldsymbol{d}(n)\|_1}_{\nabla \boldsymbol{\xi}_2}. \tag{4.31}$$

From the wave-domain Filtered-X Least Mean Square algorithm [96], the term $\nabla \boldsymbol{\xi}_1$ of (4.31) is simply represented by

$$\nabla \boldsymbol{\xi}_1 = (\mathrm{diag}(\boldsymbol{\sigma}))^* \boldsymbol{\alpha}. \tag{4.32}$$

To find $\nabla \boldsymbol{\xi}_2$ of (4.31), we use its relationship to the conjugate derivative [50]

$$\nabla \boldsymbol{\xi}_2 = 2\frac{\partial \boldsymbol{\xi}_2}{\partial \boldsymbol{w}^*}, \tag{4.33}$$

and approximate it by the summation of the real and the imaginary part

$$\frac{\partial \boldsymbol{\xi}_2}{\partial \boldsymbol{w}^*} \approx \lambda\left(\frac{\partial \|\Re(\boldsymbol{d})\|_1}{\partial \boldsymbol{w}^*} + \frac{\partial \|\Im(\boldsymbol{d})\|_1}{\partial \boldsymbol{w}^*}\right). \tag{4.34}$$

If the complex $\boldsymbol{w}$ is decomposed into its real and imaginary parts as $\boldsymbol{w} = \boldsymbol{x} + i\boldsymbol{y}$, the complex partial differentiation based on $\boldsymbol{w}^*$ can be separated [104] by

$$\begin{aligned}
\frac{\partial \|\Re(\boldsymbol{d})\|_1}{\partial \boldsymbol{w}^*} &= \frac{1}{2}\left(\frac{\partial \|\Re(\boldsymbol{d})\|_1}{\partial \boldsymbol{x}} + i * \frac{\partial \|\Re(\boldsymbol{d})\|_1}{\partial \boldsymbol{y}}\right), \\
\frac{\partial \|\Im(\boldsymbol{d})\|_1}{\partial \boldsymbol{w}^*} &= \frac{1}{2}\left(\frac{\partial \|\Im(\boldsymbol{d})\|_1}{\partial \boldsymbol{x}} + i * \frac{\partial \|\Im(\boldsymbol{d})\|_1}{\partial \boldsymbol{y}}\right).
\end{aligned} \tag{4.35}$$

Since $\boldsymbol{w} = \boldsymbol{E}\boldsymbol{d}$, each item in (4.35) in the wave domain can be given by

$$\frac{\partial \|\Re(\boldsymbol{d})\|_1}{\partial \boldsymbol{x}} = \Re((\boldsymbol{E}^{-1})^T) * \mathrm{sign}(\Re(\boldsymbol{d}))$$

$$\frac{\partial \|\Re(\boldsymbol{d})\|_1}{\partial \boldsymbol{y}} = -\Im((\boldsymbol{E}^{-1})^T) * \mathrm{sign}(\Re(\boldsymbol{d}))$$

$$\frac{\partial \|\Im(\boldsymbol{d})\|_1}{\partial \boldsymbol{x}} = \Im((\boldsymbol{E}^{-1})^T) * \mathrm{sign}(\Im(\boldsymbol{d}))$$

$$\frac{\partial \|\Im(\boldsymbol{d})\|_1}{\partial \boldsymbol{y}} = \Re((\boldsymbol{E}^{-1})^T) * \text{sign}(\Im(\boldsymbol{d})). \tag{4.36}$$

Substituting (4.36) into (4.34), $\partial \boldsymbol{\xi}_2 / \partial \boldsymbol{w}^*$ becomes

$$\begin{aligned}\frac{\partial \xi_2}{\partial \boldsymbol{w}^*} =& \frac{1}{2}\lambda\{[\Re((\boldsymbol{E}^{-1})^T) - i * \Im((\boldsymbol{E}^{-1})^T)] * [\text{sign}(\Re(\boldsymbol{E}^{-1}\boldsymbol{w})) \\ &+ i * \text{sign}(\Im(\boldsymbol{E}^{-1}\boldsymbol{w}))]\}. \end{aligned} \tag{4.37}$$

Thus, the ℓ_1-norm constrained wave-domain FxLMS algorithm (ℓ_1-WD-FxLMS) can be derived as

$$\begin{aligned}\boldsymbol{w}(n+1) =& \boldsymbol{w}(n) - \frac{1}{2}\mu(\text{diag}(\boldsymbol{\sigma}))^*\boldsymbol{\alpha} \\ &- \frac{1}{2}\mu\lambda\{[\Re((\boldsymbol{E}^{-1})^T) - i * \Im((\boldsymbol{E}^{-1})^T)] * [\text{sign}(\Re(\boldsymbol{E}^{-1}\boldsymbol{w})) \\ &+ i * \text{sign}(\Im(\boldsymbol{E}^{-1}\boldsymbol{w}))]\}. \end{aligned} \tag{4.38}$$

4.5 Simulation Results

In this section, we conduct simulations to evaluate the proposed wave-domain adaptive algorithms (WD-FxLMS and ℓ_1-WD-FxLMS) in terms of the noise reduction on the boundary, noise reduction inside the region, residual energy inside the region and convergence speed. For ℓ_1-WD-FxLMS algorithm, we also evaluate the ℓ_1 norm of the loudspeaker driving signals.

We consider following four cases: (i) single-frequency noise field, free-field environment (ii) single-frequency noise field, room reverberant environment; (iii) multi-frequency noise field, free-field environment; (iv) multi-frequency noise field, room reverberant environment. In case (i), we compare WD-FxLMS, ℓ_1-WD-FxLMS, ℓ_1-MP-FxLMS, and the conventional MP-FxLMS algorithm. In cases (ii), (iii), and (iv), we compare the WD-FxLMS and the conventional MP-FxLMS algorithm.

In the simulation, the quiet zone is a circular region of radius 1 m ($R_1 = 1$ m). We place the loudspeaker array on a circle of $R_2 = 2$ m and the microphones are equally spaced on the boundary of the quiet zone ($R_q = R_1 = 1$ m). A signal-to-noise (SNR) ratio of 40 dB is added to the microphone recordings.

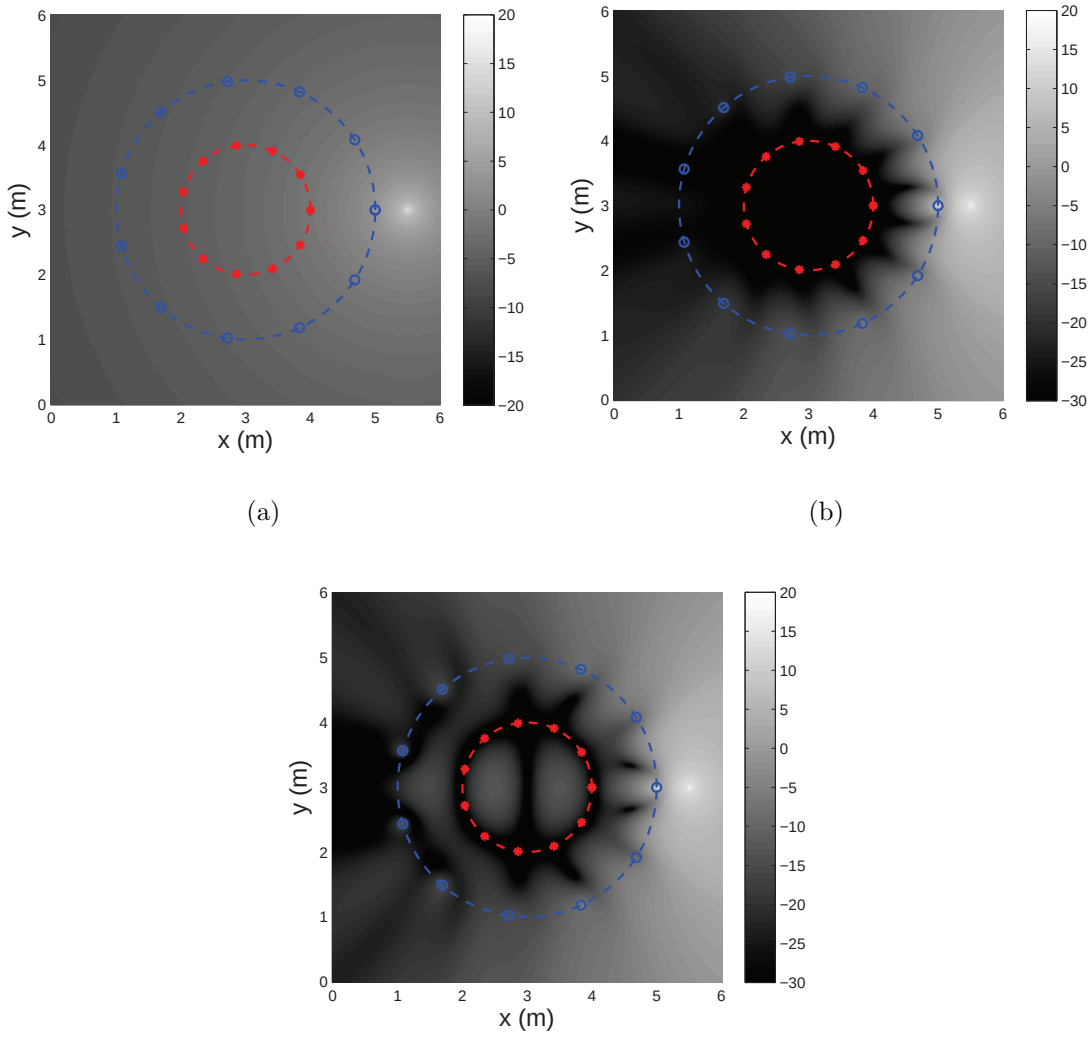

(a)

(b)

(c)

Figure 4.3: The results of ANC in the free-field. The inner array is the microphone array, outer array is the loudspeaker array. (a) The energy of the initial noise field. (b) The residual energy after 30 iterations of WD-FxLMS. (c) The residual energy after 30 iterations of MP-FxLMS.

To evaluate the noise reduction performance inside the control region, sound pressures at $Z = 1296$ points uniformly placed inside the regions $\boldsymbol{e}_{in}$ are examined. We define the instantaneous noise reduction inside the interest region $N_{\mathrm{r}}^{\mathrm{in}}(n)$ as follows,

$$N_{\mathrm{r}}^{\mathrm{in}}(n) \triangleq 10\log_{10}\frac{\sum_z E\{|e_{\mathrm{in}\_z}(n)|^2\}}{\sum_z E\{|e_{\mathrm{in}\_z}(0)|^2\}}, \tag{4.39}$$

where $e_{\mathrm{in}\_z}(n)$ denotes the residual signals at the z^{th} point inside the region at the n^{th} iteration, and $e_{\mathrm{in}\_z}(0)$ represents the primary noise field at the z^{th} point in the region.

4.5.1 Single-frequency noise field

We first investigate the ANC performance in a single-frequency noise field due to a single 2D point source. The noise source is a 2D omni-directional point source located at (5.5, 3), and operates at the frequency of 200 Hz. According to (4.3) and the rule of thumb [108], such a noise field within the desired quiet zone (radius of 1 m) needs $m \in [-5, 5]$ orthogonal modes to represent; thus, we place 11 loudspeakers and 11 microphones in each corresponding array.

Case 1—Free-field Environment

Plots in Figure 4.3 show the results of cancelling the noise field in the free-field environment using the proposed WD-FxLMS and conventional MP-FxLMS. Compared with Figure 4.3(a), after 30 iterations of wave-domain adaptive processing, Figure 4.3(b) shows that the noise energy inside the entire quiet zone has been reduced to a very low level. With the same loudspeaker array and microphone array setup, the conventional MP-FxLMS algorithm [32] however can only achieve noise cancellation at the microphone positions or at points very close to the microphones, as shown in Figure 4.3(c). Inside the quiet zone, a fairly high level of the noise field still exists.

The results in Figure 4.4 demonstrate the spatial residual signal energy over the entire control region using the proposed ℓ_1-WD-FxLMS algorithm, proposed ℓ_1-MP-FxLMS algorithm, and conventional MP-FxLMS algorithm. Compared with Figure4.4(a), Figure 4.4(d) shows a significant noise reduction in the designated

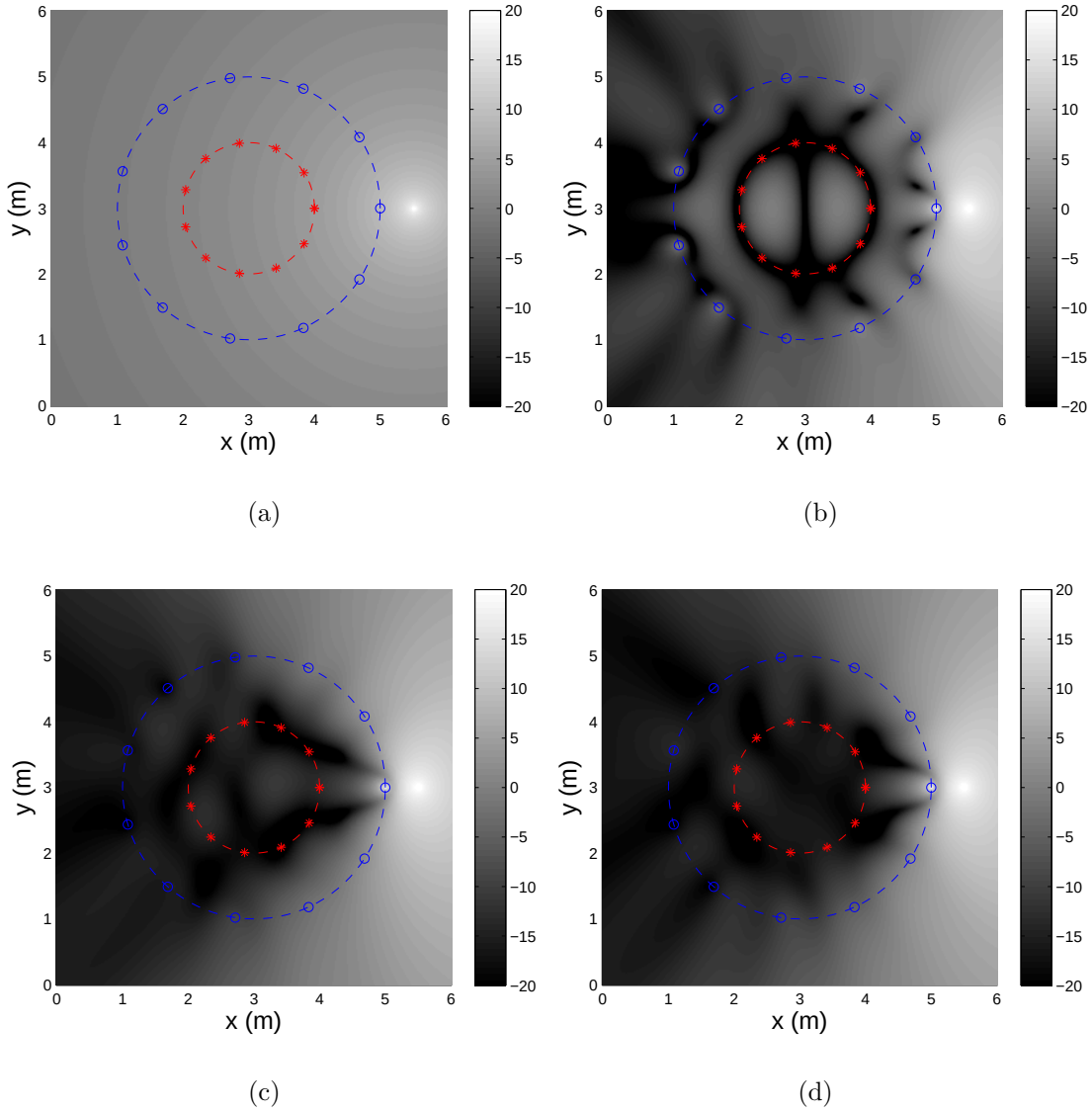

Figure 4.4: The results of ANC in the free-field. The inner array is a microphone array and the outer array is a loudspeaker array. (a) The energy of the initial sparse noise field. The residual energy after 30 iterations of (b) MP-FxLMS, (c) ℓ_1-MP-FxLMS, and (d) ℓ_1-WD-FxLMS.

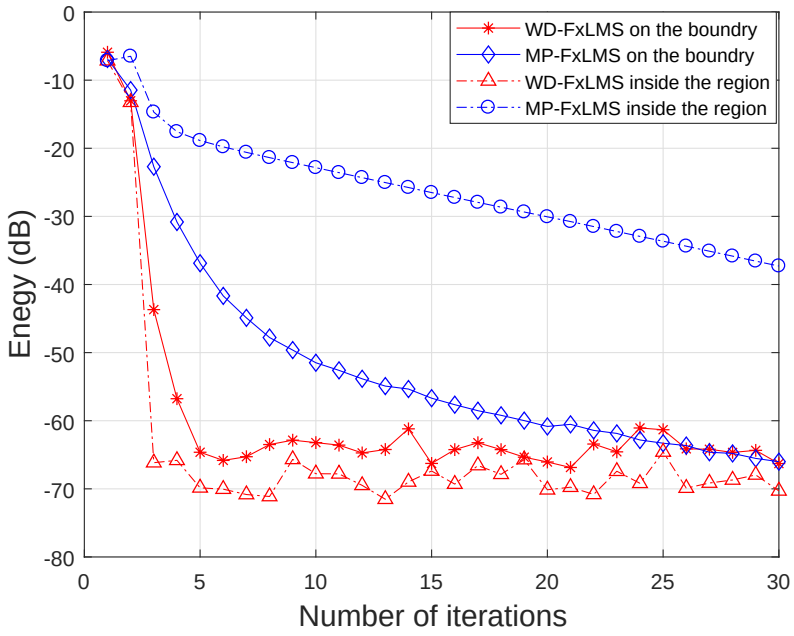

Figure 4.5: Comparison of convergence performance for noise cancellation using WD-FxLMS and MP-FxLMS algorithm in the free-field in the first 30 iterations.

region after 30 iterations of ℓ_1-WD-FxLMS. For comparison, the MP-FxLMS algorithm can only achieve noise reduction on the boundary of the region of interest after the same number of iterations, as shown in Figure 4.4(b). Here, Figure 4.4(c) demonstrates the spatial ANC performance using the ℓ_1-MP-FxLMS algorithm, which is the ℓ_1-norm constrained multi-point algorithm proposed in [113].

Figure 4.5 compares the convergence performance of the WD-FxLMS and MP-FxLMS algorithm, where 11 microphone recordings are used to evaluate the noise reduction on the boundary and measurements from 1296 points inside the regions are used to evaluate the noise reduction inside the region. The WD-FxLMS demonstrates faster convergence at both recording positions and at points inside the region. In particular, for the noise reduction inside the region, the ANC process converges after 5 iterations using the WD-FxLMS algorithm, while it has not converged after 30 iterations using the MP-FxLMS algorithm. Figure 4.6 compares the noise reduction after convergence in the same scenario. In the free-field, for both noise reduction on the boundary and noise reduction inside the region, MC-

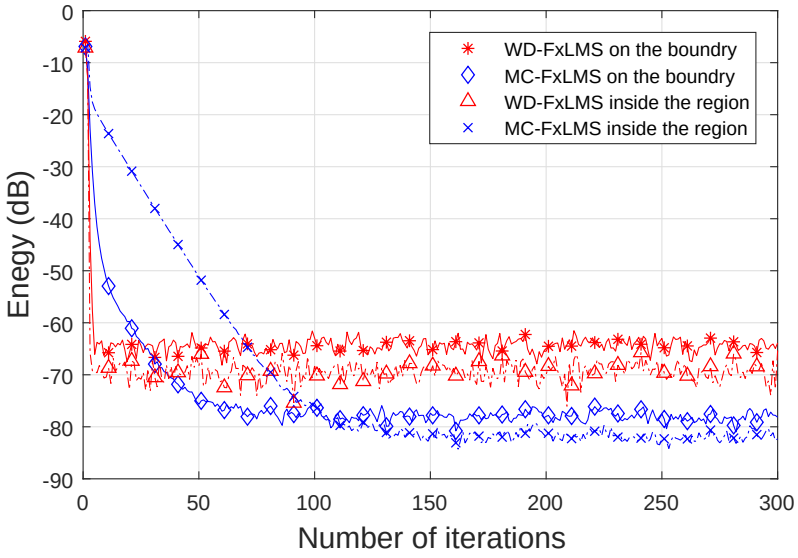

Figure 4.6: Comparison of noise cancellation after convergence using WD-FxLMS and MP-FxLMS algorithm in the free-field in the first 300 iterations.

FxLMS method (blue curves) has better noise reduction (about 10-15 dB) on the steady state compared to the WD-FxLMS method.

Plots in Figure 4.7 and Figure 4.8 compare the convergence performance for the proposed WD-FxLMS, proposed ℓ_1-WD-FxLMS, proposed ℓ_1-MP-FxLMS, and the conventional MP-FxLMS in a time-varying noise field. The amplitude of the noise field increases at iteration 50.

Figure 4.7 shows the comparison of convergence performance vs spatial noise reduction. The solid lines in Figure 4.7 show the convergence performance of ℓ_1-WD-FxLMS. As expected, the convergence speed of ℓ_1-WD-FxLMS algorithms is much faster than that of ℓ_1-MP-FxLMS for all values of λ. For each λ, the ℓ_1-WD-FxLMS demonstrates more noise reduction and faster convergence, so that it tracks the variation of the noise field and achieves better performance than the ℓ_1-MP-FxLMS. Meanwhile, compared to the solid red line with $\lambda = 0$ in Figure 4.7 (which represents the WD-FxLMS [96]), adding the sparse constraint decreases the noise reduction level of the ANC system (blue and black solid line in Figure 4.7).

The plots in Figure 4.8 show the comparison of the convergence performance vs the ℓ_1-norm of the loudspeaker weights. With the sparse constraints added in

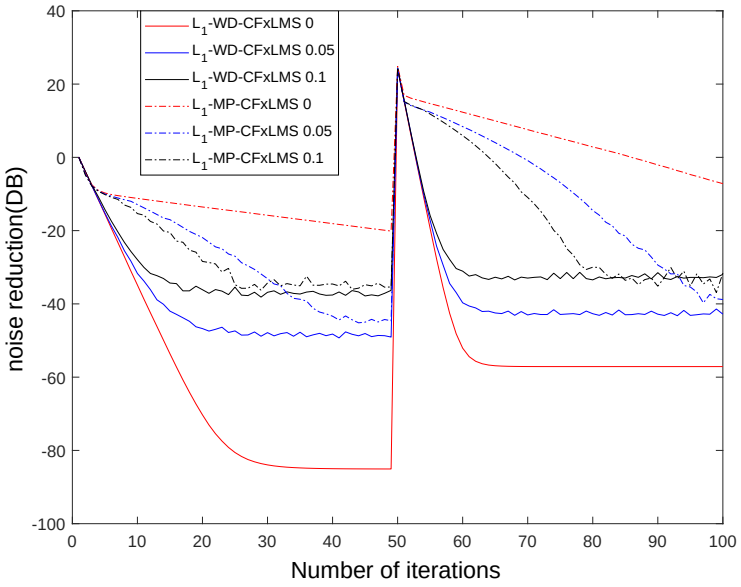

Figure 4.7: Comparison of convergence performance for noise cancellation using ℓ_1-WD-CFxLMS and ℓ_1-MP-CFxLMS algorithms with variable zero attractor strength $(\lambda = 0, 0.05, 0.1)$.

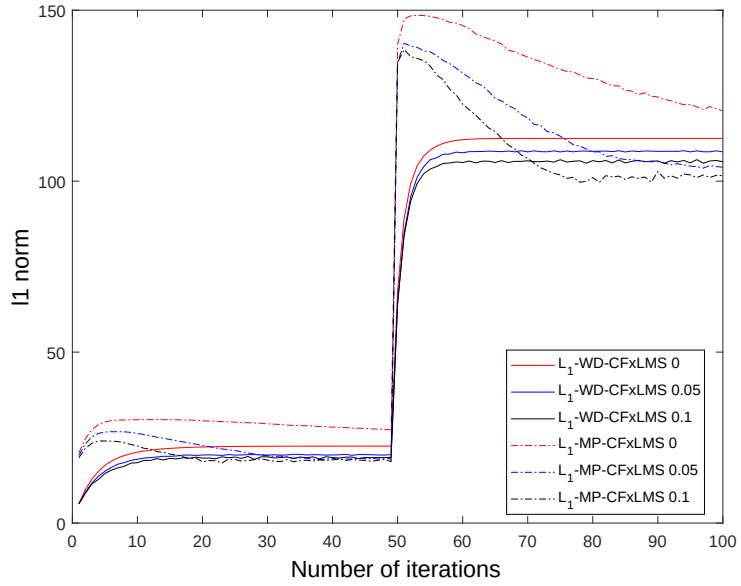

Figure 4.8: Comparison of convergence performance for ℓ_1-norm of the loudspeaker weights using ℓ_1-WD-CFxLMS and ℓ_1-MP-CFxLMS algorithms with variable zero attractor strength $(\lambda = 0, 0.05, 0.1)$.

the WD-FxLMS and MP-FxLMS algorithms, the ℓ_1-norm of loudspeaker weights can be reduced, indicating lower total energy of the loudspeaker weights.

From Figure 4.7 and Figure 4.8, we can also conclude that a large value of λ will result in less noise reduction and a lower ℓ_1 norm of the loudspeaker driving signal in the steady state, for both constrained wave-domain and constrained multi-point algorithms.

Case 2—Reverberant Environment

The simulations in the reverberant environment are made in a room 6 m×6 m with all side walls having the reflection coefficient of 0.9. The reflections are simulated by image source method [114]. The origin of the loudspeaker and microphone arrays is the centre of the room. The same noise source location as in the case of free-field environment is simulated, which generates a time-invariant noise field.

The results in Figure 4.9 demonstrate the spatial ANC performance after 30 iterations. Compared with Figure4.9(a), the proposed WD-FxLMS algorithm can cancel the noise field completely within the desired quiet zone, as shown in Figure 4.9(b). While the conventional MP-FxLMS can only cancel noises at the microphone positions or the boundary of the quiet zone, as shown in Figure 4.9(c).

Figure 4.10 compares the convergence performance of the WD-FxLMS and MP-FxLMS algorithms. Both algorithms can achieve noise cancellation at the recording positions, i.e., the boundary of the designated quiet zone. It can be seen clearly that the convergence speed of the proposed WD-FxLMS is much faster than that of the conventional MP-FxLMS algorithm. For all the points inside the designed region, only the wave-domain adaptive processing can achieve noise energy reduction to a very low level. We can conclude that the proposed WD-FxLMS algorithm is much more effective in the reverberant environment, especially for achieving noise cancellation over a spatial region.

4.5.2 Multi-frequency noise field

We next investigate the ANC performance of the proposed WD-FxLMS algorithm in multi-frequency noise field. The system is designed at the frequency of 1 kHz.

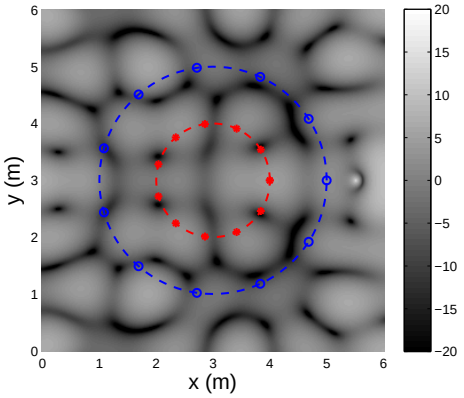

(a)

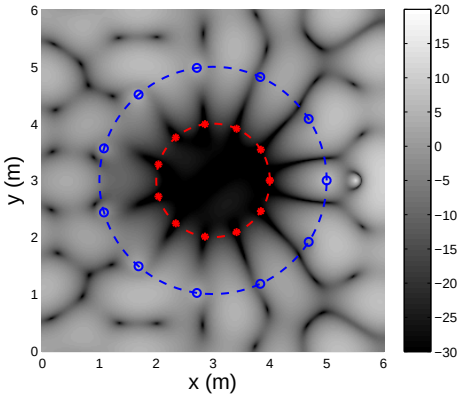

(b)

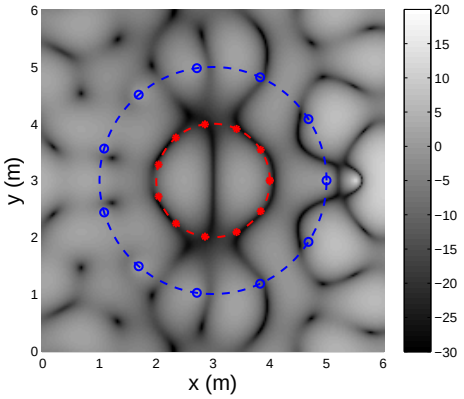

(c)

Figure 4.9: Results of ANC in reverberant environment. The inner and outer arrays are microphone array and loudspeaker array, respectively. (a) The energy of the initial noise field. The residual energy after 30 iterations of (b) WD-FxLMS, and (c) MP-FxLMS.

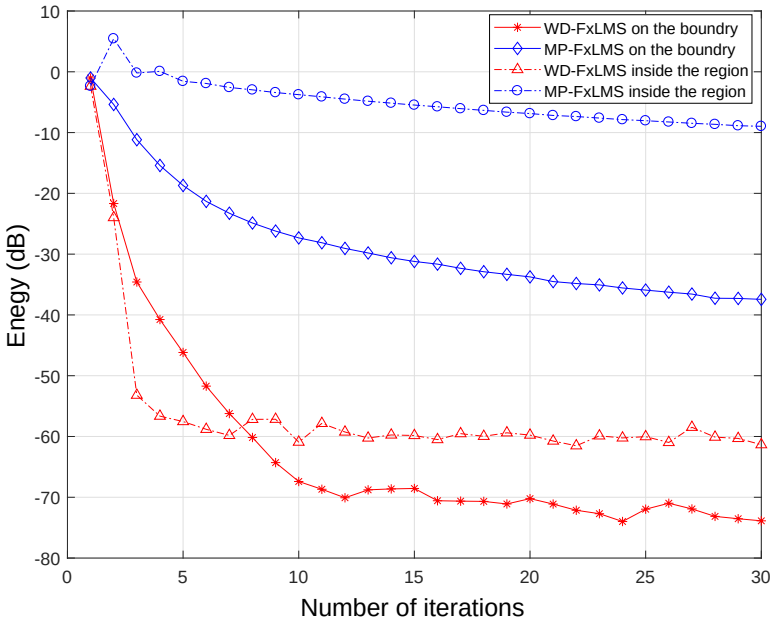

Figure 4.10: Comparison of convergence performance for noise cancellation using WD-FxLMS and MP-FxLMS algorithm in reverberant environment.

The noise field within a radius of 1 m is due to 10 noise sources uniformly distributed on a circle 2.5 m from the origin and at angles $[0 : 36 : 324]^\circ$.

Figure 4.11 shows that for all frequencies below 1 kHz, using the WD-FxLMS algorithm, the noise can be reduced significantly within the desired quiet zone. The average noise reduction is around 80 dB and 50 dB in the free-field and reverberant environment, respectively. Notice that the performance is significantly degraded at 600 Hz and 900 Hz. This is due to the fact that at these particular frequencies, the Bessel functions are close to zero (i.e., $J_m(kr) \approx 0$) and the coefficient error is amplified. This problem can be avoided by placing two closely spaced microphone arrays [76].

4.6 Summary and Contributions

In this chapter, we presented adaptive wave-domain methods to achieve noise cancellation over a spatial region using feedback control structure. We proposed a

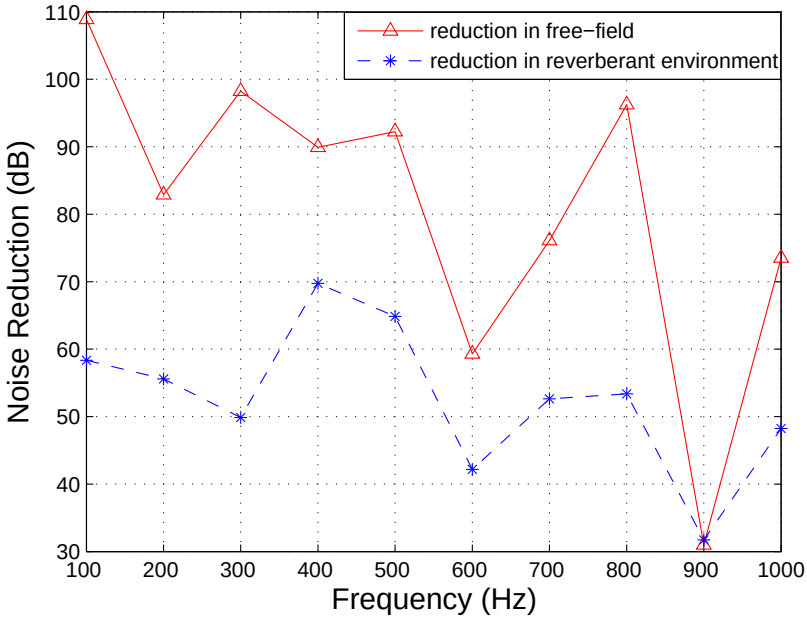

Figure 4.11: Noise reduction using WD-FxLMS algorithm after 30 iterations in multi-frequency noise field.

feedback control system using a circular microphone array to measure the residual signals and a circular loudspeaker array to produce anti-noise signals. We represented all the variables of the noise field in the wave domain and formulated the spatial ANC problem in terms of the wave-domain coefficients. We proposed the WD-FxLMS algorithm, and it was evaluated in both free-field and reverberant environments and compared with the conventional multi-point ANC algorithm. Simulation results showed that the proposed WD-FxLMS algorithm achieved significant noise reduction over the entire design region with fast convergence speed. We also introduced the sparse constraint in the WD-FxLMS which can reduce the total energy of the loudspeaker weights. There existed a trade off between noise reduction and the energy of the loudspeaker weights.

The major contributions made in this chapter are:

- We proposed a feedback control system using a circular microphone array and a circular loudspeaker array, and formulated the spatial ANC problem in terms of the wave-domain coefficients.

- We proposed a wave-domain FxLMS algorithm (WD-FxLMS) for active noise control over spatial region in general noise field.
- Weproposed a ℓ_1-norm constrained wave-domain FxLMS algorithm (ℓ_1-WD-FxLMS) for active noise control over a spatial region in a directional sparse noise field.

4.7 Related Publications

This chapter's work has been published in the following conference proceedings:

[96]: J. Zhang, W. Zhang, and T. D. Abhayapala, "Noise cancellation over spatial regions using adaptive wave domain processing", in *IEEE Workshop on Applications of Signal Processing to Audio and Acoustics (WASPAA) 2015*, New Paltz, NY, USA, Oct. 2015, pp. 1-5

[113]: J. Zhang, T.D. Abhayapala, P. N. Samarasinghe, W. Zhang and S. Jiang, "Sparse complex FxLMS for active noise cancellation over spatial regions", in *IEEE International Conference on Acoustics, Speech and Signal Processing (ICASSP) 2016*, Shanghai, China, March 2016, pp. 524-528

Chapter 5

Wave Domain ANC: Different Cost Functions and Adaptations

Overview: ***In this chapter, we investigate wave-domain spatial active noise control in terms of different cost functions and different update variables. We propose normalized wave-domain active noise control algorithms based on two minimization problems, (i) minimizing the wave-domain residual signal coefficients and (ii) minimizing the acoustic potential energy over the region. We derive the update equations with respect to two variables, (a) the loudspeaker driving signals and (b) wave-domain secondary source coefficients. Simulation results demonstrate the effectiveness of the four proposed algorithms, more specifically the convergence speed, energy of the loudspeaker driving signals, and the noise cancellation performance in terms of the noise reduction level and acoustic potential energy reduction level over the entire spatial region. We also investigate the spatial active noise control performance with limited secondary sources in the simulations.***

5.1 Introduction

As discussed in Chapter 3, the multi-point control systems minimize the sum of the squared pressures, which is equal to minimizing the potential energy density

at the microphone locations. Although these approaches lead to significant noise reduction at the target points, the consistency over a continuous spatial region is low.

In Chapter 4, we developed the wave domain ANC structure and proposed FxLMS algorithm and the ℓ_1-norm constrained FxLMS algorithm in wave domain [96, 113]. We used cylindrical/spherical harmonics as basis functions and their respective coefficients to represent the noise field and secondary field over the desired spatial region. Instead of minimizing the sum of the squared error signals [64], wave-domain ANC tends to minimize the harmonic coefficients, which in turn control the entire spatial region directly. The simulation results [96, 113] showed that wave-domain ANC achieved significant noise cancellation over the entire region of interest with faster convergence speeds.

In this chapter, we further investigate the wave domain ANC strategy. As discussed in Chapter 2, ANC using multi-point structure can be solved by (i) minimizing the squared residual signals and (ii) minimizing the energy densities. In this chapter, we investigate the spatial ANC problem by solving the minimization of (i) squared wave domain coefficients and (ii) acoustic potential energy. For each minimization problem, we update two different variables: (i) driving signals, and (ii) wave domain coefficients. We propose normalized version of the wave domain algorithms, and evaluate the proposed algorithms in terms of noise reduction over the region, acoustic potential energy reduction over the region and convergence performance. Simulations are conducted in both free field and reverberant environment, and in different numbers of loudspeaker setup.

The rest of the chapter is organized as follows. In Section 5.2, we refer back to Section 4.2, and formulate the spatial noise cancellation problem and the ANC system in the wave domain. The wave-domain multichannel ANC algorithms minimizing the squared residual signal coeffients are proposed in Section 5.3, and the wave-domain multichannel ANC algorithms minimizing the acoustic potential energy are proposed in Section 5.4. We demonstrate the simulation results to compare the ANC performance of the proposed wave-domain methods and the conventional multi-point method in Section 5.5, and draw some conclusions in Section 5.6.

5.2 Problem Formulation

In this chapter, we adopt the same array setup (Figure 5.1) as in Chapter 4, and address the ANC problem in 2-D space. The theory we develop in this chapter can be extended to 3-D space.

5.2.1 System model

The wave domain representation of all the variables in the ANC system are same as Section 4.2. In the wave domain, the primary sound field ($v(\boldsymbol{x}, k)$), secondary sound field ($s(\boldsymbol{x}, k)$), and residual sound field ($e(\boldsymbol{x}, k)$) can be represented by $\beta_m(k)$, $\gamma_m(k)$, and $\alpha_m(k)$, respectively.

For convenience, we rewrite some formulas of wave domain representation in Section 4.2.

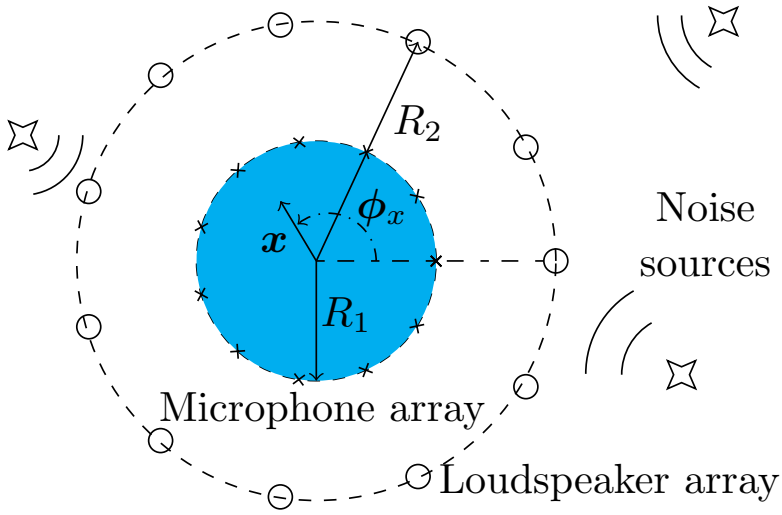

Figure 5.1: A spatial ANC region (blue) consists of a circular microphone array of radius R_1 and a circular loudspeaker array of radius R_2.

Within the circular region $r \leq R_1$, the cylindrical harmonic based wave equation solution decomposes any incident wave field $v(\boldsymbol{x}, k)$ observed at $\boldsymbol{x}$ into

$$v(\boldsymbol{x}, k) = \sum_{m=-M}^{M} \beta_m(k) J_m(kr) \exp(im\phi_{\boldsymbol{x}}). \tag{5.1}$$

Using the cylindrical harmonic expansion, the generated secondary sound field inside the control region can also be represented by

$$s(\boldsymbol{x}, k) \approx \sum_{m=-M}^{M} \gamma_m(k) J_m(kr) \exp(im\phi_{\boldsymbol{x}}). \tag{5.2}$$

In this chapter, we utilize the second strategy (4.2.2) to formulate the secondary sound field, and design the discrete loudspeaker array $\boldsymbol{d}(k)$ directly without the continuous loudspeaker assumption.

In matrix form, the relationship between the secondary source decomposition coefficients and the loudspeaker weights are given by

$$\boldsymbol{\gamma}(k) = \boldsymbol{T}\boldsymbol{d}(k). \tag{5.3}$$

In this section, ATF coefficients T are assumed to be prior knowledge obtained from pre-calibration or room modelling.

The residual signals on the microphone points can be represented by

$$e(\boldsymbol{x}, k) \approx \sum_{m=-M}^{M} \underbrace{(\beta_m(k) + \gamma_m(k))}_{\alpha_m(k)} J_m(kr) \exp(im\phi_{\boldsymbol{x}}). \tag{5.4}$$

The error signal coefficients in the wave domain are written as

$$\alpha_m(k) = \frac{1}{QJ_m(kr)} \sum_{q=1}^{Q} e(\boldsymbol{x}_q, k) \exp(-i2\pi m(q-1)/Q), \qquad m = -M, \ldots, M. \tag{5.5}$$

5.2.2 Multichannel wave-domain active noise control

In this chapter, we adopt a block-wise operation and transform the microphone measurements (residual signals) into the time-frequency domain, and decompose the residual noise field into the wave-domain coefficients using (5.5).

In the wave-domain adaptive algorithm, the residual signals in each iteration

(the n^{th} time block) can be expressed as

$$\boldsymbol{\alpha}(n,k) = \boldsymbol{\beta}(n,k) + \boldsymbol{\gamma}(n,k), \tag{5.6}$$

where $\boldsymbol{\alpha}(n,k) = [\alpha_{-M}(n,k), \ldots, \alpha_M(n,k)]^T$, the superscript $(\cdot)^T$ denotes the transpose of a vector,

$$\boldsymbol{\beta}(n,k) = [\beta_{-M}(n,k), \ldots, \beta_M(n,k)]^T,$$

and

$$\boldsymbol{\gamma}(n,k) = [\gamma_{-M}(n,k), \ldots, \gamma_M(n,k)]^T.$$

From here onwards, we omit the dependency k in each vector for notational simplicity, thus have

$$\boldsymbol{\alpha}(n) = \boldsymbol{\beta}(n) + \boldsymbol{\gamma}(n). \tag{5.7}$$

In the next two sections, we derive different wave-domain adaptive algorithms by solving two minimization problems, (a) squared residual signal coefficients, and (b) acoustic potential energy.

5.3 Wave Domain ANC Algorithms - Minimization of Squared Residual Signal Coefficients

By minimizing the sum of the squared residual signal coefficients, the cost function becomes

$$\xi_1(n) = \sum_{m=-M}^{M} |\alpha_m(n)|^2 = \boldsymbol{\alpha}^H(n)\boldsymbol{\alpha}(n), \tag{5.8}$$

where the superscript $(\cdot)^H$ denotes the conjugate transpose. Using the steepest descent algorithm, the adaptive algorithm follows the update equation

$$\boldsymbol{w}(n+1) = \boldsymbol{w}(n) - \frac{\mu}{2}\boldsymbol{\nabla}\xi_1(n), \tag{5.9}$$

where $\boldsymbol{w}$ is the update variable and μ is the step size.

Below we derive the wave-domain update function for two cases, (1) loudspeaker weights are updated directly, and (2) secondary sound field coefficients are updated

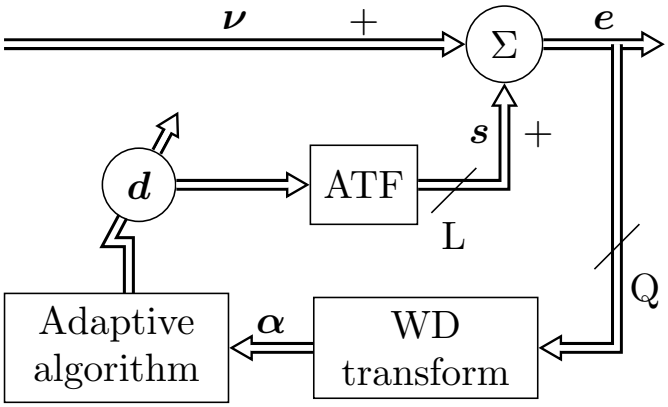

Figure 5.2: Block diagram of wave-domain ANC system, when updating the loudspeaker driving signals. The WD transform block represents the wave-domain transform for the residual signals.

directly.

5.3.1 Normalized wave-domain algorithm updating driving signals (NWD-D)

If we perform the adaptive process on the loudspeaker weights directly, we can obtain the loudspeaker weights for each iteration from the update equation. In this case, the update variable in (5.9) can be replaced by $\boldsymbol{d}$, that is $\boldsymbol{w} = \boldsymbol{d} = [d_1, \ldots, d_L]^T$.

By the complex LMS algorithm [111], taking a derivative of $\xi_1(n)$ with respect to $\boldsymbol{d}$, the gradient of the cost function can be written by

$$\nabla \xi_1(n) = 2\boldsymbol{T}^H \boldsymbol{\alpha}(n). \tag{5.10}$$

The proof is given in Appendix 5.8.1.
Substituting (5.10) into (5.9), the final adaptive equation in wave domain can be written as

$$\boldsymbol{d}(n+1) = \boldsymbol{d}(n) - \mu \boldsymbol{T}^H \boldsymbol{\alpha}(n). \tag{5.11}$$

The block diagram of the algorithm is shown in Figure 5.2.

By replacing the LMS filter by the normalized LMS filter, the final update

equation of the normalized wave-domain algorithm updating driving signals (NWD-D) can be written as

$$\boldsymbol{d}(n+1) = \boldsymbol{d}(n) - \frac{\mu_0}{\|\boldsymbol{T}^H\|_2^2}\boldsymbol{T}^H\boldsymbol{\alpha}(n), \tag{5.12}$$

where $\|\cdot\|_2$ denotes the Euclidean norm for a vector or matrix, and $\mu_0 \in [0, 1]$ denotes the normalized step size.

5.3.2 Normalized wave-domain algorithm updating mode coefficients (NWD-M)

If we update the wave-domain secondary sound field coefficients ($\boldsymbol{\gamma}$) first, and calculate the loudspeaker driving signals ($\boldsymbol{d}$) later, the update variable in (5.9) can be replaced by $\boldsymbol{\gamma}$, then we have $\boldsymbol{w} = \boldsymbol{\gamma} = [\gamma_{-M}, \ldots, \gamma_M]^T$. Taking a derivative of $\xi_1(n)$ with respect to $\boldsymbol{\gamma}$, the gradient of the cost function can be written by

$$\nabla\xi_1(n) = 2\boldsymbol{\alpha}(n). \tag{5.13}$$

The proof is given in Appendix 5.8.2.
Substituting (5.13) into (5.9), the adaptive equation in wave-domain coefficients can be written as

$$\boldsymbol{\gamma}(n+1) = \boldsymbol{\gamma}(n) - \mu\boldsymbol{\alpha}(n). \tag{5.14}$$

Thus, the final update equation of the normalized wave-domain algorithm updating mode coefficients (NWD-M) is

$$\boldsymbol{\gamma}(n+1) = \boldsymbol{\gamma}(n) - \mu_0\boldsymbol{\alpha}(n). \tag{5.15}$$

From (5.3), we obtain the loudspeaker weights $\boldsymbol{d}(n)$ by $\boldsymbol{d} = \boldsymbol{T}^+\boldsymbol{\gamma}$, where the superscript $(\cdot)^+$ denotes the pseudoinverse of a matrix. The block diagram for updating the wave-domain coefficients is shown in Figure 5.3.

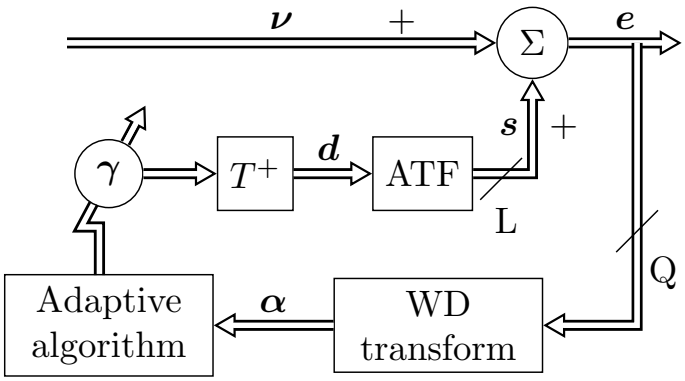

Figure 5.3: Block diagram of wave-domain ANC system, when updating the wave-domain coefficients. The WD transform block represents the wave domain transform for the residual signals.

5.4 Wave Domain ANC Algorithms - Minimization of Acoustic Potential Energy

Minimizing the total acoustic potential energy (APE) in an enclosed noise field can achieve global reduction in sound pressure throughout the enclosure [115,63]. Here we derive the acoustic potential energy in terms of the wave-domain coefficients to obtain global reduction over the control region.

By definition, acoustic potential energy is

$$E_p(k) = \frac{1}{2\rho_0 c^2} P(k), \tag{5.16}$$

where ρ_0 denotes the density of the media and $P(k)$ is the average energy of the residual signal given by

$$P(k) = \int\limits_S e^*(\boldsymbol{x}, k) e(\boldsymbol{x}, k) dS = \int_0^{2\pi} \int_0^{R_1} e^*(\boldsymbol{x}, k) e(\boldsymbol{x}, k) r dr d\phi_{\boldsymbol{x}}, \tag{5.17}$$

with superscript $(\cdot)^*$ denoting the complex conjugate. Since the potential energy is a scalar multiple of the average spatial energy, by defining $P(k)$ to be the cost function, we can effectively minimize the potential energy.

We represent $P(k)$ in the cylindrical harmonics domain by substituting (5.4) into (5.17) as,

$$P(k) = \sum_{m=-M}^{M} \alpha_m^*(k)\alpha_m(k)(\underbrace{2\pi \int_0^{R_1} (J_m(kr))^2 r dr}_{u_m(k)}), \tag{5.18}$$

where the integral in (5.18) is estimated by numerically evaluating the integral between 0 and R_1, which is the integral over the region of interest.

The above result shows that acoustic potential energy within a circular region is given by a sum of squared cylindrical harmonic coefficients with the weight $u_m(k)$. The weight $u_m(k)$ can be pre-calculated for each frequency and each harmonic order, therefore it does not incur additional computational complexity during the adaptive process.

Then, (5.18) can be written in matrix form as

$$P(k) = \boldsymbol{\alpha}^H \boldsymbol{U} \boldsymbol{\alpha}, \tag{5.19}$$

where $\boldsymbol{\alpha} = [\alpha_{-M}, \ldots, \alpha_M]^T$, $\boldsymbol{U} = \text{diag}(u_{-M}, \ldots, u_{-M})$, and

$$u_m = 2\pi \int_0^{R_1} (J_m(kr))^2 r dr.$$

Therefore, the new cost function becomes

$$\xi_p(n) = P(n) = \boldsymbol{\alpha}^H(n) \boldsymbol{U} \boldsymbol{\alpha}(n). \tag{5.20}$$

where the frequency dependency k is omitted for notational simplicity.

Similar to Section 5.3, we derive the update equation for the new cost function in two cases as follows.

5.4.1 Normalized energy-based wave domain algorithm updating driving signals (NEWD-D)

The gradient of the cost function can be written by

$$\nabla \xi_p(n) = 2\boldsymbol{T}^H \boldsymbol{U} \boldsymbol{\alpha}(n). \tag{5.21}$$

The proof is given in Appendix 5.8.3.
Substituting (5.21) into (5.9), the final adaptive equation in wave domain can be written as

$$\boldsymbol{d}(n+1) = \boldsymbol{d}(n) - \mu \boldsymbol{T}^H \boldsymbol{U} \boldsymbol{\alpha}(n). \tag{5.22}$$

Similar to (5.12), the update equation of the normalized energy-based wave domain algorithm updating driving signals (NEWD-D) can be written as

$$\boldsymbol{d}(n+1) = \boldsymbol{d}(n) - \frac{\mu_0}{\|\boldsymbol{T}^H \boldsymbol{U}\|_2^2} \boldsymbol{T}^H \boldsymbol{U} \boldsymbol{\alpha}(n). \tag{5.23}$$

5.4.2 Normalized energy-based wave domain algorithm updating mode coefficients (NEWD-M)

The gradient of the cost function can be written as

$$\nabla \xi_p(n) = 2\boldsymbol{U} \boldsymbol{\alpha}(n). \tag{5.24}$$

The proof is given in Appendix 5.8.4.
Substituting (5.24) into (5.9), the adaptive equation in the wave-domain coefficients can be written as

$$\boldsymbol{\gamma}(n+1) = \boldsymbol{\gamma}(n) - \mu \boldsymbol{U} \boldsymbol{\alpha}(n). \tag{5.25}$$

The final update equation of the normalized energy-based wave domain algorithm updating the mode coefficients (NEWD-M) can be written as

$$\boldsymbol{\gamma}(n+1) = \boldsymbol{\gamma}(n) - \frac{\mu_0}{\|\boldsymbol{U}\|_2^2} \boldsymbol{U} \boldsymbol{\alpha}(n). \tag{5.26}$$

Then the loudspeaker weights $\boldsymbol{d}(n)$ can be calculated by $\boldsymbol{d} = \boldsymbol{T}^+ \boldsymbol{\gamma}$ in each iteration.

5.5 Simulation Results Analysis

5.5.1 Simulation setup

In this section, performance of the proposed four wave domain algorithms (i) normalized wave domain algorithm updating driving signals (NWD-D), (ii) normalized wave domain algorithm updating mode coefficients (NWD-M), (iii) normalized energy-based wave domain algorithm updating driving signals (NEWD-D), and (iv) normalized energy-based wave domain algorithm updating the mode coefficients (NEWD-M) are compared with the conventional normalized multi-point (NMP) algorithm[1], in both free-field and reverberant environments. We assume the desired control zone to be a circular region of a radius of 1 m (black area in Figure 5.1), and the noise field to be generated by point sources, which are outside the control region.

We utilize a feedback ANC system for control on a 2D plane, where the circular microphone array of radius 1 m is placed on the boundary of the control region and the circular loudspeaker array of radius 2 m is placed outside the control region. The speed of sound is $c = 343$ m/s and the density of the air is $\rho_0 = 1.225$ kg/m^3. The simulation of the reverberant environment is modelled as a rectangular room 6 m×6 m with perfectly absorbing ceiling and floor, and all the side walls have a reflection coefficient of 0.75. The reverberation is simulated using the image-source method [114].

The simulation begins in the time domain. We adopt a block-wise operation and transform the microphone recordings into the time-frequency domain. Based on Equation (9), we further transfer the signal into wave-domain coefficients. A sampling rate of 8 kHz and a window length of 3200 samples are employed. White Gaussian noise with SNR of 40 dB is added to each microphone recording to model the internal thermal noise of microphones.

To evaluate the primary noise reduction performance, we study the (i) instantaneous noise reduction on the microphones $N_{\mathrm{r}}^{\mathrm{b}}(n)$, (ii) noise reduction within the

[1]Here, the NMP algorithm is the normalized version of the MC algorithm in [105].

region of interest $N_{\mathrm{r}}^{\mathrm{in}}(n)$, and (iii) acoustic potential energy over region $E_p(n)$.

The instantaneous noise reduction on the microphones can be defined as

$$N_{\mathrm{r}}^{\mathrm{b}}(n) \triangleq 10\log_{10}\frac{\sum_q E\{|e_q(n)|^2\}}{\sum_q E\{|e_q(0)|^2\}}, \tag{5.27}$$

where $e_q(n)$ represents the sound pressure received on the q^{th} microphone at the n^{th} iteration, and $e_q(0)$ represents the sound pressure received on the q^{th} microphone before the ANC process.

To evaluate the noise reduction performance within the control region, the sound pressure at $Z = 1296$ points uniformly placed within the regions $\boldsymbol{e}_{in}$ are examined. We define the instantaneous noise reduction inside the region of interest $N_{\mathrm{r}}^{\mathrm{in}}(n)$ as:

$$N_{\mathrm{r}}^{\mathrm{in}}(n) \triangleq 10\log_{10}\frac{\sum_z E\{|e_{\mathrm{in}\_z}(n)|^2\}}{\sum_z E\{|e_{\mathrm{in}\_z}(0)|^2\}}, \tag{5.28}$$

where $e_{\mathrm{in}\_z}(n)$ denotes the residual signals at the z^{th} point within the region at the n^{th} iteration, and $e_{\mathrm{in}\_z}(0)$ represents the primary noise field at the z^{th} point in the region.

As mentioned above, acoustic potential energy is another measure of the noise reduction over the entire spatial region [116], which can be considered a more insightful measure in practice. From (5.16) and (5.19), the acoustic potential energy over the control region for each iteration can be calculated by

$$E_p(n) = \frac{1}{2\rho_0 c^2}\boldsymbol{\alpha}^H(n)\boldsymbol{U}\boldsymbol{\alpha}(n), \tag{5.29}$$

where $\boldsymbol{\alpha}(n)$ can be conveniently captured by circular microphone arrays, and calculated based on (5.4).

In addition to the noise reduction measures mentioned above, we analyse two more performance measures, (i) the residual noise field in the control region, and (ii) the convergence speed. We simulate the ANC algorithms to deal with a single frequency noise field and a multi-frequency noise field as shown in the following two subsections.

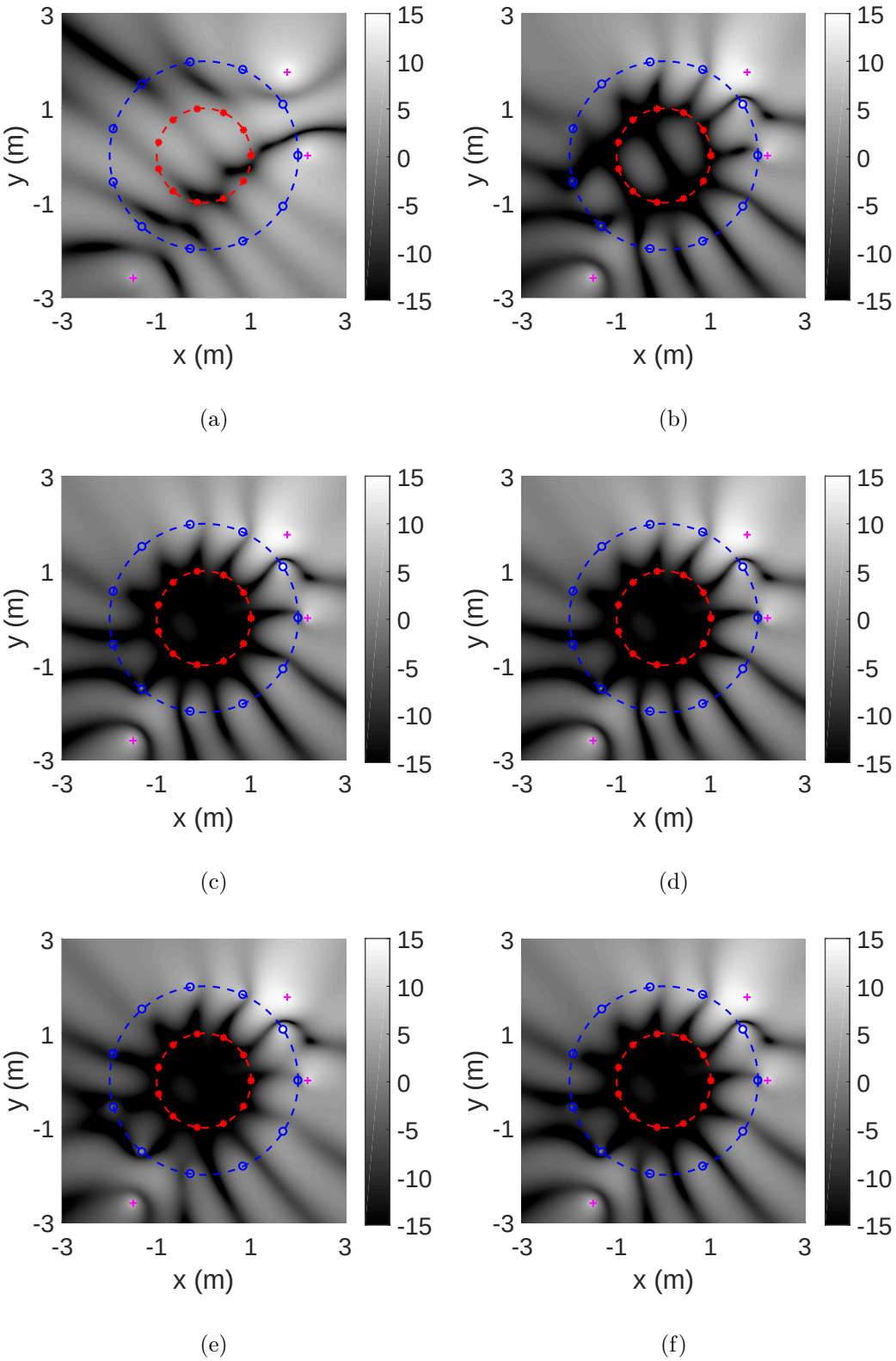

(a) (b)

(c) (d)

(e) (f)

Figure 5.4: Noise cancellation performance after 50 iterations using different ANC algorithms in free field: (a) Primary noise field (200 Hz) (b) Normalized MP (c) NWD-M (d) NWD-D (e) NEWD-M (f) NEWD-D.

5.5.2 Single frequency scenario

First, we investigate the narrowband performance of different algorithms. Three noise sources are located at $(2.2, 0°)$, $(2.5, 45°)$, and $(3, 240°)$ with the magnitude of 10, 15 and 5, which are shown as pink $'+'$ in Figure 5.4 and Figure 5.5. The frequency of the noise field is 200 Hz. The control region ($R_1 = 1$ m) in such a noise field can be represented by $m\epsilon[-5, 5]$ modes, thus, we place $2N + 1 = 11$ microphones on the boundary to capture the information of the residual noise field for each mode. We select the same normalized step values for different algorithms, $\mu_0 = 0.8$ in free field and $\mu_0 = 0.5$ in reverberant environments.

Loudspeaker number meeting the requirement

In order to control all the modes in the entire spatial region, $2N + 1 = 11$ loudspeakers are required to be placed in the corresponding array.

Figure 5.4 and Figure 5.5 demonstrate the energy of residual noise fields over region before ANC and after 50 iterations of ANC process, in free field and in reverberant environments. NWD-D, NWD-M, NEWD-D and NEWD-M can achieve noise cancellation over the entire region. Whereas NMP can only reduce the noise on the boundary close to the microphone points after 50 iterations. Compared to the primary noise field (Figure 5.4(a) and Figure 5.5(a)), we can see that all the wave-domain methods can achieve higher noise reduction over the entire region than the NMP method, in both free field and reverberation environments within 50 iterations. Figure 5.6, Figure 5.7, Figure 5.8 and Figure 5.9 compare the noise reduction level and convergence performance for each algorithm in free field and in a room environment. Figure 5.6 and Figure 5.8 are zoomed-in versions of Figure 5.7 and Figure 5.9 in the first 50 iterations, respectively. The acoustic potential energy reduction over the region shows a similar trend to the noise reduction over the region, as they both monitor the overall energy of the control region.

From Figure 5.7 and Figure 5.9, we can see that all the wave domain algorithms can cancel the noise on the boundary and over the entire region. In the steady state, different algorithms can achieve similar $N_{\mathrm{r}}^{\mathrm{in}}(n)$ attenuation, the same as for $N_{\mathrm{r}}^{\mathrm{b}}(n)$ and APE reduction.

Figure 5.6 and Figure 5.8 demonstrate the convergence speed in free field and in

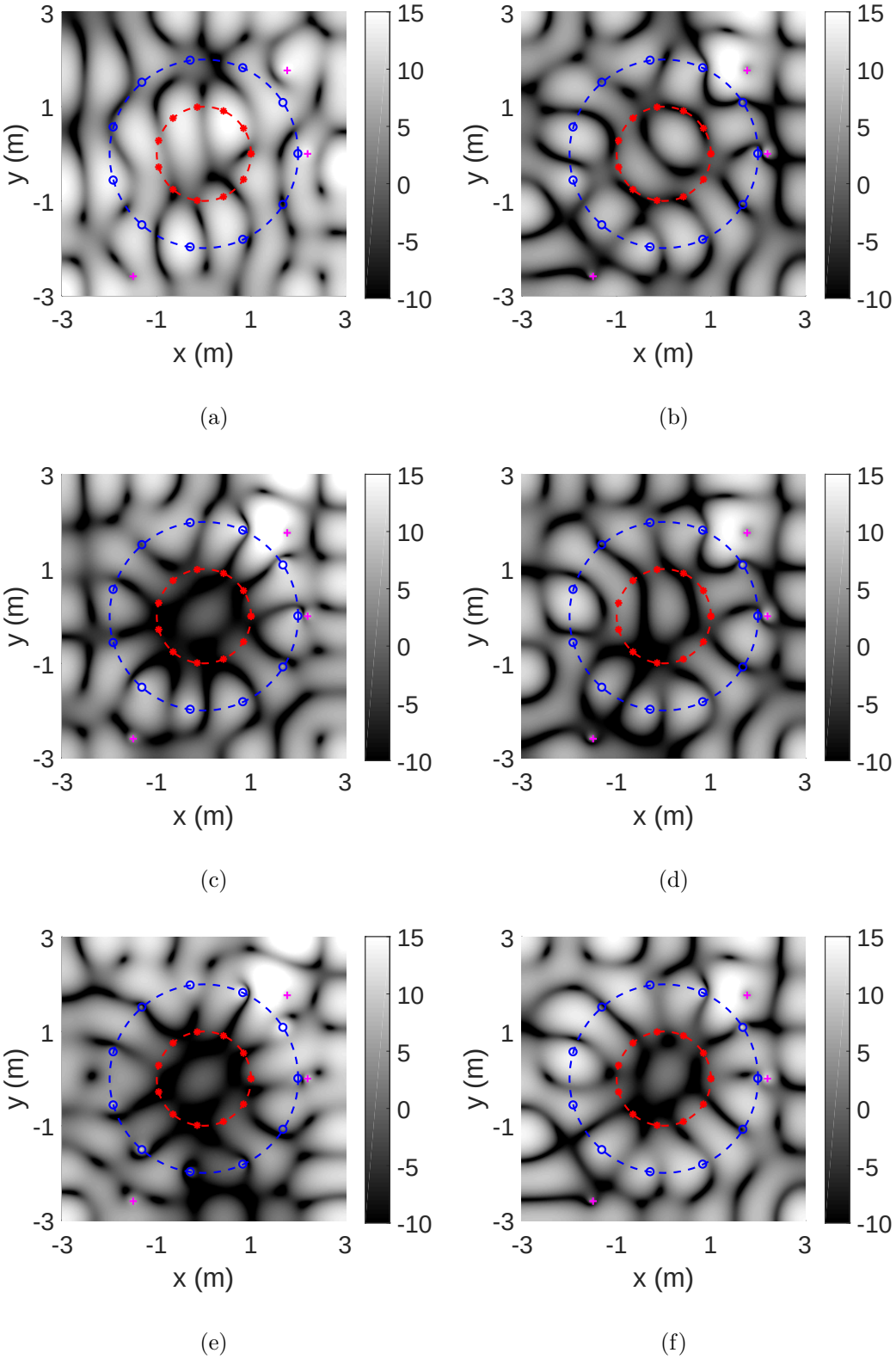

(a) (b)

(c) (d)

(e) (f)

Figure 5.5: Noise cancellation performance after 50 iterations using different ANC algorithms in reverberant environments: (a) primary noise field (200 Hz) (b)Normalized MP (c) NWD-M (d) NWD-D (e) NEWD-M (f) NEWD-D.

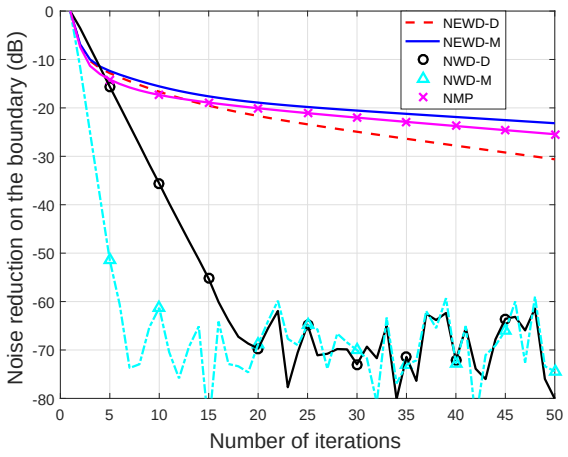

(a)

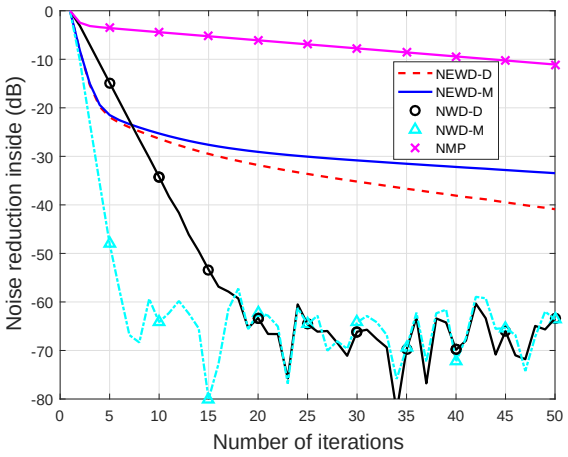

(b)

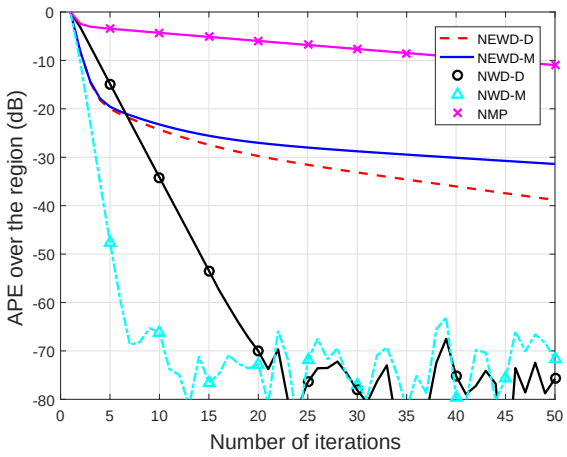

(c)

Figure 5.6: Convergence performance using different ANC algorithm in free field (50 iterations): (a) $N_{\mathrm{r}}^{\mathrm{b}}(n)$ (b) $N_{\mathrm{r}}^{\mathrm{in}}(n)$ (c) APE reduction over the region.

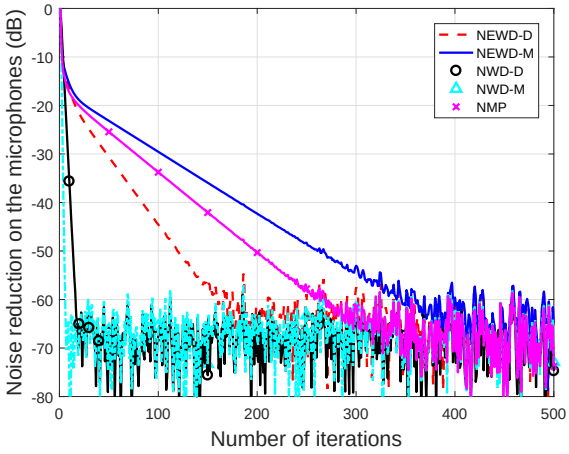

(a)

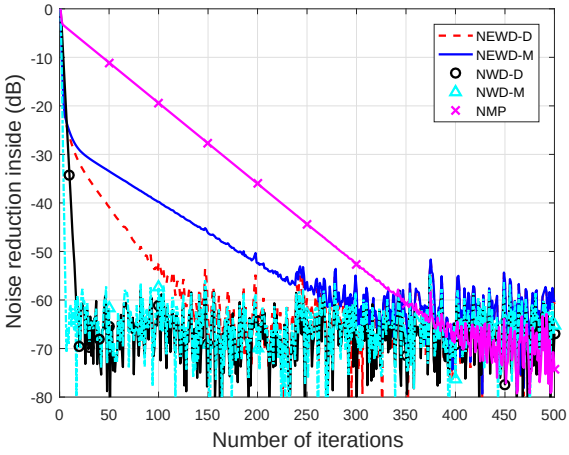

(b)

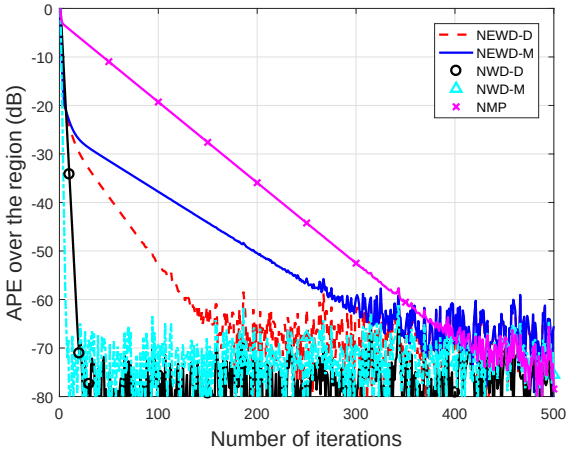

(c)

Figure 5.7: Convergence performance using different ANC algorithm in free field (500 iterations): (a) $N_{\mathrm{r}}^{\mathrm{b}}(n)$ (b) $N_{\mathrm{r}}^{\mathrm{in}}(n)$ (c) APE reduction over the region.

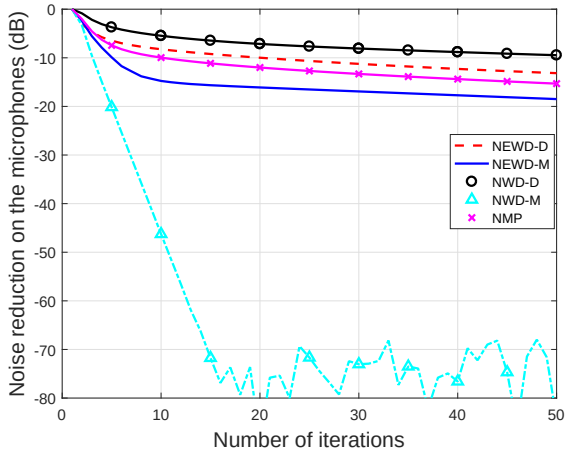

(a)

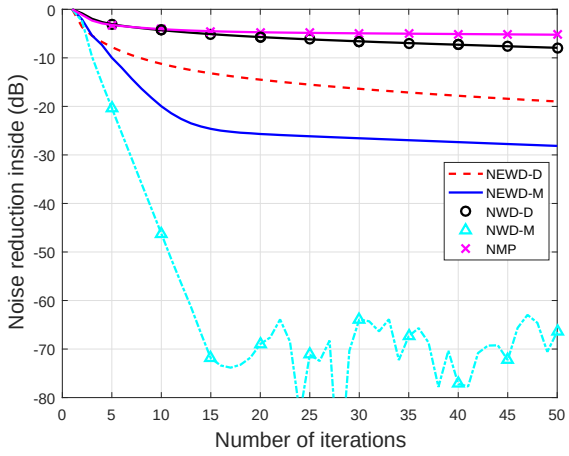

(b)

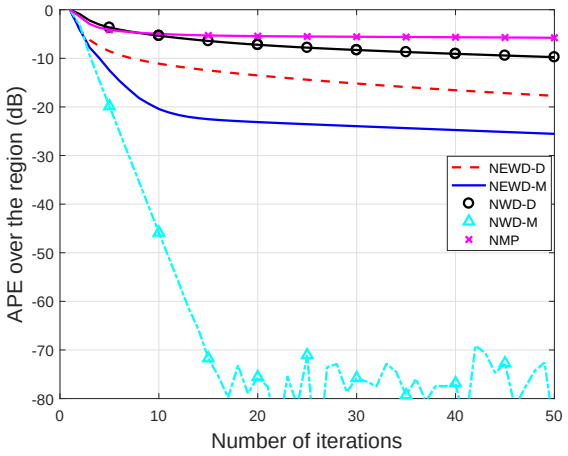

(c)

Figure 5.8: Convergence performance in reverberant environment (50 iterations): (a) $N_{\mathrm{r}}^{\mathrm{b}}(n)$ (b) $N_{\mathrm{r}}^{\mathrm{in}}(n)$ (c) APE reduction over the region.

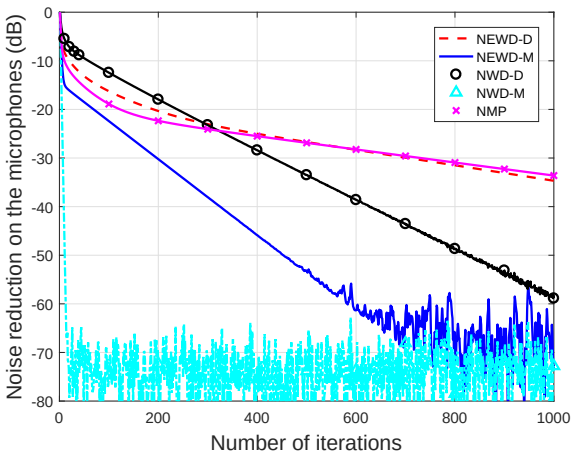

(a)

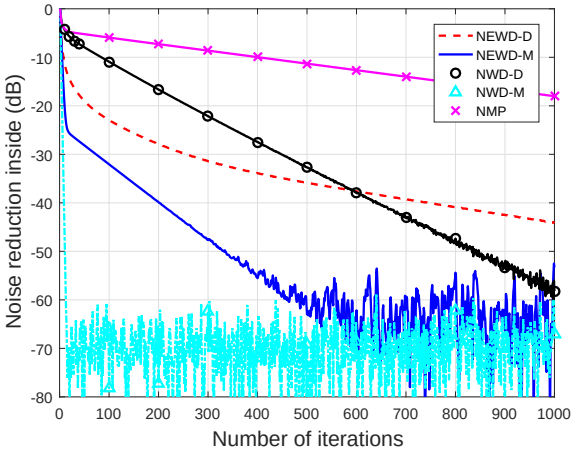

(b)

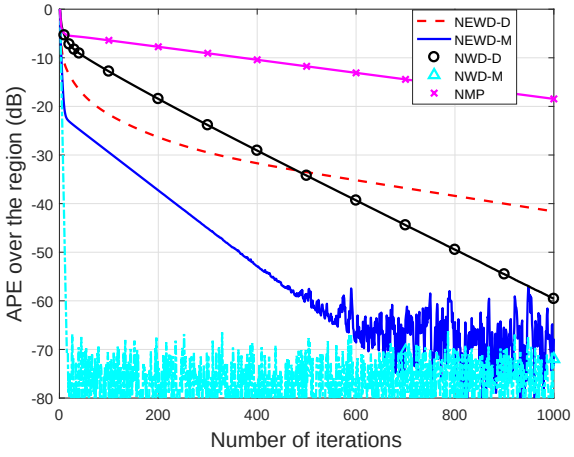

(c)

Figure 5.9: Convergence performance in reverberant environment (1000 iterations): (a) $N_{\mathrm{r}}^{\mathrm{b}}(n)$ (b) $N_{\mathrm{r}}^{\mathrm{in}}(n)$ (c) APE reduction over the region.

a room reverberant environment. NMP converges fast on the boundary, but much more slowly within the region. In free field, coefficients-based algorithms (NWD-M and NWD-D) converge faster than the energy-based WD algorithms. In the room reverberant environment, the algorithms updating wave coefficients (NWD-M and NEWD-M) have better convergence performance than the algorithms updating driving signals directly (NWD-D and NEWD-D). From the comparison of the free field case and room case, we can see that NWD-M has the fastest convergence speed in both free field and reverberant environments. While NWD-D works well in the free field, but converges much more slowly in a room.

Fewer loudspeakers than the requirement

In real applications, it is possible that secondary sources are limited, so that fewer loudspeakers are available than the requirement $(2N+1)$. In the simulation below, a small number of loudspeakers are equi-angularly placed in the circular array, which cannot cover all the modes in the spatial region.

Figure 5.10 demonstrates the convergence performance in the reverberant environment using 9 loudspeakers. The algorithms updating mode coefficients converge faster than the algorithms updating driving signals directly. The NMP algorithm has the slowest convergence speed. Since 9 loudspeakers cannot reconstruct all the modes in the control region, the noise reduction performance in the steady state degrades significantly compared to that when 11 loudspeakers are used. By minimizing the weighted $(u_m(k))$ squared sum of the wave domain residual signals, the energy-based wave domain algorithms emphasize the importance of the low order modes and reduce the importance of the high order modes. Therefore, it is found that the energy-based wave domain algorithms (NEWD-D and NEWD-M) can achieve more noise reduction over the entire control region than the other algorithms. Meanwhile, in the steady state the wave domain algorithms have better $\mathrm{NR}_{\mathrm{in}}$ and APE attenuation performance compared to the NMP algorithm.

We further reduce the loudspeaker number to 7 and 5, and evaluate the noise cancellation performance after 1000 iterations, as shown in Table 5.1. NEWD-D and NEWD-M outperform the other algorithms in each case. In general, a smaller number of loudspeakers decreases the noise reduction performance, especially the

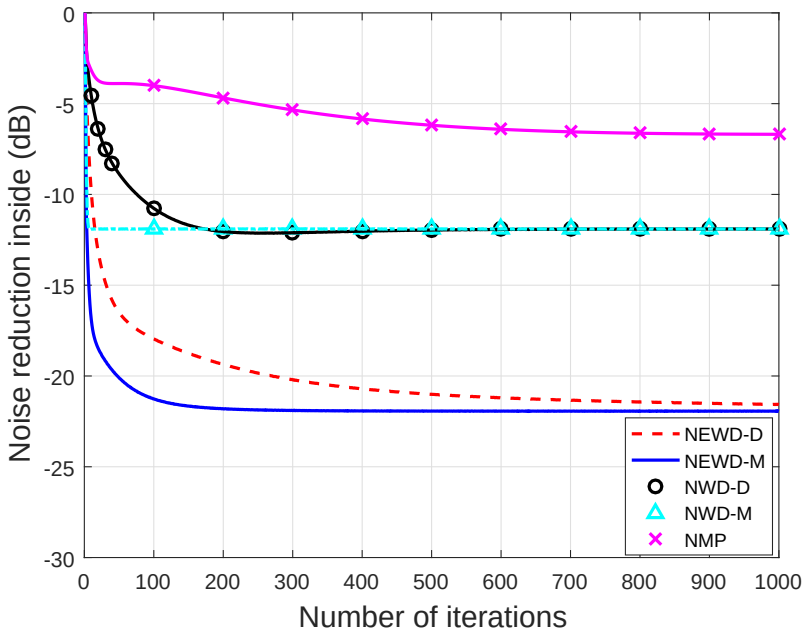

(a)

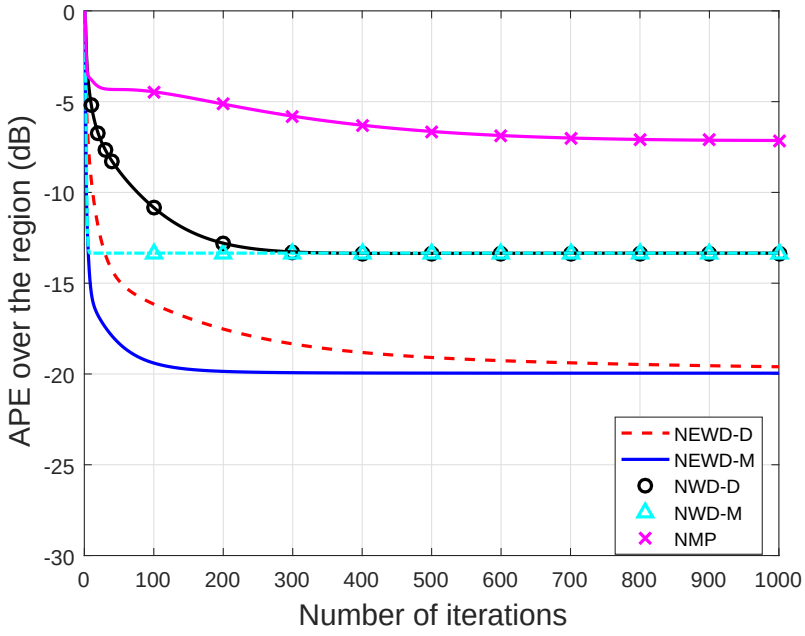

(b)

Figure 5.10: Convergence performance using 9 loudspeakers in reverberant environment (1000 iterations): (a) noise reduction inside the region (b) acoustic potential energy reduction over the region.

Table 5.1: Attenuation level using different numbers of loudspeakers.

	N_r^{in} (dB)			APE (dB)		
	9	7	5	9	7	5
NEWD-D	-22	-14	-4	-20	-14	-5
NEWD-M	-22	-14	-4	-20	-14	-5
NWD-D	-12	-6	-1	-13	-7	-2
NWD-M	-12	-6	-1	-13	-7	-2
NMP	-7	-5	0	-7	-5	-1

NR_{in} and APE attenuation. For example, when 5 loudspeakers are used, none of the algorithms can achieve more than -10 dB noise reduction, which indicates deteriorated ANC performance.

Loudspeaker energy consumption

To evaluate the loudspeaker energy consumption during the ANC process, we compare the total energy of all the loudspeakers[2] ($\boldsymbol{d}^T\boldsymbol{d}$) using different algorithms in the reverberant environment, as shown in Figure 5.11.

When 11 loudspeakers are utilized to generate the secondary sound field (Figure 5.11(a)), the algorithms which update the driving signals gradually increase the total energy, and reach the steady state smoothly. While the loudspeaker energy using NEWD-M has a peak before the steady state. All the algorithms reach the same energy level after convergence. When the resources are limited, the loudspeakers consume more energy to achieve noise cancellation, as shown in Figure 5.11(b). Meanwhile, the energy-based algorithms will end up with more loudspeaker energy compared to the other algorithms.

5.5.3 Multi-frequency scenario

For broadband noise field, we assume that only one noise source is located at $(2.5, 0°)$, and it can be synthesised by the combination of $J = 19$ dominant narrowband components. The frequency range is from 50 Hz to 500 Hz with the same pressure level in each frequency bin $f_j, j = 1, 2, ..., J$. The system is designed for

[2]Here, we evaluate the summation of squared driving signals, for all the 11 loudspeakers.

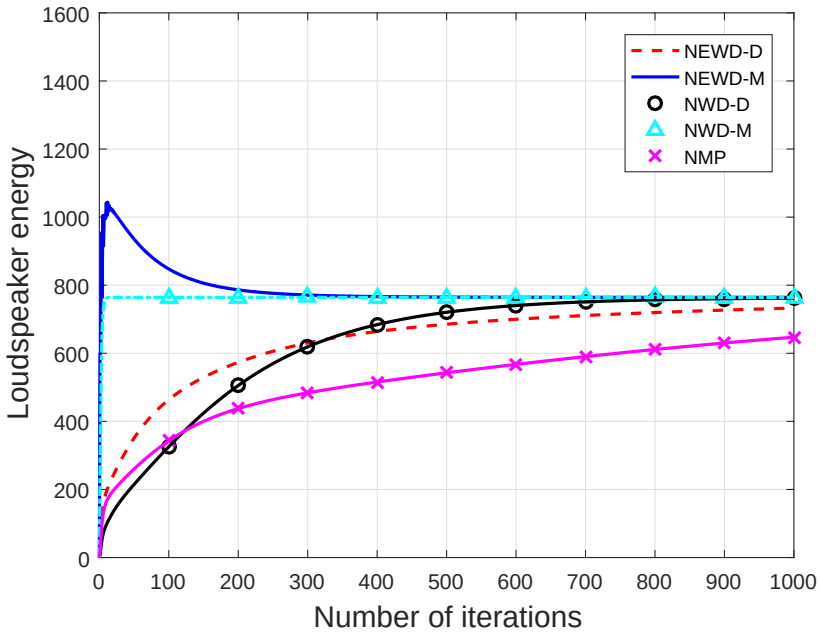

(a)

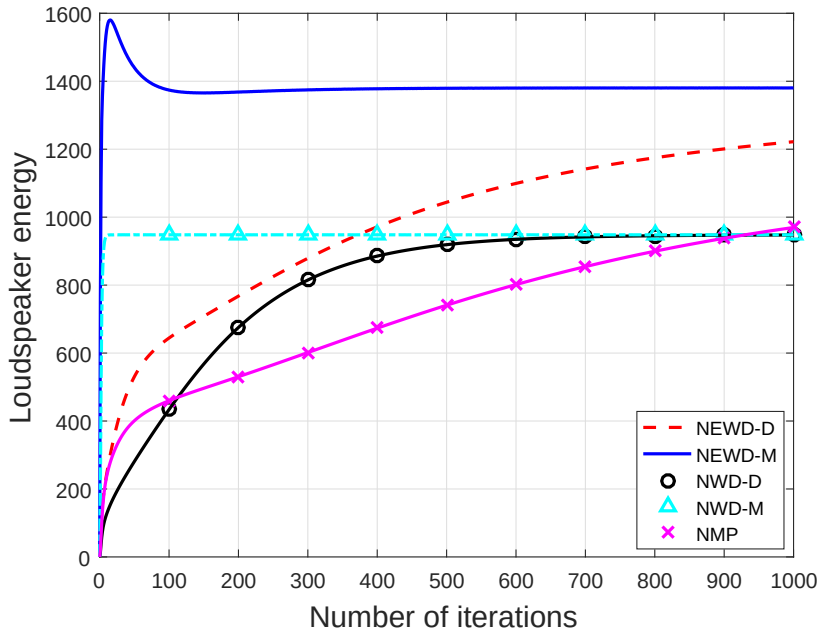

(b)

Figure 5.11: Loudspeaker energy ($\boldsymbol{d}^T\boldsymbol{d}$) using different ANC algorithms during 1000 iterations in reverberant environment: (a) 11 loudspeakers (b) 9 loudspeakers.

the frequency upper bound, so that we place $2M + 1 = 27$ loudspeakers and 27 microphones in each corresponding array.

The noise reduction performance within the control region in free field and reverberant environments are shown in Figure 5.12 and Figure 5.13 respectively. Over a wide frequency range, the wave-domain ANC algorithms can cancel the noise within the entire region. In free field, the average noise reduction is around -25 dB and -50 dB, for energy-based WD algorithms and WD algorithms, respectively. Similar results have been shown in reverberant environments. Notice that the noise reduction performance is significantly degraded at 300 Hz and 475 Hz. This is due to the 'irregular frequencies' problem, where the Bessel functions in the corresponding frequencies are close to zero and the coefficient errors are amplified. This is a limitation of the wave domain technique when using a single circular microphone array. However, there are well understood methods to tackle this problem, such as using two closely spaced microphone arrays [76,117], using multi-radii shell arrays [118], and using a planar array of differential microphones [119]. In the reverberant environment, the variation of $\mathrm{N}_{\mathrm{r}}^{\mathrm{in}}$ and APE reduction between different frequency bins are relatively larger than in the free field, especially for the WD algorithms.

5.6 Summary and Contributions

In this chapter, we presented a comprehensive analysis of adaptive wave-domain ANC based on a feedback control system. We utilized the harmonic coefficients to calculate the acoustic potential energy. We investigated multiple cost functions and multiple update variables, resulting in four different methods of implementing harmonics based wave-domain ANC systems.

The major contributions in this chapter are:

- We developed normalized wave-domain ANC algorithms in two different ways: (i) minimizing the residual sound field coefficients and (ii) minimizing the acoustic potential energy of the residual sound field.

- We derived the update equations with respect to two variables: (a) the loudspeaker weights and (b) secondary sound field coefficients.

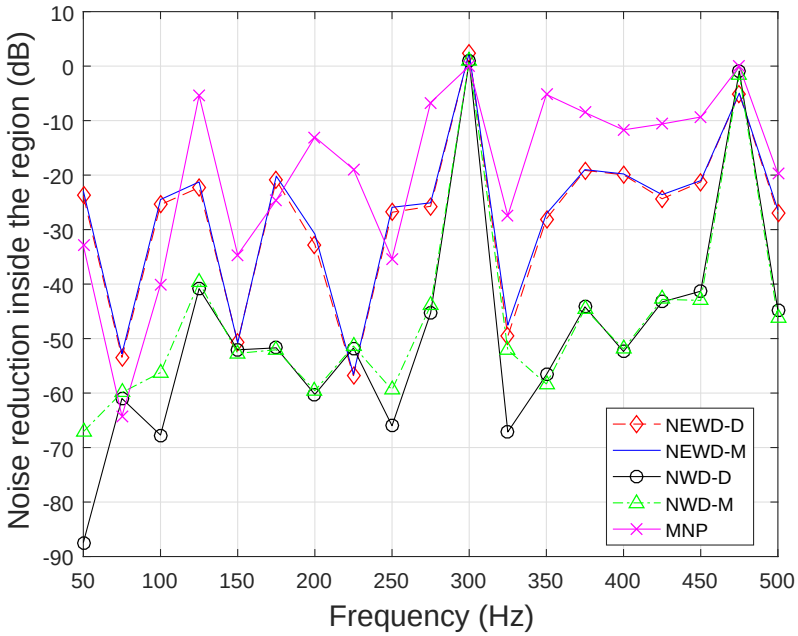

(a)

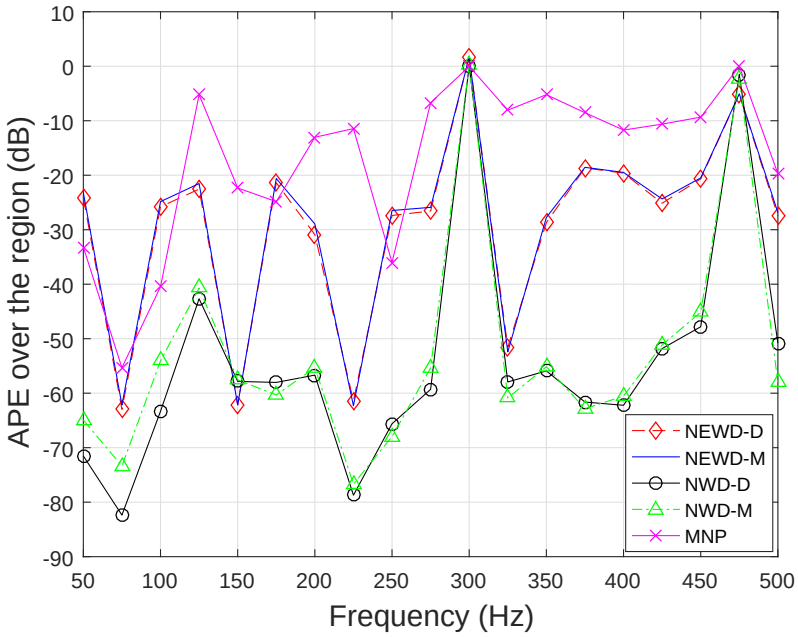

(b)

Figure 5.12: Multi-frequency performance using different wave-domain ANC algorithms in free field after 50 iterations: (a) noise reduction within the region (b) acoustic potential energy reduction over the region.

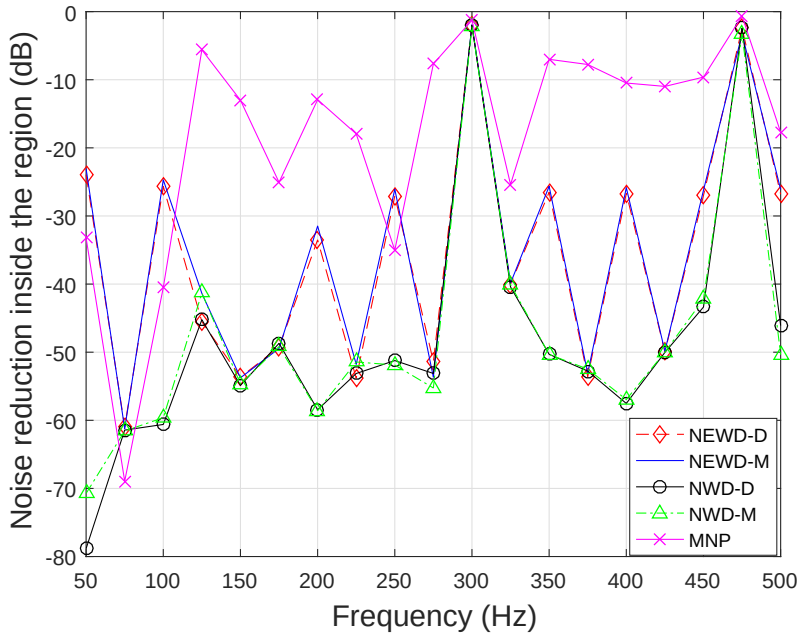

(a)

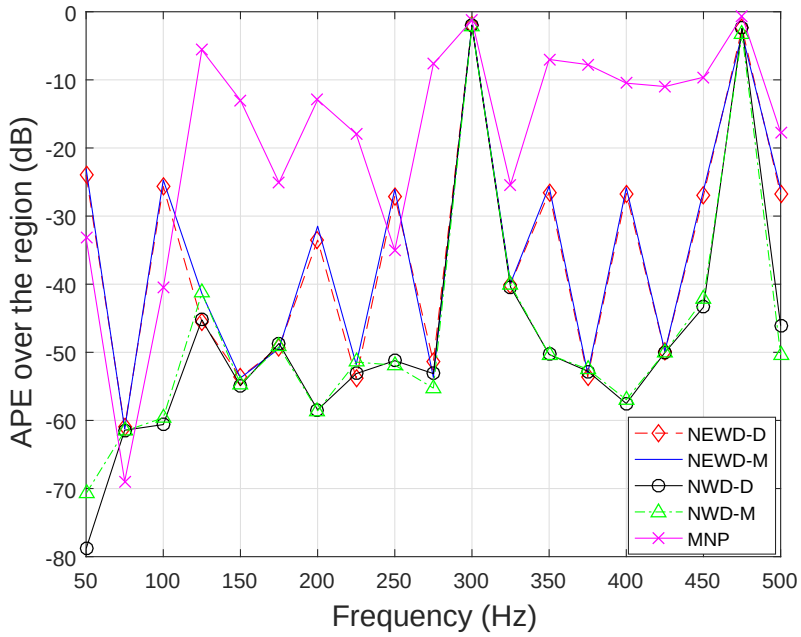

(b)

Figure 5.13: Multi-frequency performance using different wave-domain ANC algorithms in reverberant environment after 50 iterations: (a) noise reduction within the region (b) acoustic potential energy reduction over the region.

- We compared four proposed algorithms with respect to each other as well as with the conventional multi-point method. We showed that there are trade-offs in selecting any one of the four algorithms over the other. To the best of our knowledge, such detailed analyses of these four wave-domain adaptive algorithms have not been reported in the literature.

5.7 Related Publications

[120]: J. Zhang, T. D. Abhayapala, W. Zhang, P. N. Samarasinghe and S. Jiang, "Active Noise Control Over Space: A Wave Domain Approach," *IEEE/ACM Trans. Audio, Speech, Language Process.*, vol. 26, no. 4, pp. 774-786, April 2018.

[116]: H. Chen, J. Zhang, P. N. Samarasinghe, and T. D. Abhayapala, "Evaluation of spatial active noise cancellation performance using spherical harmonic analysis", in *IEEE International Workshop on Acoustic Signal Enhancement 2016*, Xi′an, China, Sept. 2016, pp. 15.

5.8 Appendices

5.8.1 Proof of equation (5.10)

The gradient vector and the conjugate derivative [50] are related by

$$\nabla\xi_1 = 2\frac{\partial\xi_1}{\partial \boldsymbol{d}^*} = 2\frac{\partial(\boldsymbol{\alpha}^H\boldsymbol{\alpha})}{\partial \boldsymbol{d}^*}, \tag{5.30}$$

where we use (5.8) and omit the iteration index n for notational simplicity. Substitute (5.3) and (5.7) into (5.30),

$$\nabla\xi_1 = 2\bigg(\frac{\partial(\boldsymbol{\beta}^H\boldsymbol{\beta})}{\partial \boldsymbol{d}^*} + \frac{\partial(\boldsymbol{\beta}^H\boldsymbol{T}\boldsymbol{d})}{\partial \boldsymbol{d}^*} + \frac{\partial(\boldsymbol{d}^H\boldsymbol{T}^H\boldsymbol{\beta})}{\partial \boldsymbol{d}^*} + \frac{\partial(\boldsymbol{d}^H\boldsymbol{T}^H\boldsymbol{T}\boldsymbol{d})}{\partial \boldsymbol{d}^*}\bigg). \tag{5.31}$$

Calculate each item separately to get,

$$\frac{\partial(\boldsymbol{\beta}^H\boldsymbol{\beta})}{\partial \boldsymbol{d}^*} = \frac{\partial(\boldsymbol{\beta}^H\boldsymbol{T}\boldsymbol{d})}{\partial \boldsymbol{d}^*} = 0,$$

$$\frac{\partial(\boldsymbol{d}^H\boldsymbol{T}^H\boldsymbol{\beta})}{\partial\boldsymbol{d}^*} = \boldsymbol{T}^H\boldsymbol{\beta},$$

$$\frac{\partial(\boldsymbol{d}^H\boldsymbol{T}^H\boldsymbol{T}\boldsymbol{d})}{\partial\boldsymbol{d}^*} = \boldsymbol{T}^H\boldsymbol{T}\boldsymbol{d}. \tag{5.32}$$

Substituting (5.32) into (5.31),

$$\nabla\xi_1 = 2\boldsymbol{T}^H(\boldsymbol{\beta} + \boldsymbol{T}\boldsymbol{d}). \tag{5.33}$$

Substituting (5.3) and (5.7) into (5.33), we complete the proof.

5.8.2 Proof of equation (5.13)

The gradient vector and the conjugate derivative are related by

$$\nabla\xi_1 = 2\frac{\partial\xi}{\partial\boldsymbol{\gamma}^*} = 2\frac{\partial(\boldsymbol{\alpha}^H\boldsymbol{\alpha})}{\partial\boldsymbol{\gamma}^*}. \tag{5.34}$$

Substitute (5.3) and (5.7) into (5.34),

$$\nabla\xi_1 = 2\left(\frac{\partial(\boldsymbol{\beta}^H\boldsymbol{\beta})}{\partial\boldsymbol{\gamma}^*} + \frac{\partial(\boldsymbol{\beta}^H\boldsymbol{\gamma})}{\partial\boldsymbol{\gamma}^*} + \frac{\partial(\boldsymbol{\gamma}^H\boldsymbol{\beta})}{\partial\boldsymbol{\gamma}^*} + \frac{\partial(\boldsymbol{\gamma}^H\boldsymbol{\gamma})}{\partial\boldsymbol{\gamma}^*}\right). \tag{5.35}$$

Calculate each item separately,

$$\frac{\partial(\boldsymbol{\beta}^H\boldsymbol{\beta})}{\partial\boldsymbol{\gamma}^*} = \frac{\partial(\boldsymbol{\beta}^H\boldsymbol{\gamma})}{\partial\boldsymbol{\gamma}^*} = 0,$$

$$\frac{\partial(\boldsymbol{\gamma}^H\boldsymbol{\beta})}{\partial\boldsymbol{\gamma}^*} = \boldsymbol{\beta},$$

$$\frac{\partial(\boldsymbol{\gamma}^H\boldsymbol{\gamma})}{\partial\boldsymbol{\gamma}^*} = \boldsymbol{\gamma}. \tag{5.36}$$

Substituting (5.7) and (5.36) into (5.35), we complete the proof.

5.8.3 Proof of equation (5.21)

The gradient vector and the conjugate derivative [50] are related by

$$\nabla \xi_p = 2\frac{\partial \xi_p}{\partial \boldsymbol{d}^*}, \tag{5.37}$$

where the iteration index n has been omitted for notational simplicity.
Therefore the gradient is expressed as

$$\nabla \xi_p = 2\frac{\partial (\boldsymbol{\alpha}^H \boldsymbol{U} \boldsymbol{\alpha})}{\partial \boldsymbol{d}^*}. \tag{5.38}$$

Substitute (5.3) and (5.7) into (5.38),

$$\nabla \xi_p = 2\left(\frac{\partial (\boldsymbol{\beta}^H \boldsymbol{U} \boldsymbol{\beta})}{\partial \boldsymbol{d}^*} + \frac{\partial (\boldsymbol{\beta}^H \boldsymbol{U} \boldsymbol{T} \boldsymbol{d})}{\partial \boldsymbol{d}^*} + \frac{\partial (\boldsymbol{d}^H \boldsymbol{T}^H \boldsymbol{U} \boldsymbol{\beta})}{\partial \boldsymbol{d}^*} + \frac{\partial (\boldsymbol{d}^H \boldsymbol{T}^H \boldsymbol{U} \boldsymbol{T} \boldsymbol{d})}{\partial \boldsymbol{d}^*} \right). \tag{5.39}$$

Calculate each item separately,

$$\frac{\partial (\boldsymbol{\beta}^H \boldsymbol{U} \boldsymbol{\beta})}{\partial \boldsymbol{d}^*} = \frac{\partial (\boldsymbol{\beta}^H \boldsymbol{U} \boldsymbol{T} \boldsymbol{d})}{\partial \boldsymbol{d}^*} = 0,$$

$$\frac{\partial (\boldsymbol{d}^H \boldsymbol{T}^H \boldsymbol{U} \boldsymbol{\beta})}{\partial \boldsymbol{d}^*} = \boldsymbol{T}^H \boldsymbol{U} \boldsymbol{\beta},$$

$$\frac{\partial (\boldsymbol{d}^H \boldsymbol{T}^H \boldsymbol{U} \boldsymbol{T} \boldsymbol{d})}{\partial \boldsymbol{d}^*} = \boldsymbol{T}^H \boldsymbol{U} \boldsymbol{T} \boldsymbol{d}. \tag{5.40}$$

Substituting (5.40) into (5.39),

$$\nabla \xi_p = 2\boldsymbol{T}^H \boldsymbol{U} (\boldsymbol{\beta} + \boldsymbol{T} \boldsymbol{d}). \tag{5.41}$$

Substituting (5.3) and (5.7) into (5.41), we complete the proof.

5.8.4 Proof of equation (5.24)

The gradient vector and the conjugate derivative are related by

$$\nabla \xi_p = 2\frac{\partial \xi_p}{\partial \boldsymbol{\gamma}^*} = 2\frac{\partial (\boldsymbol{\alpha}^H \boldsymbol{U} \boldsymbol{\alpha})}{\partial \boldsymbol{\gamma}^*}. \tag{5.42}$$

Substitute (5.3) and (5.7) into (5.42),

$$\nabla\xi_p = 2\left(\frac{\partial(\boldsymbol{\beta}^H\boldsymbol{U}\boldsymbol{\beta})}{\partial\boldsymbol{\gamma}^*} + \frac{\partial(\boldsymbol{\beta}^H\boldsymbol{U}\boldsymbol{\gamma})}{\partial\boldsymbol{\gamma}^*} + \frac{\partial(\boldsymbol{\gamma}^H\boldsymbol{U}\boldsymbol{\beta})}{\partial\boldsymbol{\gamma}^*} + \frac{\partial(\boldsymbol{\gamma}^H\boldsymbol{U}\boldsymbol{\gamma})}{\partial\boldsymbol{\gamma}^*}\right). \tag{5.43}$$

Calculate each item separately,

$$\frac{\partial(\boldsymbol{\beta}^H\boldsymbol{U}\boldsymbol{\beta})}{\partial\boldsymbol{\gamma}^*} = \frac{\partial(\boldsymbol{\beta}^H\boldsymbol{U}\boldsymbol{\gamma})}{\partial\boldsymbol{\gamma}^*} = 0,$$

$$\frac{\partial(\boldsymbol{\gamma}^H\boldsymbol{U}\boldsymbol{\beta})}{\partial\boldsymbol{\gamma}^*} = \boldsymbol{U}\boldsymbol{\beta},$$

$$\frac{\partial(\boldsymbol{\gamma}^H\boldsymbol{U}\boldsymbol{\gamma})}{\partial\boldsymbol{\gamma}^*} = \boldsymbol{U}\boldsymbol{\gamma}. \tag{5.44}$$

Substituting (5.7) and (5.44) into (5.43), we complete the proof.

Chapter 6

ANC Subspace Performance Analysis

***Overview:** In this chapter, we investigate the maximum active noise control performance over a three-dimensional spatial space, by investigating the capability of secondary sources in particular environment. We first formulate the spatial ANC problem in a 3-D room. Then we discuss a wave-domain least square method by matching the secondary sound field to the primary sound field in wave domain. Furthermore, we extract the subspace from wave-domain coefficients of the secondary paths. We propose a subspace method by matching the secondary sound field to the projection of primary sound field in the subspace. Simulation results demonstrate the comparison between the wave-domain least square method and the subspace method, in terms of energy of the loudspeaker driving signals, noise reduction inside the region, and residual noise field outside the region. We also investigate the ANC performance under different loudspeaker configurations and noise source positions.*

6.1 Introduction

As discussed in Section 5.5.2, when the number of loudspeakers cannot control all the modes in the spatial region, using the proposed adaptive algorithms and conventional adaptive algorithms, simulation results demonstrated that the noise reduction performance in the steady state degrades significantly. In practical applications, numbers and locations of the loudspeakers have more constraints compared to simulation setups in Section 5.5.2. For instance, in a vehicle, the numbers and positions of the loudspeakers are highly constrained by the vehicle size and passenger convenience. It is valuable for design engineers to estimate whether the available numbers and positions of the loudspeakers are sufficient to the noise reduction requirements, before they implement an ANC system in a real environment.

Meanwhile, since the noise reduction performance varies with different ANC algorithms, it is important to investigate the maximum performance for the given system, which should only be dependent on the secondary source characteristics and locations, room environments and the sound field characteristics.

In literature, for spatial ANC performance estimation over an entire region, Chen et al. investigated ANC performance by noise pattern analysis of the primary noise field [121, 6]. Buerger et al. investigated the coherence between two observation points in the noise field evoked by given continuous source distributions, which can be applied to predict the upper bound of ANC performance in the region of interest [122]. However, capability of secondary sources in particular room environments has not yet been explored.

In this chapter, we investigate the maximum noise control performance by investigating capability of secondary sources in particular room environments. We find the subspace spanned by the wave-domain secondary path coefficients, and evaluate the ANC performance in the subspace. Using the proposed subspace method, the design engineers can predict the noise cancelation performance before an actual ANC system is implemented in a product. Simulations are conducted in a 3-D room environment under different noise source positions, when the loudspeakers have constraints on numbers and positions. The solution in the subspace method is more feasible than the wave-domain least square method.

The rest of this chapter is organized as follows. In Section 6.2, we formulate

the ANC problem in a 3-D room. We investigate the maximum ANC performance using the wave-domain least square method in Section 6.3, and investigate the maximum ANC performance using the subspace method in Section 6.4. The simulation validation is demonstrated in Section 6.5. We draw some conclusions in Section 6.6.

6.2 Problem Formulation

In this section, we formulate the ANC problem in a 3-D room.

As shown in Figure 6.1, let the quiet zone of interest (blue area) be a spherical region (S) with a radius R_1. Assume that the noise sources (red loudspeakers) and the secondary sources (black loudspeakers) are located outside the region of interest. In the ANC process, we measure the noise field by placing a spherical microphone array (dark blue stars) on the boundary of the region.

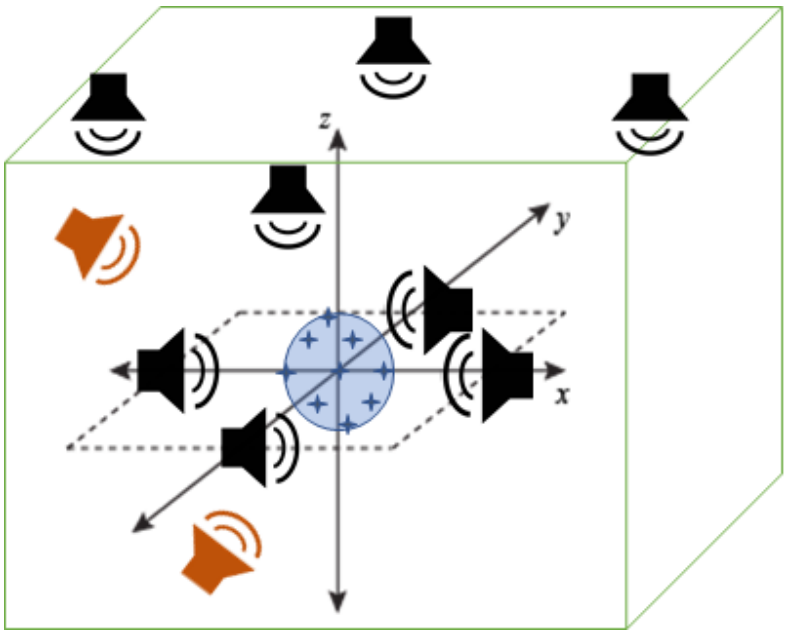

Figure 6.1: ANC system in a 3-D room.

Instead of using measurements of the microphone points directly, the wave-domain approach employs the wave equation solutions as basis functions to express

any wave field over the spatial region, and designs the secondary sound field based on the wave-domain decomposition coefficients.

In the ANC system, the residual signal at any arbitrary observation point is given by (3.1), which we rewrite here for convenience,

$$e(\boldsymbol{x}, k) = \nu(\boldsymbol{x}, k) + s(\boldsymbol{x}, k), \tag{6.1}$$

where the secondary sound field generated by a discrete loudspeaker array with L loudspeakers can be represented by

$$s(\boldsymbol{x}, k) = \sum_{l=1}^{L} d_l(k) G(\boldsymbol{x}|\boldsymbol{y}_l, k). \tag{6.2}$$

Here, $d_l(k)$ is the driving signal for the l^{th} loudspeaker. Note that in the reverberant environment, $G(\boldsymbol{x}|\boldsymbol{y}_l, k)$ includes the room reflections.

We then represent the primary sound field and secondary sound field in the wave domain.

As described in (2.40), the spherical harmonics based wave equation solution decomposes any homogeneous incident wave field $\nu(\boldsymbol{x}, k)$ observed at $\boldsymbol{x}$ into

$$\nu(\boldsymbol{x}, k) = \sum_{u=0}^{\infty} \sum_{m=-u}^{u} \beta_{um}(k) j_u(kr) Y_{um}(\phi_{\boldsymbol{x}}, \psi_{\boldsymbol{x}}), \tag{6.3}$$

where $j_u(\cdot)$ is the spherical Bessel function of order u and $Y_{um}(\cdot)$ denotes the spherical harmonics. Here, ψ and ϕ are the elevation angle and the azimuthal angle, respectively. Therefore, the decomposition coefficients $\beta_{um}(k)$ represent the primary noise field in the wave domain. In the vector version, $\boldsymbol{\beta}(k) = [\beta_{0,0}(k), \beta_{1,-1}(k), \ldots, \beta_{N,N}(k)]^T$. Within the region of interest $r \leq R_1$, a finite number of modes can be used to approximate the noise field [108]. Thus, the primary sound field in (6.3) can be truncated by

$$\nu(\boldsymbol{x}, k) \approx \sum_{u=0}^{N} \sum_{m=-u}^{u} \beta_{um}(k) j_u(kr) Y_{um}(\phi_{\boldsymbol{x}}, \psi_{\boldsymbol{x}}), \tag{6.4}$$

where the number of $N = \lceil ekR_1/2 \rceil$ [108, 109, 123].

Using the spherical harmonic expansion, the secondary sound field within the quiet zone can also be represented by

$$s(\boldsymbol{x}, k) = \sum_{u=0}^{\infty} \sum_{m=-u}^{u} \gamma_{um}(k) j_u(kr) Y_{um}(\phi_{\boldsymbol{x}}, \psi_{\boldsymbol{x}}). \tag{6.5}$$

The coefficients $\gamma_{um}(k)$ represent the secondary sound field in the wave domain. Similar to the primary noise field, inside the region of interest with the radius of R_1, the secondary sound field can be truncated by

$$s(\boldsymbol{x}, k) \approx \sum_{u=0}^{N} \sum_{m=-u}^{u} \gamma_{um}(k) j_u(kr) Y_{um}(\phi_{\boldsymbol{x}}, \psi_{\boldsymbol{x}}). \tag{6.6}$$

The acoustic transfer function (ATF) in (6.2) can be parameterized in the wave domain [76] as

$$G(\boldsymbol{x}|\boldsymbol{y}_l, k) \approx \sum_{u=0}^{N} \sum_{m=-u}^{u} \eta_{um}^{(l)}(k) j_u(kr) Y_{um}(\phi_{\boldsymbol{x}}, \psi_{\boldsymbol{x}}). \tag{6.7}$$

where $\eta_{um}^{(l)}(k)$ is the ATF in wave domain for each loudspeaker.

Substituting (6.7) and (6.6) into (6.2), the secondary sound coefficients $\gamma_{um}(k)$ can also be represented by

$$\gamma_{um}(k) = \sum_{l=1}^{L} d_l(k) \eta_{um}^{(l)}(k). \tag{6.8}$$

In matrix form, the relationship between the secondary source decomposition coefficients and the loudspeaker driving signals are given by

$$\boldsymbol{\gamma}(k) = \boldsymbol{\eta}(k) \boldsymbol{d}(k), \tag{6.9}$$

where

$$\boldsymbol{\eta}(k) = \begin{bmatrix} \eta_{00}^{(1)}(k) & \eta_{00}^{(2)}(k) & \cdots & \eta_{00}^{(L)}(k) \\ \eta_{-11}^{(1)}(k) & \eta_{-11}^{(2)}(k) & \cdots & \eta_{-11}^{(L)}(k) \\ \vdots & \vdots & \ddots & \vdots \\ \eta_{NN}^{(1)}(k) & \eta_{NN}^{(2)}(k) & \cdots & \eta_{NN}^{(L)}(k) \end{bmatrix}, \tag{6.10}$$

and $\boldsymbol{d}(k) = [d_1(k), \ldots, d_L(k)]^T$.

We investigate the maximum ANC performance based on the primary sound field coefficients $\boldsymbol{\beta}(k)$ and the secondary-path information $\boldsymbol{\eta}(k)$ in the wave domain, and derive loudspeaker driving signals using two methods: the wave-domain least square method and the subspace method.

6.3 Wave-domain Least Square Method

In the following two sections, we analyse noise cancellation capability using wave-domain coefficients of the primary noise field and the secondary path.

One method for deriving the loudspeaker driving signal $\boldsymbol{d}(k)$ is to match the secondary sound field coefficients to the primary sound field coefficients, in the region of interest. Therefore,

$$\boldsymbol{\eta}(k)\boldsymbol{d}(k) = -\boldsymbol{\beta}(k). \tag{6.11}$$

Here, we denote the set of all linear combinations of the columns in $\boldsymbol{\eta}(k)$ as column space $\boldsymbol{C}$. The dimension of the column space $\boldsymbol{C}$ is called the rank of matrix $\boldsymbol{\eta}(k)$.

In equation (6.11), (i) the number of loudspeakers, (ii) the rank of $\boldsymbol{\eta}(k)$ and (iii) the rank of matrix $\boldsymbol{\eta}(k)$ augmented by $\boldsymbol{\beta}(k)$ specify the number of solutions for the linear system (6.11).

- Case 1: $L = (N+1)^2$

If the number of loudspeakers is same as the number of modes in the region of interest, (6.11) has one unique solution, which is given by

$$\boldsymbol{d}(k) = -(\boldsymbol{\eta}(k))^{-1}\boldsymbol{\beta}(k). \tag{6.12}$$

- Case 2: $L > (N+1)^2$

If the number of loudspeakers is greater than the mode requirement, (6.11) is an under-determined system. There is either no solution or an infinite number of solutions. In practice, however, this case rarely happens, as extra loudspeakers do not result in better ANC results but increase the device cost and computational cost.

- Case 3: $L < (N+1)^2$

If the loudspeaker number L is less than the number of modes $(N+1)^2$ in the region of interest, (6.11) is an over-determined system. There are more equations than unknowns, resulting in either a single unique solution or no solution.

When the measurements are in a very special case, which requires

$$\text{rank}(\boldsymbol{\eta}|\boldsymbol{\beta}) = \text{rank}(\boldsymbol{\eta}), \tag{6.13}$$

equation (6.11) has an exact solution. Here, rank($\boldsymbol{\eta}$) denotes the rank of $\boldsymbol{\eta}$, and rank($\boldsymbol{\eta}|\boldsymbol{\beta}$) denotes the rank of the matrix $\boldsymbol{\eta}(k)$ augmented by $\boldsymbol{\beta}(k)$.
When

$$\text{rank}(\boldsymbol{\eta}|\boldsymbol{\beta}) \neq \text{rank}(\boldsymbol{\eta}), \tag{6.14}$$

equation (6.11) has no exact solution.

The solution can be approximated using the least square method [124]. The least square method tries to find the best approximation which results in minimum mean square errors [125], by solving the following problem

$$\min\|\boldsymbol{\eta}(k)\boldsymbol{d}(k) - (-\boldsymbol{\beta}(k))\|^2. \tag{6.15}$$

The optimal solution of this minimization problem can be written as

$$\boldsymbol{d}(k) = -(\boldsymbol{\eta}(k))^{\dagger}\boldsymbol{\beta}(k), \tag{6.16}$$

where $(\cdot)^{\dagger}$ denotes the pseudoinverse of a matrix.

For some circumstances, $\boldsymbol{\beta}(k)$ could be totally inside the column space $\boldsymbol{C}$. While most of time, $\boldsymbol{\beta}(k)$ have components outside the space $\boldsymbol{C}$. In general, the result of the driving signal in (6.16) is achieved by solving the equation as follows:

$$\boldsymbol{\eta}(k)\boldsymbol{d}(k) = -\text{Proj}_{\boldsymbol{C}}\boldsymbol{\beta}(k), \tag{6.17}$$

where $\text{Proj}_{\boldsymbol{C}}\boldsymbol{\beta}(k)$ denotes the projected part of the primary noise field coefficients $\boldsymbol{\beta}(k)$ in the column space $\boldsymbol{C}$. The projection matrix can be also written by

$$\text{Proj}_{\boldsymbol{C}}\boldsymbol{\beta}(k) = \boldsymbol{\eta}(k)(\boldsymbol{\eta}^H(k)\boldsymbol{\eta}(k))^{-1}\boldsymbol{\eta}^H(k). \tag{6.18}$$

In most applications, the number of loudspeakers is less than the requirement. Then the driving signals can be designed by least square solutions in (6.16). Therefore, this method is here called the 'wave-domain least square method' (WDLS).

6.4 Subspace Method

In the second method, we obtain the secondary-path coefficient $\boldsymbol{\eta}^{(l)}(k)$, extract the subspace spanned by secondary-path coefficients which represents the secondary sources in this environment, and only cancel the primary noise field which can be projected into this subspace.

6.4.1 Principal component analysis of the secondary path

Let $\boldsymbol{\eta}^{(l)}(k)$ the wave-domain secondary-path coefficients for the l_{th} loudspeaker. Matrix $\boldsymbol{\eta}(k)$ in (6.10) for the entire loudspeaker array represents the secondary path, where

$$\boldsymbol{\eta}(k) = [\boldsymbol{\eta}^{(1)}(k), \ldots, \boldsymbol{\eta}^{(L)}(k)]. \tag{6.19}$$

In an arbitrary loudspeaker array setup, each column of matrix $\boldsymbol{\eta}(k)$ is not necessarily orthogonal. We use the principal component analysis (PCA) of the correlation matrix to obtain an orthonormal eigen-basis for the space of the secondary path in the wave domain.

We take the correlation matrix $E\{\boldsymbol{\eta}^H(k)\boldsymbol{\eta}(k)\}$, and then decompose this matrix into a set of orthonormal eigenvectors and their corresponding eigenvalues, as follows:

$$E\{\boldsymbol{\eta}^H\boldsymbol{\eta}\} = \boldsymbol{u}\boldsymbol{\lambda}\boldsymbol{v}, \tag{6.20}$$

where $\boldsymbol{u} = [\boldsymbol{u}_1, \ldots, \boldsymbol{u}_i, \ldots, \boldsymbol{u}_L]$ are the eigenvectors of the wave-domain ATF, $\boldsymbol{v} = \boldsymbol{u}^T$, and the i^{th} column corresponds to the eigenvalue λ_i. Here onwards, the frequency dependent k is omitted for notational simplicity.

The eigenvalues in the matrix form are

$$\boldsymbol{\lambda} = \begin{bmatrix} \lambda_1 & 0 & \cdots & 0 \\ 0 & \lambda_2 & \cdots & 0 \\ \vdots & \vdots & \ddots & \vdots \\ 0 & 0 & \cdots & \lambda_L \end{bmatrix}. \tag{6.21}$$

Here, the vectors $\boldsymbol{u}$ are written in order of descending eigenvalues $\boldsymbol{\lambda}$ [126].
On this basis $\boldsymbol{u}$, the largest eigenvalues correspond to the principal components of the secondary path in wave domain ($\boldsymbol{\eta}$), which contain the most useful information.

Depending on the acoustic environment and the loudspeaker placement, the first B components are used to represent the loudspeakers, then the corresponding eigenvectors are $\boldsymbol{u}^{\diamond} = [\boldsymbol{u}_1, \ldots, \boldsymbol{u}_B]$,

$$\boldsymbol{O} = \boldsymbol{\eta}\boldsymbol{u}^{\diamond}, \tag{6.22}$$

where the dimension of $\boldsymbol{u}^{\diamond}$ is $L \times B$, and $B \leq L$.
By normalizing each column of matrix $\boldsymbol{O}$, the orthonormal vectors $\boldsymbol{o}_1, \ldots, \boldsymbol{o}_B$ are obtained. These vectors generate a subspace, which represents the loudspeaker array and the acoustic environment. The dimensions of basis $\boldsymbol{O}$ are $(N+1)^2 \times B$.

For the l^{th} loudspeaker, the average ATF coefficients over certain short frames can be represented in this space as

$$\overline{\boldsymbol{\eta}}^{(l)} = \sum_{b=1}^{B} \kappa_b^{(l)} \boldsymbol{o}_b, \tag{6.23}$$

where $\kappa_b^{(l)}$ are the projection coefficients. In vector form, (6.23) can be written by

$$\overline{\boldsymbol{\eta}}^{(l)} = \boldsymbol{O}\boldsymbol{\kappa}^{(l)}, \tag{6.24}$$

where $\boldsymbol{\kappa}^{(l)} = \{\kappa_1^{(l)}, \ldots, \kappa_b^{(l)}, \ldots, \kappa_B^{(l)}\}^T$ and

$$\kappa_b^{(l)} = < \boldsymbol{\eta}^{(l)}, \boldsymbol{o}_b > . \tag{6.25}$$

Here, $< \cdot, \cdot >$ is the inner product of two vectors. $\boldsymbol{\kappa}$ is the secondary-path coeffi-

cients in the subspace $\boldsymbol{O}$, with the dimension of $B \times L$.

6.4.2 Projection from the primary sound field into the subspace

Below we project the wave-domain coefficients of the primary sound field into the subspace $\boldsymbol{O}$.

For a new primary sound field represented by vector $\boldsymbol{\beta}$, by projecting $\boldsymbol{\beta}$ into the subspace $\boldsymbol{O}$, we can obtain

$$\text{Proj}_{\boldsymbol{O}}\boldsymbol{\beta} = \sum_{b=1}^{B} < \boldsymbol{\beta}, \boldsymbol{o}_b > \boldsymbol{o}_b = < \boldsymbol{\beta}, \boldsymbol{o}_1 > \boldsymbol{o}_1 + \cdots + < \boldsymbol{\beta}, \boldsymbol{o}_B > \boldsymbol{o}_B, \tag{6.26}$$

where $\text{Proj}_{\boldsymbol{O}}\boldsymbol{\beta}$ denotes the projection of vector $\boldsymbol{\beta}$ into subspace $\boldsymbol{O}$. The matrix form of the projection is represented by

$$\text{Proj}_{\boldsymbol{O}}\boldsymbol{\beta} = \boldsymbol{O}\boldsymbol{y}, \tag{6.27}$$

where $\boldsymbol{y} = \{y_1, y_2, \ldots, y_B\}^T$ are the primary sound field coefficients in the subspace, and $y_b = < \boldsymbol{\beta}, \boldsymbol{o}_b >$.

Therefore, the primary sound field can be separated by two parts: the projected part and the remaining part,

$$\boldsymbol{\beta} = \text{Proj}_{\boldsymbol{O}}\boldsymbol{\beta} + R(\boldsymbol{\beta}), \tag{6.28}$$

where $R(\boldsymbol{\beta})$ is the orthogonal complement of the subspace $\boldsymbol{O}$. The projected part indicates the primary sound field which can be cancelled in this system setup, and the orthogonal complement indicates the primary sound field which can not be cancelled in this system.

If $R(\boldsymbol{\beta}) = 0$, $\boldsymbol{\beta}$ lies in the subspace, then the primary sound field can be completely cancelled by the loudspeaker array.

In more general cases, $R(\boldsymbol{\beta}) \neq 0$. This indicates the limitation of noise cancellation over the region of interest, under the particular loudspeaker placement and acoustic environment.

Next, we design the driving signal of loudspeaker $d_l(k)$ to cancel the primary noise field projected into the subspace ($\text{Proj}_{\boldsymbol{O}}\boldsymbol{\beta}$).

6.4.3 Noise control in the subspace

In the subspace, matching the secondary sound field coefficients to the projected primary sound field coefficients, the optimal solution of the secondary sound field coefficients can be written by

$$\boldsymbol{\gamma} = -\text{Proj}_{\boldsymbol{O}}\boldsymbol{\beta}. \tag{6.29}$$

The projection from the primary sound field into the loudspeaker subspace $\text{Proj}_{\boldsymbol{O}}\boldsymbol{\beta}$ can be calculated by (6.27).

In a given loudspeaker setup, substituting (6.24) into (6.9), the representation of secondary sound field coefficients can be rewritten by

$$\boldsymbol{\gamma} = \boldsymbol{O}\boldsymbol{\kappa}\boldsymbol{d}, \tag{6.30}$$

where $\boldsymbol{d} = \{d_1, \ldots, d_L\}^T$, $\boldsymbol{\kappa} = \{\boldsymbol{\kappa}^{(1)}, \ldots, \boldsymbol{\kappa}^{(L)}\}$.

Substituting (6.30) and (6.27) into (6.29), we can get

$$\boldsymbol{O}\boldsymbol{\kappa}\boldsymbol{d} = -\boldsymbol{O}\boldsymbol{y}. \tag{6.31}$$

Multiplying the left inverse of $\boldsymbol{O}$ on both sides, (6.31) becomes

$$\boldsymbol{O}^{\dagger}\boldsymbol{O}\boldsymbol{\kappa}\boldsymbol{d} = -\boldsymbol{O}^{\dagger}\boldsymbol{O}\boldsymbol{y}. \tag{6.32}$$

Further simplifying (6.32), the final equation to design the driving signal can be written as

$$\boldsymbol{\kappa}\boldsymbol{d} = -\boldsymbol{y}. \tag{6.33}$$

The loudspeaker driving signals can be calculated by solving the system of linear equations described by (6.33). The number of principal components specifies whether the linear system (6.33) can be solved exactly.

- Case 1: $B = L$

When we reserve all the information in the PCA, (6.33) has only one unique solution. In that case, the driving signals can be represented by

$$\boldsymbol{d} = -(\boldsymbol{\kappa})^{-1}\boldsymbol{y}. \tag{6.34}$$

- Case 2: $B < L$

  When we only use the largest components to generate the subspaces, instead of solving the over-determined system in (6.11), equation (6.33) solves an under-determined system. In that case, the driving signals $\boldsymbol{d}$ can be derived by

  $$\boldsymbol{d} = -(\boldsymbol{\kappa})^{\dagger}\boldsymbol{y}, \tag{6.35}$$

  where $(\boldsymbol{\kappa})^{\dagger}$ is the pseudoinverse of the secondary-path coefficients in the subspace, with the dimension of $L \times B$.

Loudspeaker driving signals $\boldsymbol{d}$ are designed by the secondary-path information in the subspace $\boldsymbol{\kappa}$ and the primary sound field coefficients in the subspace $\boldsymbol{y}$, as shown in (6.35). Therefore, the method is here called the 'subspace method'.

6.5 Simulation Results

In this section, we conduct simulations to investigate the maximum ANC performance in the 3-D sound field by using the WDLS and the proposed subspace method.

When the driving signal is unit amplitude, and only the l^{th} loudspeaker produces sound, $\eta_{um}^{(l)}(k) = \gamma_{um}^{(l)}(k)$. Therefore, we can capture $\eta_{um}^{(l)}(k)$ from the measurement of $s(\boldsymbol{x}, k)$ based on (6.6). For the subspace method, following the PCA, from (6.22), we can extract the subspace $\boldsymbol{O}$ from the loudspeaker coefficients $\eta_{um}^{(l)}(k)$. Representing the $\eta_{um}^{(l)}(k)$ in the subspace as $\boldsymbol{\kappa}$, and projecting the primary source into the subspace as $\boldsymbol{y}$, we can derive the driving signals by solving (6.33).

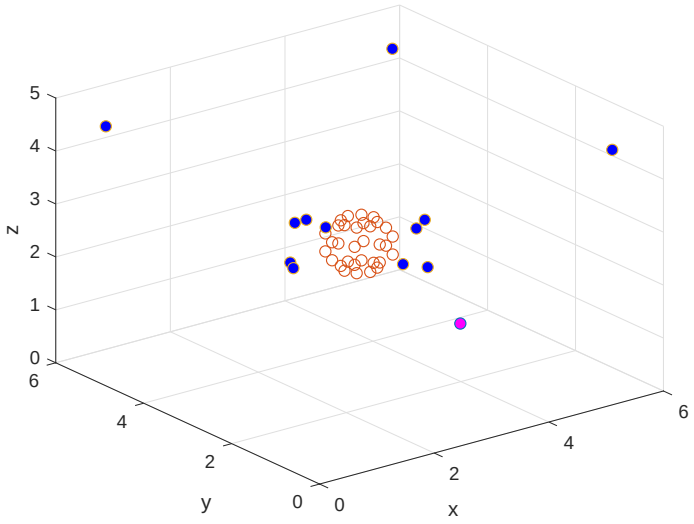

(a)

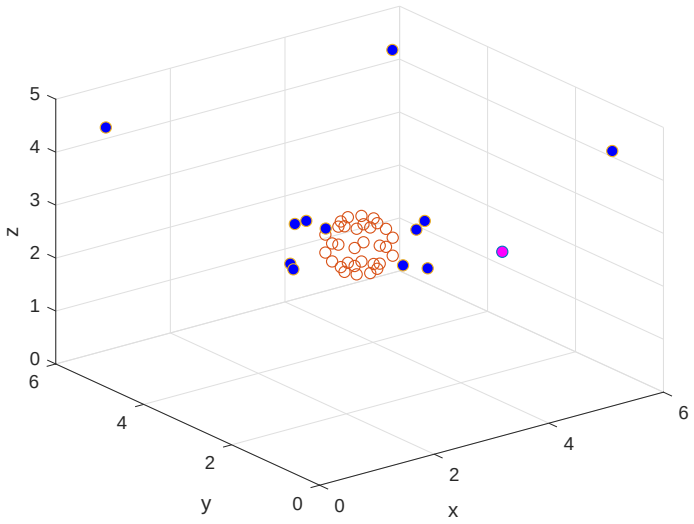

(b)

Figure 6.2: ANC system setup, where the pink point is the noise source position, blue points are loudspeaker positions, and red points are microphone positions: (a) case 1; (b) case 2.

6.5.1 Simulation setup

In this simulation, we investigate the ANC performance in the reverberant environment. The reverberant environment is modelled as a cuboid room of 6 m ×6 m ×5 m. The reflection coefficients are [0.75, 0.8, 0.77, 0.85, 0.1, 0.1]. The reverberation is simulated by the image source method with the image order of 5. The origin of the room is on the left bottom corner. The region of interest is a spherical area with a radius of 0.5 m, and the center of the region is (3, 3, 1.5) with respect to the origin.

We assume that the noise field only contains a single-frequency component. In the following investigations, the primary noise field is a spherical wave coming from a point source located at (r, ϕ, ψ) with respect to the center of the region, with a constant magnitude of 10. The locations of primary sources are different in each case, as shown in Table 6.1.

We assume the frequency of the noise field is 200 Hz. From (6.4), the region of interest in such a noise field can be represented by $N = \lceil ekR_1/2 \rceil = 3$ modes. Thus, at least $(N+1)^2 = 16$ microphones must be placed on the boundary to capture the information of the residual noise field for each mode. In this simulation, we place 32 microphones on the spherical boundary, following the Gauss-Legendre sampling method. White Gaussian noise is added to each microphone recording to simulate the internal thermal noise of microphones.

To control all the modes, 16 loudspeakers are required to be placed outside the control region. To emulate a practical scenario, however, in this simulation, only 12 loudspeakers are placed outside the region. 8 loudspeakers are placed in the x-y plane with two different geometries, as shown in Table 6.1. In both cases, four loudspeakers are placed on another plane, which is on the plane close to the ceiling. The loudspeaker positions for each case are shown in Table 6.2.

We evaluate the ANC performance in terms of residual noise field, noise reduction on the sample points inside the region N_r^{in}, and the energy of the driving signals E_d.

To evaluate the actual noise reduction performance within the control region, residual sound fields $\boldsymbol{e}_{in}$ at $Z = 1296$ points uniformly placed within the cross section between the region of interest and the x-y plane are examined. As in

Table 6.1: Loudspeaker array setup and noise source location in each case.

Noise source position \ Loudspeaker array	non-symmetry	symmetry
$(2, 315°, 45°)$	case 1	
$(2, 315°, 90°)$	case 2	
24 position candidates	case 3	case 4

Table 6.2: Loudspeaker positions for non-symmetric placement and symmetric placement.

loudspeakers in the x-y plane			loudspeakers outside the x-y plane	
No.	non-symmetry	symmetry	No.	
1	(4, 3, 2.5)	(4.5, 3, 2.5)	9	(0.5, 0.5, 4.5)
2	(1.8, 3, 2.5)	(1.5, 3, 2.5)	10	(5.5, 5.5, 4.5)
3	(3, 2, 2.5)	(3, 1.5, 2.5)	11	(5.5, 0.5, 4.5)
4	(3, 4.2, 2.5)	(3, 4.5, 2.5)	12	(0.5, 5.5, 4.5)
5	(4.3, 3.2, 2.5)	(4.2, 1.8, 2.5)		
6	(1.7, 2.8, 2.5)	(1.8, 1.8, 2.5)		
7	(3.2, 1.7, 2.5)	(4.2, 4.2, 2.5)		
8	(2.8, 4.2, 2.5)	(1.8, 4.2, 2.5)		

Chapter 5 (5.28), the noise reduction inside the region of interest over Z points $N_{\mathrm{r}}^{\mathrm{in}}$ can be written by

$$N_{\mathrm{r}}^{\mathrm{in}} \triangleq 10\log_{10}\frac{\sum_z E\{|e_{\mathrm{in}\_z}|^2\}}{\sum_z E\{|e_{\mathrm{in}\_z}(0)|^2\}}, \tag{6.36}$$

where $E\{|e_{\mathrm{in}\_z}(0)|^2\}$ is the energy of the primary sound field at the z^{th} sample point, and $E\{|e_{\mathrm{in}\_z}|^2\}$ is the energy of the residual sound field at the z^{th} sample point.

To evaluate the loudspeaker energy consumption, we compare the total energy of all the loudspeakers E_d. The loudspeaker energy consumption can be represented by

$$E_d = \boldsymbol{d}^T\boldsymbol{d}. \tag{6.37}$$

For the subspace method, during the PCA process for the secondary path, we only reserve the principle components in $\boldsymbol{u}$. Components in $\boldsymbol{u}$ which correspond to λ_i occupied less than 5% of the largest eigenvalue $\boldsymbol{\lambda}_1$ are omitted in $\boldsymbol{u}^{\diamond}$.

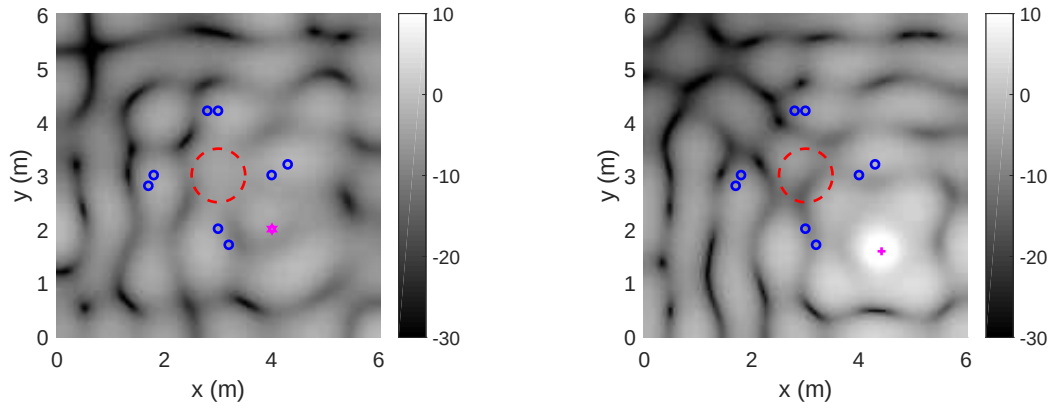

(a) (b)

Figure 6.3: Energy of the primary noise field, where pink point is the projection of the primary source on the x-y plane, blue points are the loudspeaker points located on the x-y plane, and the red dashed circle is the boundary of the region of interest: (a) case 1; (b) case 2.

6.5.2 Cancellation performance using different methods

We first compare cancellation performance using the subspace method and the WDLS method in two different noise source positions. In this simulation, white Gaussian noise with SNR[1] of 60 dB is added to each microphone recording. For simplicity of plotting, the cancellation performance over the region is confined to horizontal planes at elevation of 90° (x-y plane) of the 3-D region.

As shown in Figure 6.2, we assume noise field is generated by a point source located at $(2, 315°, 45°)$(case 1) or $(2, 315°, 90°)$ (case 2) in the spherical coordinates. The geometry of loudspeakers in the x-y plane is not symmetrical. The energy of the primary sound field is shown in Figure 6.3.

Figure 6.4 demonstrates the energy of the residual noise field in the x-y plane. As we expected, since the number of loudspeakers (12) can-not cover all the modes (16) in the region, in all four figures, the primary noise field in the region of interest can-not be fully cancelled. In case 2, compared with the primary noise field (Figure 6.3(b)), both the WDLS method and the subspace method can achieve significant noise reduction in the region of interest, which are dark areas in the middle of Figure 6.4(b) and Figure 6.4(d). In case 1, since the noise source is located in a different hemisphere as the loudspeaker array, compared with Figure 6.3(a), cancellation performance inside the region is fairly limited for both WDLS and the subspace method, as shown in Figure 6.4(a) and Figure 6.4(c).

Meanwhile, compared with Figure 6.4(a) and Figure 6.4(b), in Figure 6.4(c) and Figure 6.4(d), the subspace method results in lower energy of the residual noise field outside the region of interest. the WDLS method increases the sound energy outside the region, especially when the noise reduction level is fairly limited inside the region. Using the subspace method, we reduce the sound amplification to people sitting outside the control area.

[1]Here, the SNR level is with respect to the primary noise field level on virtual microphone in the center of the region.

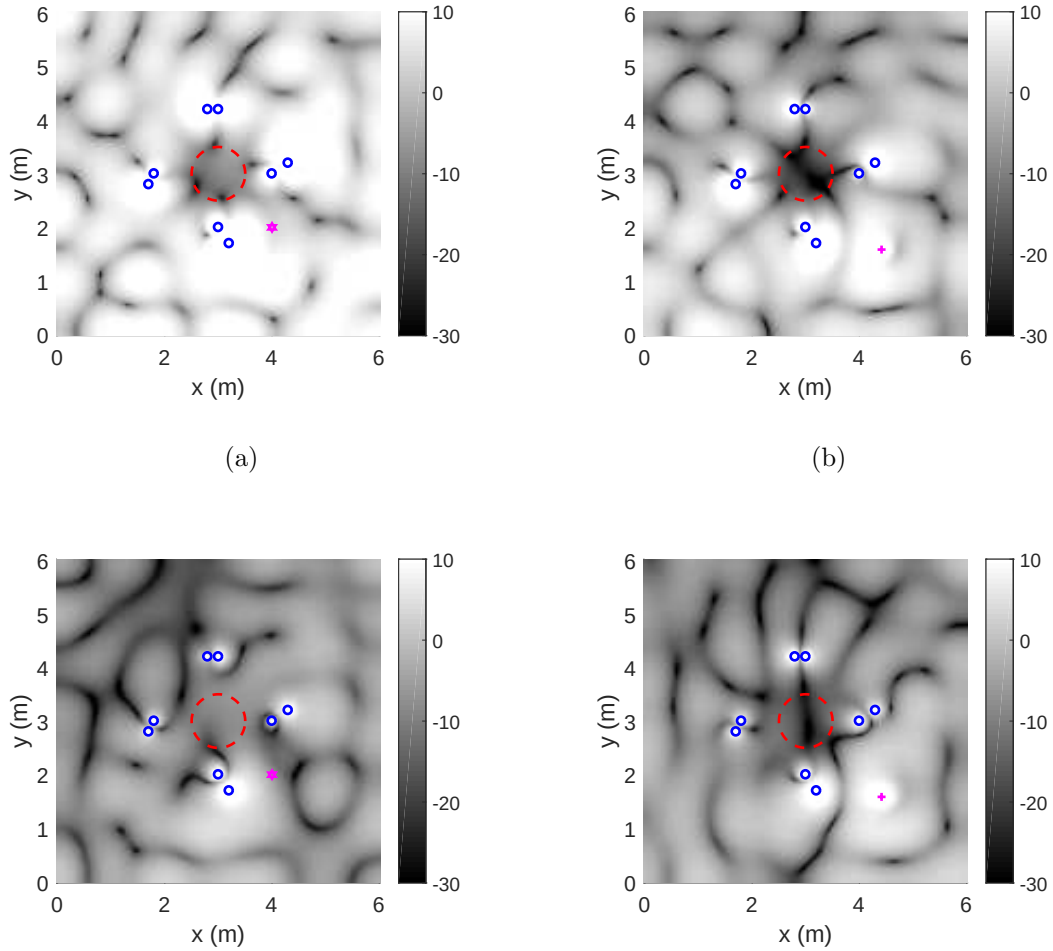

(a) (b)

(c) (d)

Figure 6.4: Energy of the residual noise field, when the noise field is generated by one primary source using different methods. Here, pink point is the projection of the primary source on the x-y plane and blue points are the loudspeaker points located on the x-y plane: (a) the WDLS method in case 1; (b) the WDLS method in case 2; (c) the subspace method in case 1; (d) the subspace method in case 2.

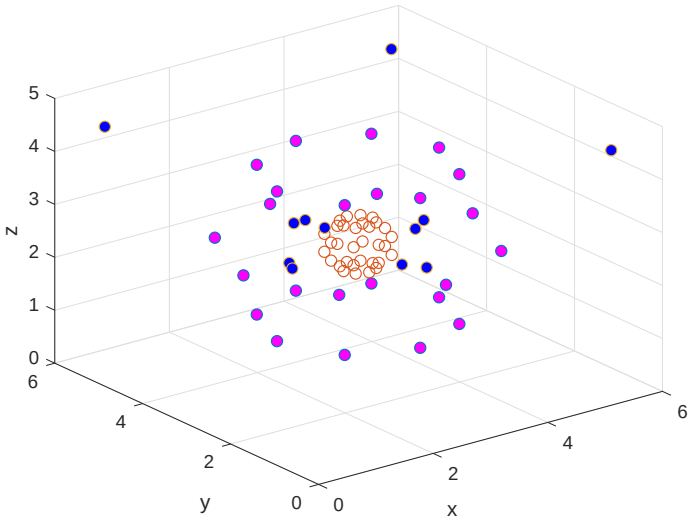

(a)

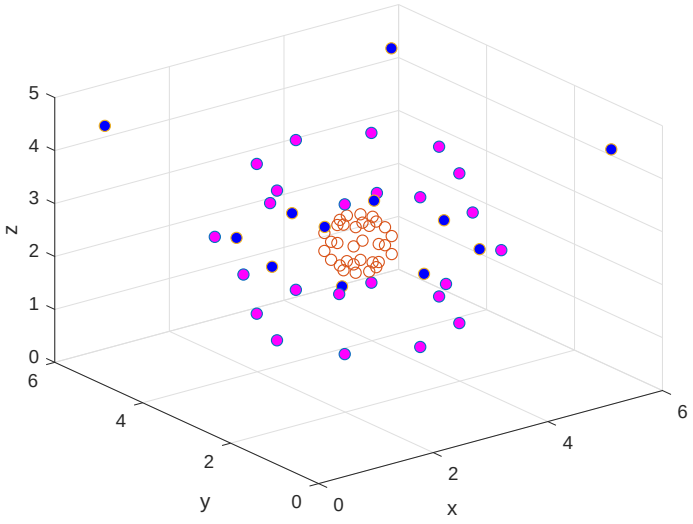

(b)

Figure 6.5: Two different array setups, when the noise source moves around a sphere, where in both setups, pink points are the primary source positions, blue points are loudspeaker positions, and red points are microphone positions: (a) Case 3; (b) Case 4.

6.5.3 Comparison of the effect of different noise source positions

After investigating the cancellation performance in two different noise source positions, we move the source position around different elevations (45°, 90°, 135°) and different azimuthal angles ($0°, 45°, 90°, 135°, 180°, 225°, 270°, 315°$). As shown in Figure 6.5(a), 24 source position candidates are chosen on the sphere with radius of 2 m. We measure the primary sound field coefficients and secondary sound field coefficients by microphones with different SNR levels, which are 60 dB and 30 dB, respectively, for each source position candidate.

Figure 6.6 demonstrates the noise reduction performance for different source positions. For most of the positions, the WDLS method can achieve slightly better noise reduction than the subspace method. This is due to the subspace method only uses the principal components while the WDLS method considers all the information of the secondary path. Since 8 out of 12 loudspeakers are located in the x-y plane, the noise source positions indicated better noise reduction levels in Figure 6.6(a) and Figure 6.6(b) are position No. 2, 5, 8, 11, 14, 17, 20, 23, which are the candidates on the x-y plane. As the accuracy of the microphone recordings is reduced, the performance prediction becomes less accurate. As shown in Figure 6.6(b), at the noise source position 15, using both methods, the noise reduction levels are positive, which indicates the opposite result as Figure 6.6(a).

Figure 6.7 demonstrates the energy of the loudspeaker driving signals using different methods. As shown in Figure 6.7(a) and Figure 6.7(b), in both cases, compared with the WDLS method, the proposed subspace method can reduce the total energy on the loudspeakers significantly, which can avoid the overloading of the secondary sources.

6.5.4 Comparison of the effect of different loudspeaker placements

Since the loudspeaker placements effect the numbers of principal components in the subspace method, we investigate the noise reduction performance and energy of driving signal under different loudspeaker configurations. The ANC systems

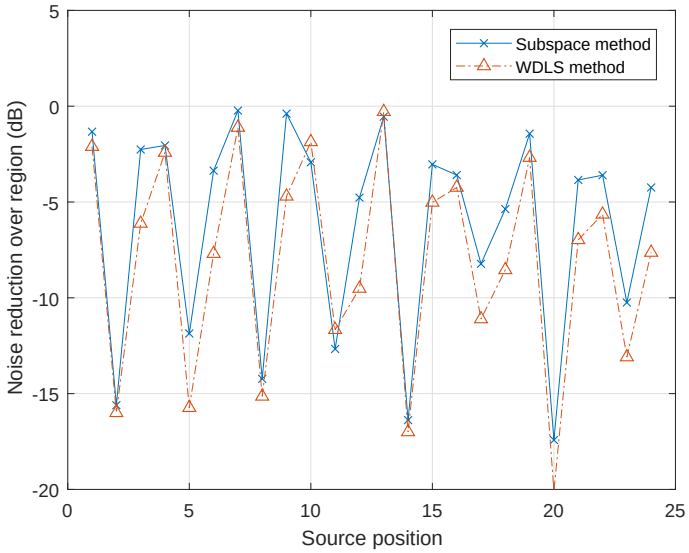

(a)

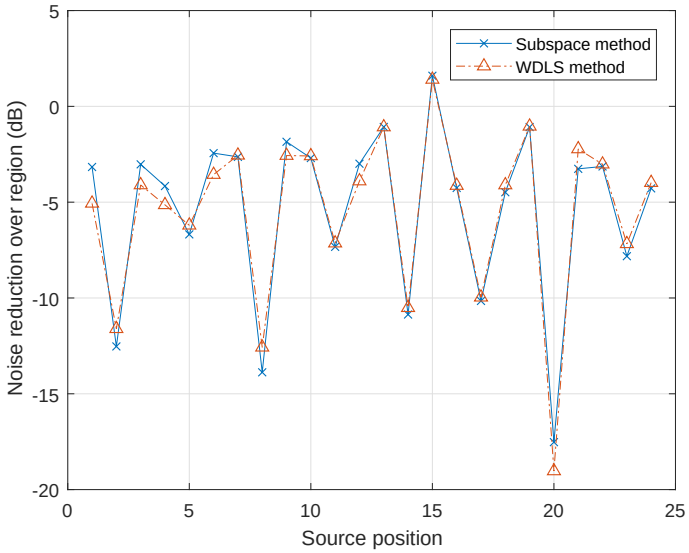

(b)

Figure 6.6: Noise reduction performance in case 3, when the noise field is generated by one primary source moving around the sphere using different methods: (a) with SNR = 60 dB white noise on the microphone recordings; (b) with SNR = 30 dB white noise on the microphone recordings.

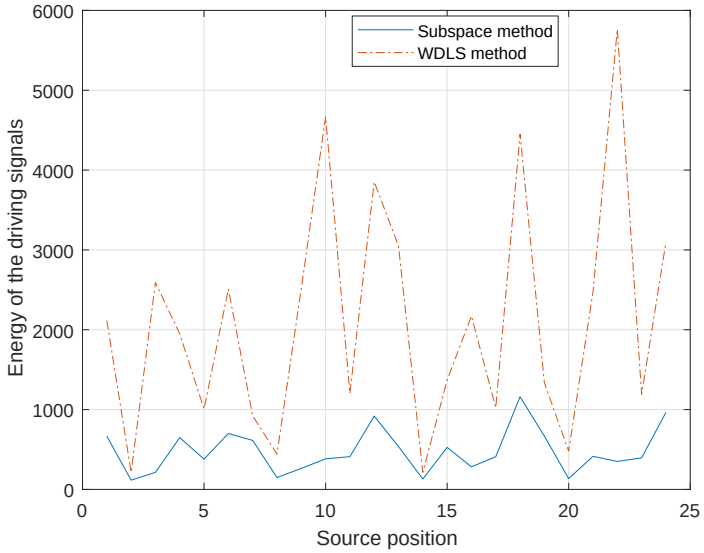

(a)

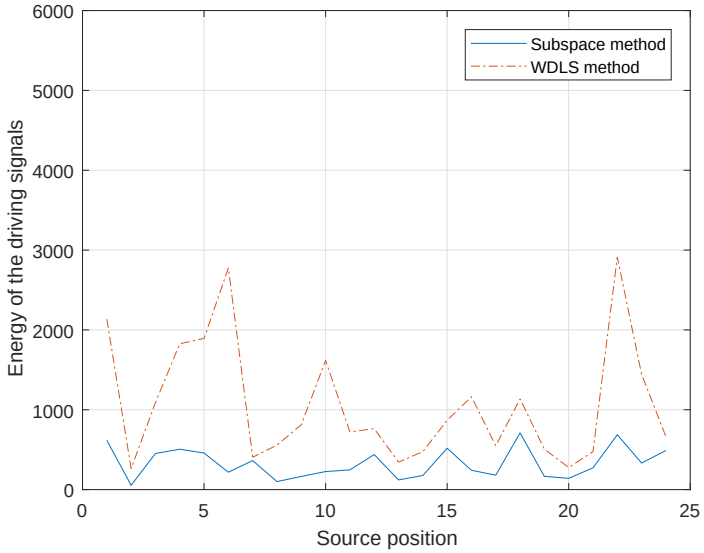

(b)

Figure 6.7: Energy of the driving signals in case 3, when the noise field is generated by one primary source moving around the sphere using different methods: (a) with SNR = 60 dB white noise on the microphone recordings; (b) with SNR = 30 dB white noise on the microphone recordings.

with two configurations are shown in Figure 6.5. Figure 6.8 and Figure 6.9 demonstrate the noise reduction and the energy of the loudspeaker driving signals for each noise source positions. For both loudspeaker configurations, compared with the WDLS method, the proposed subspace method achieves less noise reduction and less total energy on the loudspeakers. The significantly reduced energy of the driving signals can avoid the overloading of the secondary sources and reduce the sound amplification to people outside the control area. In case 3, the correlation between different loudspeakers is higher than that in case 4. In case 4, the numbers of principal components is larger than that in case 3. Therefore, compared with Figure 6.8(a) and Figure 6.9(a), in Figure 6.8(b) and Figure 6.9(b), there are less difference between the subspace method and the WDLS method.

6.6 Summary and Contributions

In this chapter, we analysed the noise cancellation performance in 3-D reverberant environments, especially when the secondary sources have constraints on numbers and locations. We discussed a wave-domain least square method to analyse the maximum ANC performance by matching the secondary sound field to the primary sound field in wave domain. We proposed a subspace method to analyse the maximum ANC performance by investigating the subspace of secondary path coefficients. We validated the noise reduction performance, energy of the loudspeakers, and energy of the residual signals outside the region under different loudspeaker configurations and different noise source positions.

The major contributions in this chapter are:

- By principal component analysis of the secondary path coefficients, we extracted the basis of the subspace generated by the secondary path.
- We derived the loudspeaker driving signals by matching the projection of the primary noise field coefficients to the secondary noise field coefficients in the subspace.
- We compared the proposed subspace method with the wave-domain least square method, when the number of secondary sources could not control

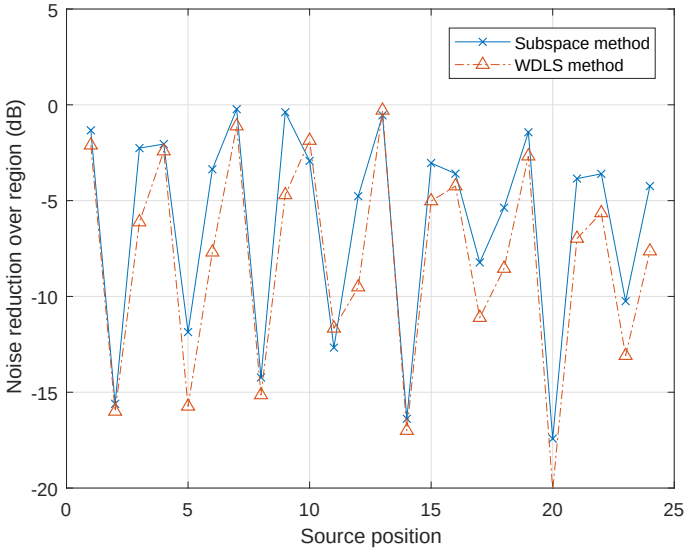

(a)

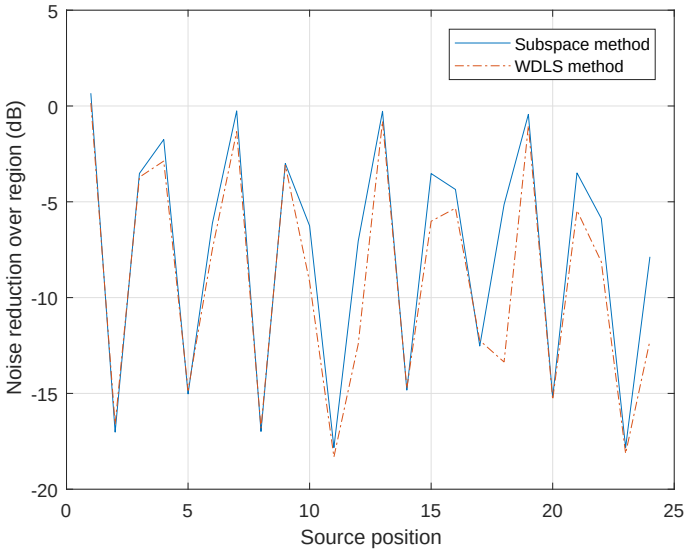

(b)

Figure 6.8: Noise reduction over the region using different loudspeaker setups, when the noise field generated by one primary source moving around the sphere using different methods: (a) case 3; (b) case 4.

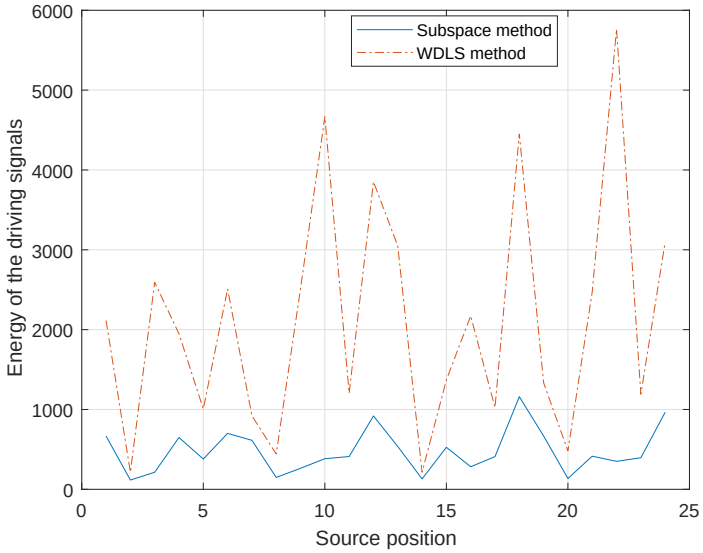

(a)

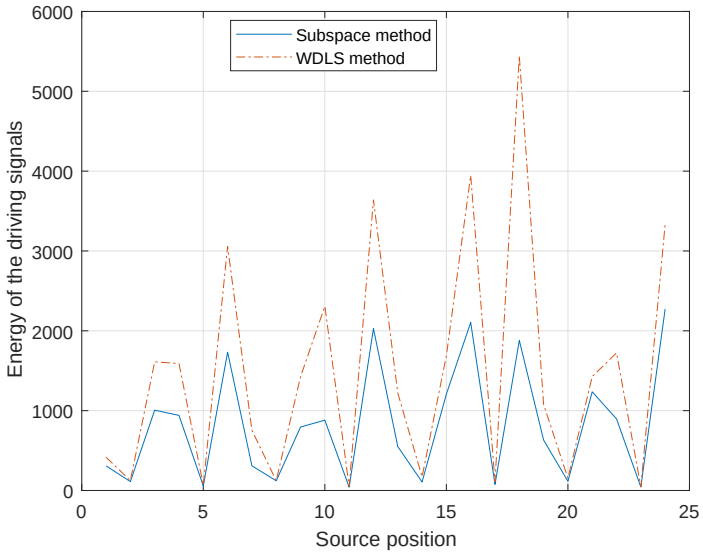

(b)

Figure 6.9: Energy of the driving signals generated by one primary source moving around the sphere using different methods: (a) case 3; (b) case 4.

all the modes in the region. Using the subspace method, we obtained a feasible solution with slightly lower noise reduction level inside the region, significantly less energy on the secondary sources, and significantly less energy on the residual noise field outside the control region.

6.7 Related Publications

[127]: J. Zhang, T. D. Abhayapala, W. Zhang, and P. N. Samarasinghe, "Active Noise Control over Space: A Subspace Method for Performance Analysis," *Applied Sciences*, vol. 9, no. 6, pp. 1250, March 2019.

Chapter 7

Conclusion and Future Research Directions

In this chapter, we state the general conclusions drawn from this thesis. We also outline future research directions arising from this work.

7.1 Conclusions

This thesis aimed to develop new theory to effectively control the noise field over a large spatial region. In particular, we investigated spatial ANC in a general noise field, as well as in a sparse noise field. For the general noise field, we proposed the wave-domain ANC structure, developed wave-domain algorithms in different cost functions and adaptations, and investigated ANC performance in subspace of the wave-domain secondary path. For the sparse noise field, we incorporated the sparse constraints to the conventional multi-point ANC and the proposed wave-domain ANC. The works which have been done in this thesis are represented as blue blocks in Figure 7.1.

In the literature, spatial ANC in a general noise field has been addressed using multichannel control structures, as reviewed in Chapter 2. In particular, multiple microphones and multiple loudspeakers formulate the basic setup, and well-known algorithms such as NLMS and FxLMS have been applied to iteratively create the secondary source driving signals. Although these algorithms lead to significant

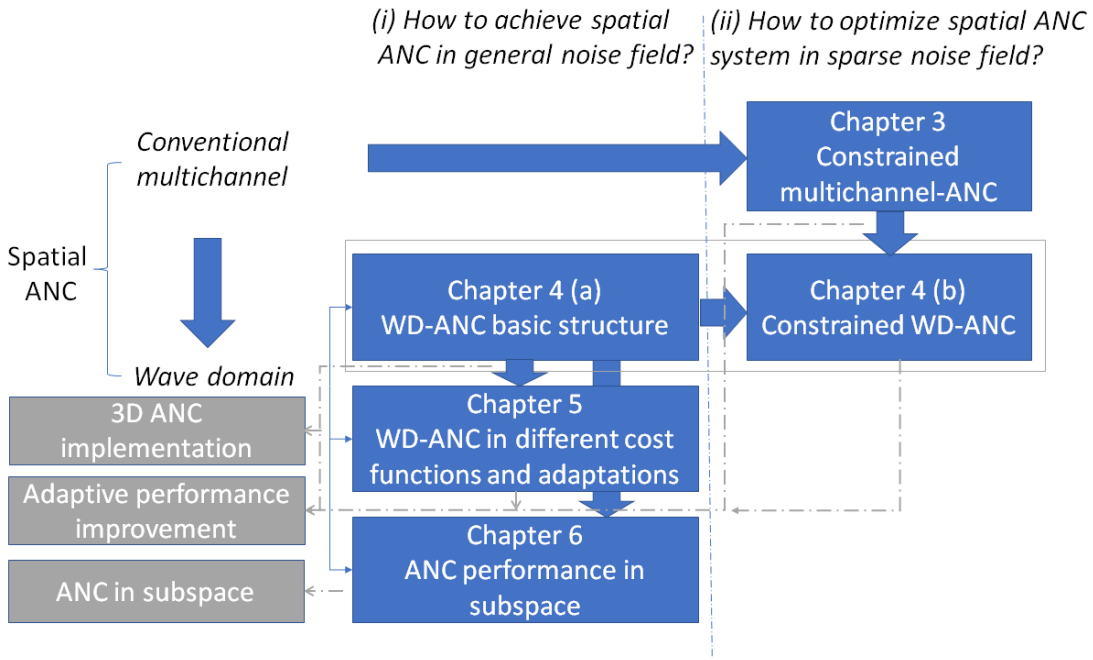

Figure 7.1: Conclusion and future works for spatial ANC over region. The blue blocks represent the works have been done in this thesis, and the grey blocks represent the future research directions.

noise reduction at the sensor points, the consistency over a continuous spatial region is low. Meanwhile, conventional multi-point algorithms utilize massive systems requiring a large number of loudspeakers to generate a secondary sound field.

We solved the problem of *'(ii) How to reduce the number of secondary sources in the array, and how to reduce the computational complexity of the algorithms'* using the multi-point structure in Chapter 3, and solved this problem using the wave-domain structure in Chapter 4.

In Chapter 3, to reduce the active loudspeaker number of the multi-point ANC system in a directional sparse noise field, we incorporated the ℓ_1-norm penalty from the compressive sensing technique into the multi-point structure, resulting in $C\ell_1$-MP and $S\ell_1$-MP algorithms. The proposed Cℓ_1-MP and Sℓ_1-MP demonstrated faster convergence speed and fewer active loudspeaker numbers in the directional sparse noise field. In Chapter 4, we incorporated the ℓ_1-norm penalty into the wave domain filtered-x least mean square, resulting in the ℓ_1-constrained FxLMS algorithm.

We solved the problem *'(i) How to achieve ANC over a large continuous region in a general noise field'* using wave-domain structure in Chapter 4 and Chapter 5.

We formulated the spatial ANC problem using the wave domain signal processing technique in Chapter 4. For spatial ANC in the general noise field, we implemented the conventional filtered-x least mean square framework in wave domain, resulting in the wave-domain FxLMS algorithm. To the best of our knowledge, we are the first team to systematically formulate the wave-domain ANC into different minimization problems and different updating variables in Chapter 5. The algorithms we proposed have been evaluated in free field and room environment through numerical simulations. Meanwhile, in the numerical simulations, we exploited the spatial ANC performance using different numbers of secondary sources. In the scenario of fewer secondary source than the requirement, we demonstrated that normalized energy based wave-domain algorithms could achieve better noise reduction performance over the region. Meanwhile, the reduced noise reduction performance in the steady state demonstrated the limit of wave-domain ANC using finite resources.

We solved the problem *'(i) How to achieve ANC in a large contin-*

***uous region in a general noise field'* by investigating the ANC performance in Chapter 6.**

We mathematically formulated the ANC performance in 3-D reverberant environments. By principal component analysis of the secondary path coefficients, we extracted the basis of the subspace generated from the secondary path coefficients, and projected the primary noise field coefficients onto this subspace. We derived the optimal solution by matching the projection of the primary noise field coefficients to the secondary noise field coefficients in the subspace. By utilising main components rather than all components of the secondary path coefficients, the subspace method can avoid overloading the loudspeakers, specifically when the ANC capability was very limited in the given secondary sources and acoustic environment. Using the proposed subspace method, we can achieve feasible solutions with reasonable noise reduction inside the region and less energy on the sound field outside the region.

Overall, it can be concluded that this thesis provides a number of significant and original contributions to the field of spatial ANC. The outcomes of this research can underpin the future development of the use of spatial ANC in industry and can be applied across a number of applications such as automobiles, theatres, and aeroplanes.

Despite this achievement, a number of challenges still require further research.

7.2 Future Work

Based on the material in this thesis, we list three future research directions, which could lead to deeper understanding of ANC over spatial regions: (i) spatial ANC implementation in 3D noise fields, (ii) adaptive performance improvement using variable step size, and (iii) spatial ANC in subspace. The future research directions are represented as grey blocks in Figure 7.1.

(i) Spatial ANC implementation in 3-D noise fields

We developed ANC theory in Chapter 3, Chapter 4 and Chapter 5 based on 2-D noise fields. One possible future direction is to extend these theories to 3-D and investigate the related spatial ANC problems in 3-D noise fields. In general, 3-D wave-domain signal processing can be implemented by using spherical microphone

arrays [128] and spherical loudspeaker arrays. However, the spherical shape and high cost of spherical arrays make the system impractical. Meanwhile, the computational complexity of multichannel ANC algorithms increases significantly with the number of secondary sources and error sensors, which reduces the feasibility of the system. There are some recent works addressing the spherical array problem. For the microphone arrays, a compact hybrid microphone array distributed on a 2-D plane was presented for 3-D sound field analysis [119, 129, 130]. For the spherical loudspeaker arrays, P. Chen et al. proposed a planar array of dipole loudspeakers to reproduce a full 3-D exterior sound field [131]. It is possible to apply these two arrays on spatial ANC implementations. Applying feed-forward structure to cancel broadband noise field is also a future work in 3-D ANC implementation, and the additional computation cost due to the multiple reference signals need to be well addressed to increase the feasibility of the system.

(ii) Adaptive performance improvement using variable step size

We applied the LMS, FxLMS and NLMS adaptive structures in this thesis, and utilized the fixed step size in all iterations. One possible future research is to investigate wave-domain adaptive algorithms with variable step size. When we use fixed step sizes, a large step size will increase the tracking capability, while it will also increase the mean-square error in the steady state. Variable step size can solve the conflict between convergence speed and mean-square error in the steady state [132, 133]. It can be applied to the wave-domain algorithms to improve the convergence speed as well as the steady-state behavior.

(iii) Spatial ANC in subspace

In Chapter 6, we derived the subspace based on information about secondary source and acoustic environment, and evaluated the maximum noise reduction performance for some specific loudspeaker array arrangements. Since the primary noise field and secondary noise field have been represented in this new subspace, it is possible to derive the adaptive algorithm in this subspace. In this subspace, it is possible to directly cancel the primary noise field which can be controlled by the current secondary source configuration and acoustic environment.

Bibliography

[1] "Engineering acoustics/sound absorbing structures and materials," https://en.wikibooks.org/wiki/Engineering_Acoustics/Sound_Absorbing_Structures_and_Materials, accessed: 2018-07-08.

[2] T. Betlehem, W. Zhang, M. A. Poletti, and T. D. Abhayapala, "Personal sound zones: Delivering interface-free audio to multiple listeners," *IEEE Signal Process. Mag.*, vol. 32, no. 2, pp. 81–91, Mar. 2015.

[3] S. M. Kuo and D. R. Morgan, "Active noise control: A tutorial review," *Proceedings of the IEEE*, vol. 87, no. 6, pp. 943–973, June 1999.

[4] R. F. Barron, "Industrial noise control and acoustics," 2003.

[5] C. M. Harris, *Handbook of acoustical measurements and noise control*. McGraw-Hill New York, 1991.

[6] H. Chen, "Theory and design of spatial active noise control systems," Ph.D. dissertation, The Australian National University, 2017.

[7] M. Alves-Pereira and N. C. Branco, "Vibroacoustic disease: Biological effects of infrasound and low-frequency noise explained by mechanotransduction cellular signalling," *Progress in Biophysics and Molecular Biology*, vol. 93, no. 1, pp. 256 – 279, 2007.

[8] J. Duan, "Active control of vehicle powertrain and road noise," Thesis, University of Cincinnati, 2011.

[9] S. M. Kuo and D. R. Morgan, *Active Noise Control Systems: Algorithms and DSP Implementations*. New York: Wiley, 1996.

[10] M. Bergamasco, F. D. Rossa, and L. Piroddi, "Active noise control with online estimation of non-Gaussian noise characteristics," *Journal of Sound and Vibration*, vol. 331, no. 1, pp. 27 – 40, Jan. 2012.

[11] C. C. Fuller, S. Elliott, and P. A. Nelson, *Active Control of Vibration*. San Diego, CA: Academic, 1996.

[12] J. McIntosh, "Active noise cancellation aircraft headset system," https://www.google.com/patents/US6278786, Aug. 2001, US Patent 6,278,786.

[13] S. Kuo, S. Mitra, and W. Gan, "Active noise control system for headphone applications," *IEEE Trans. Control Systems Technology*, vol. 14, no. 2, pp. 331–335, Mar. 2006.

[14] R. Reddy, I. Panahi, and R. Briggs, "Hybrid FxRLS-FxNLMS adaptive algorithm for active noise control in fMRI application," *IEEE Trans. Control Systems Technology*, vol. 19, no. 2, pp. 474–480, Mar. 2011.

[15] T. J. Sutton, S. J. Elliott, A. M. McDonald, and T. J. Saunders, "Active control of road noise inside vehicles," *Noise Control Engineering Journal*, vol. 42, no. 4, pp. 9–12, July 1994.

[16] H. Sano, T. Inoue, A. Takahashi, K. Terai, and Y. Nakamura, "Active control system for low-frequency road noise combined with an audio system," *IEEE Trans. Speech and Audio Process.*, vol. 9, no. 7, pp. 755–763, Oct. 2001.

[17] J. Cheer and S. J. Elliott, "The design and performance of feedback controllers for the attenuation of road noise in vehicles," *International Journal of Acoustics and Vibration*, vol. 19, no. 3, pp. 155–164, Jan. 2014.

[18] P. N. Samarasinghe, W. Zhang, and T. D. Abhayapala, "Recent advances in active noise control inside automobile cabins: Toward quieter cars," *IEEE Signal Process. Mag.*, vol. 33, no. 6, pp. 61–73, Nov. 2016.

[19] M. D. P. Emilio, "Reducing unwanted noise in automobiles," https://www.electronicdesign.com/automotive/reducing-unwanted-noise-automobiles, June 2017.

[20] S. J. Elliott and P. A. Nelson, "Active noise control," *IEEE Signal Process. Mag.*, vol. 10, no. 4, pp. 12–35, 1993.

[21] H. Chen, P. N. Samarasinghe, T. D. Abhayapala, and W. Zhang, "Spatial noise cancellation inside cars: Performance analysis and experimental results," in *2015 IEEE Workshop on Applications of Signal Processing to Audio and Acoustics (WASPAA)*, Oct. 2015, Conference Proceedings, pp. 1–5.

[22] "Active noise control: Wiping up unwanted sound," https://fisitech.wordpress.com/2010/07/06/active-noise-control-wiping-up-unwanted-sound/, 2010.

[23] S. M. Kuo and D. R. Morgan, "Active noise control: A tutorial review," *Proceedings of the IEEE*, vol. 87, no. 6, pp. 943–973, June 1999.

[24] S. J. Elliot, P. A. Nelson, I. M. Stothers, and C. C. Boucher, "In-flight experiments on the active control of propeller-induced cabin noise," *Journal of Sound and Vibration*, vol. 140, no. 2, pp. 219 – 238, 1990.

[25] J. Cheer and S. J. Elliott, "Multichannel control systems for the attenuation of interior road noise in vehicles," *Mechanical Systems and Signal Processing*, vol. 60 61, pp. 753 – 769, 2015.

[26] J. I. Mohammad, S. J. Elliott, and A. Mackay, "The performance of active control of random noise in cars," *J. Acoust. Soc. Am.*, vol. 123, no. 4, pp. 1838–1841, 2008.

[27] Y. Kajikawa, W. S. Gan, and S. M. Kuo, "Recent advances on active noise control: Open issues and innovative applications," *APSIPA Transactions on Signal and Information Processing*, vol. 1, p. 21, Apr. 2012.

[28] A. Barkefors, S. Berthilsson, and M. Sternad, "Extending the area silenced by active noise control using multiple loudspeakers," in *Proc. IEEE International Conference on Acoustics, Speech, and Signal Processing 2012*, Kyoto, Japan, Mar. 2012, pp. 325–328.

[29] M. Bouchard and S. Quednau, "Multichannel recursive-least-square algorithms and fast-transversal-filter algorithms for active noise control and sound reproduction systems," *IEEE Trans. Speech and Audio Process.*, vol. 8, no. 5, pp. 606–618, Sept. 2000.

[30] J. Benesty and D. Morgan, "Frequency-domain adaptive filtering revisited, generalization to the multi-channel case, and application to acoustic echo cancellation," in *Proc. IEEE International Conference on Acoustics, Speech, and Signal Processing 2000*, vol. 2, Istanbul, Turkey, June 2000, pp. II789–II792.

[31] J. Lorente, M. Ferrer, M. De Diego, and A. González, "GPU implementation of multichannel adaptive algorithms for local active noise control," *IEEE/ACM Trans. Audio, Speech, Language Process.*, vol. 22, no. 11, pp. 1624–1635, Nov. 2014.

[32] T. Kosaka, S. J. Elliott, and C. C. Boucher, "A novel frequency domain filtered-x LMS algorithm for active noise reduction," in *Proc. IEEE International Conference on Acoustics, Speech, and Signal Processing 1997*, vol. 1, Munich, Germany, Apr. 1997, pp. 403–406.

[33] S. J. Elliott, I. Stothers, and P. A. Nelson, "A multiple error LMS algorithm and its application to the active control of sound and vibration," *IEEE Trans. Acoust., Speech, Signal Process.*, vol. 35, no. 10, pp. 1423–1434, Oct. 1987.

[34] A. J. Berkhout, "A holographic approach to acoustic control," *Journal of the audio engineering society*, vol. 36, no. 12, pp. 977–995, 1988.

[35] A. J. Berkhout, D. de Vries, and P. Vogel, "Acoustic control by wave field synthesis," *J. Acoust. Soc. Am.*, vol. 93, no. 5, pp. 2764–2778, 1993.

[36] Y. J. Wu, "Spatial soundfield reproduction in complex environments," Thesis, The Australian National University, 2010.

[37] S. Spors and J. Ahrens, "Comparison of higher-order ambisonics and wave field synthesis with respect to spatial aliasing artifacts," in *In 19th International Congress on Acoustics*. Citeseer, 2007, Conference Proceedings.

[38] S. Spors, H. Buchner, R. Raebnstein, and W. Herbordt, "Active listening room compensation for massive multichannel sound reproduction systems using wave-domain adaptive filtering," *J. Acoust. Soc. Am.*, vol. 122, no. 1, pp. 354–369, July 2007.

[39] S. Spors, R. Rabenstein, and J. Ahrens, "The theory of wave field synthesis revisited," in *124th AES Convention*, 2008, Conference Proceedings, pp. 17–20.

[40] S. Spors and H. Buchner, "An approach to massive multichannel broadband feedforward active noise control using wave-domain adaptive filtering," in *2007 IEEE Workshop on Applications of Signal Processing to Audio and Acoustics (WASPAA)*, Oct. 2007, pp. 171–174.

[41] ——, "Efficient massive multichannel active noise control using wave-domain adaptive filtering," in *Proc. 3rd International Symposium on Communications, Control and Signal Processing*, St. Julians, Malta, Mar. 2008, pp. 1480–1485.

[42] T. D. Abhayapala, "Modal analysis and synthesis of broadband nearfield beamforming arrays," Ph.D. dissertation, The Australian National University, 1999.

[43] T. D. Abhayapala and D. B. Ward, "Theory and design of high order sound field microphones using spherical microphone array," in *2002 IEEE International Conference on Acoustics, Speech, and Signal Processing*, vol. 2, 2002, Conference Proceedings, pp. 1949–1952.

[44] T. D. Abhayapala, "Generalized framework for spherical microphone arrays: Spatial and frequency decomposition," in *IEEE International Conference on Acoustics, Speech and Signal Processing (ICASSP) 2008*, March 2008, pp. 5268–5271.

[45] C. Fan, S. A. Salehin, and T. D. Abhayapala, "Practical implementation and analysis of spatial soundfield capture by higher order microphones." in *APSIPA*, 2014, pp. 1–8.

[46] Y. Kajikawa, W. S. Gan, and S. M. Kuo, "Recent applications and challenges on active noise control," in *2013 8th International Symposium on Image and Signal Processing and Analysis (ISPA)*, Sept. 2013, pp. 661–666.

[47] J. C. Burgess, "Active adaptive sound control in a duct: A computer simulation," *J. Acoust. Soc. Am.*, vol. 70, no. 3, pp. 715–726, June 1981.

[48] C. Hansen, S. Snyder, X. Qiu, L. Brooks, and D. Moreau, *Active control of noise and vibration.* CRC press, 2012.

[49] E. A. Wan, "Adjoint LMS: an efficient alternative to the filtered-x LMS and multiple error LMS algorithms," in *IEEE International Conference on Acoustics, Speech, and Signal Processing 1996*, vol. 3, May 1996, pp. 1842–1845 vol. 3.

[50] S. Haykin, *Adaptive Filter Theory.* Prentice Hall, 2001.

[51] S. J. Elliott and P. A. Nelson, "The application of adaptive filtering to the active control of sound and vibration," *NASA STI/Recon Technical Report N*, vol. 86, Sept. 1985.

[52] L. J. Eriksson and M. C. Allie, "Use of random noise for on-line transducer modeling in an adaptive active attenuation system," *The Journal of the Acoustical Society of America*, vol. 85, no. 2, pp. 797–802, 1989.

[53] W. Zhang, C. Hofmann, M. Buerger, T. D. Abhayapala, and W. Kellermann, "Spatial noise-field control with online secondary path modeling: A wave-domain approach," *IEEE/ACM Transactions on Audio, Speech and Language Processing (TASLP)*, vol. 26, no. 12, pp. 2355–2370, 2018.

[54] O. J. Tobias and R. Seara, "Leaky-FXLMS algorithm: stochastic analysis for Gaussian data and secondary path modeling error," *IEEE Trans. Speech and Audio Process.*, vol. 13, no. 6, pp. 1217–1230, 2005.

[55] "A generalized leaky FxLMS algorithm for tuning the waterbed effect of feedback active noise control systems," *Mechanical Systems and Signal Processing*, vol. 106, pp. 13 – 23, 2018.

[56] J. Benesty and Y. Huang, *Adaptive signal processing: applications to real-world problems*. Springer Science & Business Media, 2013.

[57] "Advances in active noise control: A survey, with emphasis on recent nonlinear techniques," *Signal Processing*, vol. 93, no. 2, pp. 363 – 377, 2013.

[58] T. Wang and W. S. Gan, "Stochastic analysis of FXLMS-based internal model control feedback active noise control systems," *Signal Processing*, vol. 101, pp. 121 – 133, 2014.

[59] A. Ganguly, I. Panahi, and F. Dufour, "Exploring feedback active noise control with ambisonics," in *IEEE Circuits and Systems Conference (DCAS)*, 2010.

[60] J. K. Thomas, S. P. Lovstedt, J. D. Blotter, and S. D. Sommerfeldt, "Eigenvalue equalization filtered-x algorithm for the multichannel active noise control of stationary and nonstationary signals," *J. Acoust. Soc. Am.*, vol. 123, no. 6, pp. 4238–49.

[61] M. Bouchard, "Multichannel affine and fast affine projection algorithms for active noise control and acoustic equalization systems," *IEEE Trans. Speech Audio Process.*, vol. 11, no. 1, pp. 54–60, Jan. 2003.

[62] R. Schirmacher, "Current status and future development of anc systems," *SOUND and VIBRATION*, p. 17, 2016.

[63] J. Romeu, A. Balastegui, T. Pamies, and R. Arcos, "Optimal acoustic error sensing for global active control in a harmonically excited enclosure," *Acoustical Physics*, vol. 60, no. 1, pp. 77–85, 2014.

[64] J. Cheer and S. J. Elliott, "Active noise control of a diesel generator in a luxury yacht," *Applied Acoustics*, vol. 105, pp. 209 – 214, 2016.

[65] A. Kuntz and R. Rabenstein, "An approach to global noise control by wave field synthesis," in *2004 12th European Signal Processing Conference*, 2004, Conference Proceedings, pp. 1999–2002.

[66] A. Montazeri, J. Poshtan, and M. H. Kahaei, "Analysis of the global reduction of broadband noise in a telephone kiosk using a MIMO modal ANC system," *International Journal of Engineering Science*, vol. 45, no. 28, pp. 679 – 697, 2007.

[67] J. W. Parkins, S. D. Sommerfeldt, and J. Tichy, "Error analysis of a practical energy density sensor," *J. Acoust. Soc. Am.*, vol. 108, no. 1, pp. 211–222, 2000.

[68] ——, "Narrowband and broadband active control in an enclosure using the acoustic energy density," *J. Acoust. Soc. Am.*, vol. 108, no. 1, pp. 192–203, 2000.

[69] B. Xu, S. D. Sommerfeldt, and T. W. Leishman, "Generalized acoustic energy density," *J. Acoust. Soc. Am.*, vol. 130, no. 3, pp. 1370–1380.

[70] B. Xu and S. D. Sommerfeldt, "Generalized acoustic energy density based active noise control in single frequency diffuse sound fields," *J. Acoust. Soc. Am.*, vol. 136, no. 3, pp. 1112–1119, 2014.

[71] D. Li and M. Hodgson, "Optimal active noise control in large rooms using a locally global control strategy," *J. Acoust. Soc. Am.*, vol. 118, no. 6, pp. 3653–3661.

[72] D. Ward and T. Abhayapala, "Reproduction of a plane-wave sound field using an array of loudspeakers," *IEEE Trans. Speech and Audio Process.*, vol. 9, no. 6, pp. 697–707, Sept. 2001.

[73] H. Buchner, S. Spors, and W. Kellermann, "Wave-domain adaptive filtering: Acoustic echo cancellation for full-duplex systems based on wave-field synthesis," in *Proc. IEEE International Conference on Acoustics, Speech, and Signal Processing 2004*, vol. 4, Montreal, Quebec, Canada, May 2004, pp. iv117–iv120.

[74] M. Schneider and W. Kellermann, "A wave-domain model for acoustic MIMO systems with reduced complexity," in *Proc. IEEE HSCMA*, Edinburgh, UK, May 2011, pp. 133 – 138.

[75] ——, "Adaptive listening room equalization using a scalable filtering structure in the wave domain," in *Proc. IEEE International Conference on Acoustics, Speech, and Signal Processing 2012*, Kyoto, Japan, Mar. 2012, pp. 13–16.

[76] T. Betlehem and T. D. Abhayapala, "Theory and design of sound field reproduction in reverberant rooms," *J. Acoust. Soc. Am.*, vol. 117, no. 4, pp. 2100–2111, Apr. 2005.

[77] D. Talagala, W. Zhang, and T. Abhayapala, "Efficient multi-channel adaptive room compensation for spatial soundfield reproduction using a modal decomposition," *IEEE/ACM Trans. Audio, Speech, Language Process.*, vol. 22, no. 10, pp. 1522–1532, Oct. 2014.

[78] P. N. Samarasinghe, T. D. Abhayapala, and M. A. Poletti, "Room reflections assisted spatial sound field reproduction," in *2014 22nd European Signal Processing Conference (EUSIPCO)*, Sept 2014, pp. 1352–1356.

[79] T. D. Abhayapala and Y. Wu, "Spatial soundfield reproduction with zones of quiet," in *Proc. 127th Audio Engineering Society Convention*, New York, USA, Oct. 2009, p. 7887.

[80] Y. J. Wu and T. D. Abhayapala, "Spatial multizone soundfield reproduction," in *IEEE International Conference on Acoustics, Speech and Signal Processing (ICASSP) 2009*, 2009, pp. 93–96.

[81] Y. Wu and T. Abhayapala, "Spatial multizone soundfield reproduction: Theory and design," *IEEE Trans. Audio, Speech, Language Process.*, vol. 19, no. 6, pp. 1711–1720, Aug. 2011.

[82] T. Betlehem, W. Zhang, M. Poletti, and T. Abhayapala, "Personal sound zones: Delivering interface-free audio to multiple listeners," *IEEE Signal Process. Mag.*, vol. 32, no. 2, pp. 81–91, Mar. 2015.

[83] Z. Han, M. Wu, Q. Zhu, and J. Yang, "Two-dimensional multizone sound field reproduction using a wave-domain method," *J. Acoust. Soc. Am.*, vol. 144, no. 3, pp. EL185–EL190, 2018.

[84] J. Donley, C. Ritz, and W. B. Kleijn, "Multizone soundfield reproduction with privacy-and quality-based speech masking filters," *IEEE/ACM Trans. Audio, Speech, Language Process.*, vol. 26, no. 6, pp. 1041–1055, 2018.

[85] M. A. Poletti and T. D. Abhayapala, "Interior and exterior sound field control using general two-dimensional first-order sources," *J. Acoust. Soc. Am.*, vol. 129, no. 1, pp. 234–244, 2011.

[86] M. A. Poletti, T. D. Abhayapala, and P. N. Samarasinghe, "Interior and exterior sound field control using two dimensional higher-order variable-directivity sources," *J. Acoust. Soc. Am.*, vol. 131, no. 5, pp. 3814–3823, 2012.

[87] P. N. Samarasinghe, M. A. Poletti, S. M. A. Salehin, T. D. Abhayapala, and F. M. Fazi, "3D soundfield reproduction using higher order loudspeakers," in *2013 IEEE International Conference on Acoustics, Speech and Signal Processing (ICASSP)*, May 2013, pp. 306–310.

[88] F. Dunn, W. Hartmann, D. Campbell, and N. H. Fletcher, *Springer handbook of acoustics*. Springer, 2015.

[89] R. Duraiswami, D. N. Zotkin, and N. A. Gumerov, "Fast evaluation of the room transfer function using multipole expansion," *IEEE Trans. Audio, Speech, Language Process.*, vol. 15, no. 2, pp. 565–576, 2007.

[90] G. Williams, *Fourier acoustics: sound radiation and nearfield acoustical holography*. Academic press, 1999.

[91] T. Jonsson and J. Yngvason, *Waves and Distributions*. Singapore: World Scientific, 1995.

[92] D. Colton and R. Kress, *Inverse acoustic and electromagnetic scattering theory*. Springer Science & Business Media, 2012, vol. 93.

[93] G. Lilis, D. Angelosante, and G. Giannakis, "Sound field reproduction using the lasso," *IEEE Trans. Audio, Speech, Language Process.*, vol. 18, no. 8, pp. 1902–1912, Nov. 2010.

[94] Y. Chen, Y. Gu, and A. Hero, "Sparse LMS for system identification," in *IEEE International Conference on Acoustics, Speech, and Signal Processing 2009*, Apr. 2009, pp. 3125–3128.

[95] K. Shi and X. Ma, "Transform domain LMS algorithms for sparse system identification," in *Proceeding International Conference on Acoustics Speech and Signal Processing 2010*, Mar. 2010, pp. 3714–3717.

[96] J. Zhang, W. Zhang, and T. D. Abhayapala, "Noise cancellation over spatial regions using adaptive wave domain processing," in *IEEE Workshop on Applications of Signal Processing to Audio and Acoustics 2015*, New Paltz, NY, USA, Oct. 2015, pp. 1–5.

[97] P. A. Nelson and S. J. Elliott, *Active control of sound*. Acadamic Press, 1994.

[98] K. Mayyas and T. Aboulnasr, "Leaky LMS algorithm: MSE analysis for gaussian data," *IEEE Trans. Signal Process.*, vol. 45, no. 4, pp. 927–934, 1997.

[99] M. Kamenetsky and B. Widrow, "A variable leaky LMS adaptive algorithm," in *Signals, Systems and Computers, 2004. Conference Record of the Thirty-Eighth Asilomar Conference on*, vol. 1. IEEE, 2004, pp. 125–128.

[100] H. Huang, X. Qiu, and J. Kang, "Active noise attenuation in ventilation windows," *J. Acoust. Soc. Am.*, vol. 130, no. 1, pp. 176–188, 2011.

[101] S. Elliott, *Signal processing for active control*. Academic press, 2000.

[102] E. J. Candes and M. B. Wakin, "An introduction to compressive sampling," *IEEE Signal Process. Mag.*, vol. 25, no. 2, pp. 21–30, 2008.

[103] J. Weston, A. Elisseeff, B. S. Schölkopf, and M. Tipping, "Use of the zero norm with linear models and kernel methods," *The Journal of Machine Learning Research*, vol. 3, pp. 1439–1461, 2003.

[104] D. Sarason, *Complex Function Theory*. American Mathematical Soc., 2007.

[105] J. Zhang, T. D. Abhayapala, P. N. Samarasinghe, W. Zhang, and S. Jiang, "Multichannel active noise control for spatially sparse noise fields," *J. Acoust. Soc. Am.*, vol. 140, no. 6, pp. EL510–EL516, 2016.

[106] Q. Shen and A. Spanias, "Frequency-domain adaptive algorithms for multichannel active sound control," in *Proc. Recent Advances in Active Control of Sound Vibration*, 1993, pp. 755–766.

[107] P. Peretti, S. Cecchi, L. Palestini, and F. Piazza, "A novel approach to active noise control based on wave domain adaptive filtering," in *2007 IEEE Workshop on Applications of Signal Processing to Audio and Acoustics (WASPAA)*, New Paltz, NY, USA, Oct. 2007, pp. 307–310.

[108] R. Kennedy, P. Sadeghi, T. D. Abhayapala, and H. M. Jones, "Intrinsic limits of dimensionality and richness in random multipath fields," *IEEE Trans. Signal Process.*, vol. 55, no. 6, pp. 2542–2556, June 2007.

[109] T. D. Abhayapala, T. Pollock, and R. Kennedy, "Characterization of 3D spatial wireless channels," in *2003 IEEE 58th Vehicular Technology Conference VTC 2003-Fall*, vol. 1, Orlando, FL, USA, Oct. 2003, pp. 123–127.

[110] Y. J. Wu and T. D. Abhayapala, "Theory and design of soundfield reproduction using continuous loudspeaker concept," *IEEE Trans. Audio, Speech, Language Process.*, vol. 17, no. 1, pp. 107–116, Jan. 2009.

[111] B. Widrow, J. McCool, and M. Ball, "The complex LMS algorithm," *Proceedings of the IEEE*, vol. 63, no. 4, pp. 719–720, Apr. 1975.

[112] J. Yang and G. Sobelman, "Sparse LMS with segment zero attractors for adaptive estimation of sparse signals," in *Circuits and Systems (APCCAS), 2010 IEEE Asia Pacific Conference on*, Dec. 2010, pp. 422–425.

[113] J. Zhang, T. D. Abhayapala, P. N. Samarasinghe, W. Zhang, and S. Jiang, "Sparse complex FxLMS for active noise cancellation over spatial regions," in *IEEE International Conference on Acoustics, Speech and Signal Processing (ICASSP) 2016*, Shanghai, China, Mar. 2016, pp. 524–528.

[114] J. B. Allen and D. A. Berkley, "Image method for efficiently simulating small-room acoustics," *J. Acoust. Soc. Am.*, vol. 65, no. 4, pp. 943–950, 1979.

[115] M. R. Bai and S. Chang, "Active noise control of enclosed harmonic fields by using bem-based optimization techniques," *Applied Acoustics*, vol. 48, no. 1, pp. 15–32, 1996.

[116] H. Chen, J. Zhang, P. N. Samarasinghe, and T. D. Abhayapala, "Evaluation of spatial active noise cancellation performance using spherical harmonic analysis," in *IEEE International Workshop on Acoustic Signal Enhancement 2016*, Xi'an, China, Sept. 2016, pp. 1–5.

[117] I. Balmages and B. Rafaely, "Open-sphere designs for spherical microphone arrays," *IEEE Trans. Audio, Speech, Language Process.*, vol. 15, no. 2, pp. 727–732, Feb. 2007.

[118] B. Rafaely, "The spherical-shell microphone array," *IEEE Trans. Audio, Speech, Language Process.*, vol. 16, no. 4, pp. 740–747, 2008.

[119] H. Chen, T. D. Abhayapala, and W. Zhang, "Theory and design of compact hybrid microphone arrays on two-dimensional planes for three-dimensional soundfield analysis," *J. Acoust. Soc. Am.*, vol. 138, no. 5, pp. 3081–3092, 2015.

[120] J. Zhang, T. D. Abhayapala, W. Zhang, P. N. Samarasinghe, and S. Jiang, "Active noise control over space: A wave domain approach," *IEEE/ACM Trans. Audio, Speech, Language Process.*, vol. 26, no. 4, pp. 774–786, 2018.

[121] H. Chen, P. N. Samarasinghe, and T. D. Abhayapala, "In-car noise field analysis and multi-zone noise cancellation quality estimation," in *2015 Asia-Pacific Signal and Information Processing Association Annual Summit and Conference (APSIPA)*, Dec. 2015, pp. 773–778.

[122] M. Buerger, T. D. Abhayapala, C. Hofmann, H. Chen, and W. Kellermann, "The spatial coherence of noise fields evoked by continuous source distributions," *J. Acoust. Soc. Am.*, vol. 142, no. 5, pp. 3025–3034, 2017.

[123] R. A. Kennedy and T. D. Abhayapala, "Spatial concentration of wave-fields : Towards spatial information content in arbitrary multipath scattering," in *4th Aust. Commun. Theory Workshop, AusCTW*, 2003, pp. 4–5.

[124] G. H. Golub and C. F. Van Loan, *Matrix Computations*. JHU Press, 1996, pp. 236–247.

[125] Y. L. Parodi and P. Rubak, "Objective evaluation of the sweet spot size in spatial sound reproduction using elevated loudspeakers," *J. Acoust. Soc. Am.*, vol. 128, no. 3, pp. 1045–1055, 2010.

[126] S. Wold, K. Esbensen, and P. Geladi, "Principal component analysis," *Chemometrics and Intelligent Laboratory Systems*, vol. 2, no. 1, pp. 37–52.

[127] J. Zhang, T. D. Abhayapala, W. Zhang, and P. N. Samarasinghe, "Active noise control over space: A subspace method for performance analysis," *Applied Sciences*, vol. 9, no. 6, 2019.

[128] B. Rafaely, "Analysis and design of spherical microphone arrays," *IEEE Trans. Speech Audio Process.*, vol. 13, no. 1, pp. 135–143, Jan. 2005.

[129] P. N. Samarasinghe, H. Chen, A. Fahim, and T. D. Abhayapala, "Performance analysis of a planar microphone array for three dimensional soundfield analysis," in *2017 IEEE Workshop on Applications of Signal Processing to Audio and Acoustics (WASPAA)*, Oct. 2017, pp. 249–253.

[130] T. D. Abhayapala, P. N. Samarasinghe, and H. Chen, "A planar array of differential microphones for 3D sound capture," *J. Acoust. Soc. Am.*, vol. 143, no. 3, pp. 1823–1823, 2018.

[131] P. Chen, P. N. Samarasinghe, and T. D. Abhayapala, "3D exterior soundfield reproduction using a planar loudspeaker array," in *2018 IEEE International Conference on Acoustics, Speech and Signal Processing (ICASSP)*, Apr. 2018, pp. 471–475.

[132] R. H. Kwong and E. W. Johnston, "A variable step size LMS algorithm," *IEEE Trans. Signal Process.*, vol. 40, no. 7, pp. 1633–1642, July 1992.

[133] H. Huang and J. Lee, "A new variable step-size NLMS algorithm and its performance analysis," *IEEE Trans. Signal Process.*, vol. 60, no. 4, pp. 2055–2060, 2012.